

School of Civil and Mechanical Engineering

Investigation on Conventional and Improved Macro Polypropylene Fibre-Reinforced Concrete Subjected to Static and Dynamic Loads

Feng Shi

**This thesis is presented for the Degree of
Doctor of Philosophy
of
Curtin University**

October 2020

Declaration

To the best of my knowledge and belief, this thesis contains no material previously published by any other person except where due acknowledgement has been made.

This thesis contains no material which has been accepted for the award of any other degree or diploma in any university.

Signature:



Date: 02/11/2020

Abstract

The main weaknesses of conventional concrete are its low tensile strength and brittle characteristic. Traditionally, steel bars are used to improve the overall cracking resistance of concrete elements. However, problems such as chloride corrosion and concrete cover requirement limit the effect of crack control by using steel bars.

In recent years, fibre-reinforced concrete (FRC) has been widely used to replace traditional steel reinforcements in different concrete structures such as precast elements, shotcrete tunnel linings and concrete footpaths. Fibres can effectively improve the mechanical performance of concrete such as reducing shrinkage, improving post-cracking performance and converting brittle to ductile performance. Among different types of fibres, macro PP fibres become increasingly popular as a concrete reinforcing material because of their advantages such as low carbon emission during manufacture, economy and good performance. However, due to their low Young's modulus and weak chemical bonding with concrete, their reinforcing effects are limited. Besides, the performance of macro PP fibre-reinforced concrete (PFRC) structures under dynamic loadings has not been well studied yet and requires more investigations.

In this dissertation, the concept of hybrid fibres was adopted and presented in Chapter 2 to overcome the problems due to low Young's modulus of PP fibres by utilizing short basalt fibres with high Young's modulus. The mechanical properties of basalt-macro PP hybrid fibre-reinforced concrete were experimentally studied through the slump, compressive strength and flexural capacity tests of fibre-reinforced concrete specimens. The failure mode was observed and a new behaviour classification was introduced for hybrid fibre-reinforced concrete. The hybrid fibre-reinforced concrete showed excellent flexural strength, initial post-cracking strength and energy absorption as compared to plain concrete and concrete reinforced with only macro PP fibres.

Meanwhile, ultra-high performance concrete (UHPC) has high compressive and tensile strengths. Therefore, it requires fibres to have a good bonding with the concrete matrix in order to make full use of the high-strength of UHPC. To improve the bonding strength between PP fibres and concrete matrix, methods of modifying the surface by grafting hydrophilic groups and silane groups on PP fibres were investigated and compared in Chapter 3. Characterisation of fibre modification, fibre pullout performance from concrete, and flexural behaviour of fibre-reinforced UHPC were studied. From the Fourier transform infrared (FTIR) and water contact

angle measurements, both the hydrophilic groups and silane groups demonstrated successful and efficient surface grafting on the PP fibres, which helped to significantly improve the bonding behaviour of the grafted fibres. The silane groups and hydrophilic groups grafted PP fibres showed significant improvement in the bond behaviour and much more energy absorption capacity. The silane groups grafted PP fibre-reinforced UHPC showed outstanding toughness and deflection-hardening performance. Besides, the flexural performance of 27 kg/m³ silane groups grafted PP fibre-reinforced UHPC was found comparable with the 78 kg/m³ steel fibre-reinforced UHPC.

After proving that hybrid fibres can be successfully used to improve the mechanical properties of concrete due to the contribution of multiple sizes and functions of fibres, Chapter 4 further investigated the dynamic compressive and splitting tensile properties of basalt-macro PP hybrid fibre-reinforced concrete. High strain rate impacts tests were conducted using the split Hopkinson pressure bar (SHPB). The experimental results showed that basalt-macro PP hybrid FRC exhibited better impact resistance compared with plain concrete in both dynamic compression and splitting tension tests. FRC exhibited a smaller number of crack initiation and propagation, ductile failure pattern and smaller crack mouth opening displacement (CMOD) as compared to the unreinforced specimens. The CMOD of hybrid FRC was significantly reduced (75.8% and 90.3% for 1.1% and 2.1% hybrid FRC, respectively) at 2 milliseconds after impact. The hybrid FRC specimen remained intact with CMOD less than 1 mm when impacted with a dynamic stress rate of 180 GPa/s while plain concrete fully split into two parts in the tests. The sensitivity of hybrid FRC to strain rate was found more significant than plain concrete. Empirical formulae were derived for the dynamic increase factor (DIF) versus strain rate for both the dynamic compressive and split tensile strength of hybrid FRC.

After comprehensive investigations of FRC material properties, Chapter 5 investigated the mechanical performance of concrete slabs and beams reinforced with macro PP fibres and other types of reinforcements. Ground slabs reinforced with steel meshes, steel fibres or macro PP fibres were subjected to central concentrated loading until failure. The fracture behaviour of the slabs on the ground and the performance enhancement with the inclusion of steel and macro PP fibres were discussed. There was a significant increase in the flexural strength of fibre or steel mesh reinforced slabs on the ground. The flexural behaviours of fibre-reinforced concrete beams were also investigated to evaluate the effectiveness of using various fibres in beams and slabs. The flexural strength of fibre-reinforced beams was utilized to predict the load-carrying capacity of concrete ground slabs and compared with the test results.

In summary, this dissertation studied the performance of concrete reinforced with macro PP fibres through static and dynamic material testing and structural tests. The performance of macro PP fibre-reinforced concrete was improved by combining with other fibres. In addition, fibre modification methods were conducted to enhance the bond strength between fibres and concrete matrix. Intensive laboratory tests were carried out with different concrete grades and different reinforcements to quantify the performances of fibre reinforcements. The performance of hybrid FRC under dynamic loadings was also comprehensively investigated. Additionally, the structural performance of ground slabs with various types of reinforcements was examined and compared with the ground slab reinforced with traditional reinforcement meshes. The results from this dissertation suggest that hybrid basalt- macro PP fibres can be used to significantly improve the mechanical properties of the material and hence the structural performances. All the findings of these investigations are summarised in Chapter 6 and suggestions for further studies are also presented.

List of Publications

This thesis is assembled by accepted and submitted publications, which form the individual chapters and are listed below.

Chapter 2

Feng Shi, Thong M. Pham, Hong Hao, Yifei Hao. Post-cracking behaviour of basalt and macro polypropylene hybrid fibre reinforced concrete with different compressive strengths. *Construction and Building Materials*, 2020, 262: 120108.

DOI: 10.1016/j.conbuildmat.2020.120108

Chapter 3

Feng Shi, Shi Yin, Thong M. Pham, Rabin Tuladhar, Hong Hao. Pullout and Flexural Performance of Silane Groups and Hydrophilic Groups Grafted Polypropylene Fibre-reinforced UHPC. *Construction and Building Materials* 2021, 277: 122335.

DOI: 10.1016/j.conbuildmat.2021.122335

Chapter 4

Feng Shi, Thong M. Pham, Hong Hao. Mechanical Properties of Hybrid Fibre-Reinforced Concrete under Dynamic Compression and Split Tension (under review).

Chapter 5

Feng Shi, Thong M. Pham, Rabin Tuladhar, Zongcai Deng, Shi Yin, Hong Hao. Experimental Study on the Performance of Ground Slabs and Beams Reinforced with Macro Polypropylene Fibre, Steel Fibre and Steel Mesh (under review).

Acknowledgement

I would like to express my deepest gratitude to my supervisors Prof. Hong Hao, Dr. Thong M. Pham and Prof. Yifei Hao. Without the help of Prof. Yifei Hao and Prof. Hong Hao, I did not have the chance to study at Curtin University. I thank Dr. Thong M. Pham for providing a highly supportive and inspiring environment. Dr Thong's help extends far beyond the academic aspects of this project.

I would also like to express my sincere thanks to Dr. Xihong Zhang, Dr. Cheng Yuan, Dr. Haoran Zuo, Dr. Zhejian Li, Ms Yuwen Chiu, Mr Zhixing Li, Mr Canjun Li, Mr. Chong Chen and other research colleagues in Prof. Hao's research group for their help, encourage and friendship during my PhD study.

I would also like to thank technicians Ashley Hughes, Darren Isaac and Mark Whittaker for their help and patience in solving all the problems in the civil engineering lab. I cannot finish my degree without their help.

I would also like to thank my friends Ran Yang, Simon Zeng and Wilson for their friendship.

It would not have been possible to write this doctoral thesis without the help and support of my mother Xiangrong Yin, my father Heng Shi, my brother Shi Yin.

Statement of Contribution of Others

The work presented in this dissertation was primarily designed, experimentally executed, analytically evaluated, analysed and written by the first author (Feng Shi) of the individual manuscripts. Contributions by others are described as follows. The signed contribution forms are attached in the appendix.

Chapter 2

Prof. Hong Hao, Dr. Thong M. Pham and Prof. Yifei Hao revised and edited the manuscript, provided intellectual input towards data processing, analysis, and discussion of the results. The financial support was provided by the Australian Research Council Laureate Fellowships FL 180100196.

Chapter 3

Prof. Hong Hao, Dr. Thong M. Pham, A/Prof Rabin Tuladhar and Dr. Shi Yin revised and edited the manuscript, provided intellectual input towards data processing, analysis, and discussion of the results. Dr Shi Yin helped to manufacture modified PP fibres. The financial support was provided by the Australian Research Council Laureate Fellowships FL 180100196.

Chapter 4

Prof. Hong Hao, Dr. Thong M. Pham revised and edited the manuscript, provided intellectual input towards data processing, analysis, and discussion of the results. The financial support was provided by the Australian Research Council Laureate Fellowships FL 180100196.

Chapter 5

Prof. Hong Hao, Dr. Thong M. Pham, A/Prof Rabin Tuladhar and Dr. Shi Yin revised and edited the manuscript, provided intellectual input towards data processing, analysis, and discussion of the results. Prof Deng helped with the experimental setup. The financial support was provided by the Australian Research Council Laureate Fellowships FL 180100196.

Table of Contents

Declaration.....	1
Abstract.....	3
List of Publications	6
Acknowledgement	7
Statement of Contribution of Others.....	8
Table of Contents.....	9
1. Introduction.....	11
1.1 Preamble	11
1.2 Objectives	13
1.3 Research Outline.....	14
Chapter 2. Post-cracking behaviour of basalt and macro polypropylene hybrid fibre-reinforced concrete.....	16
Abstract.....	16
2.1. Introduction.....	16
2.2. Experimental program	19
2.2.1 Concrete mix design and fibre properties	19
2.2.2 Test setup and procedure	22
2.3. Results and discussion	23
2.3.1 Slump of hybrid fibre-reinforced concrete	23
2.3.2 Compressive strength of hybrid fibre-reinforced concrete	26
2.3.3 Flexural performance of hybrid fibre-reinforced concrete	30
2.4. Conclusion	42
Chapter 3. Pullout and flexural performance of silane groups and hydrophilic groups grafted polypropylene fibre-reinforced UHPC	44
Abstract.....	44
3.1. Introduction.....	44
3.2. Experimental investigation	47
3.2.1 Material properties	47
3.2.2 Modification of fibres	49
3.2.3. Characterisation of fibres.....	50
3.2.4. Mechanical properties of fibre-reinforced UHPC.....	51
3.3. Results and discussion	53
3.3.1. Characterisation of PP fibres	53
3.3.2 Pullout performance of fibres	54
3.3.3. Flexural performance of fibre-reinforced UHPC.....	58
3.4. Conclusion	62
Chapter 4. Mechanical properties of hybrid fibre-reinforced concrete under dynamic compression and split tension	63
Abstract.....	63
4.1 Introduction.....	63
4.2. Materials and experimental methods	66
4.2.1 Concrete mix and fibre properties	66
4.2.2. Sample preparation	67
4.2.3. Test methods and equipment details	67
4.3 Results and discussions.....	70

4.3.1. Quasi-static compressive and splitting tensile tests	70
4.3.2. Dynamic compressive strength of plain and hybrid FRC	73
4.3.3. Dynamic splitting tensile strength of plain and hybrid FRC	81
4.4. Conclusion	92
Chapter 5. Experimental study on the performance of ground slabs and beams reinforced with macro polypropylene fibre, steel Fibre and steel mesh	94
Abstract	94
5.1. Introduction.....	94
5.2. Methodology and procedures.....	97
5.2.1 Fibre, steel mesh and concrete mix.....	97
5.2.2 Slab testing configuration	99
5.2.3 Fibre-reinforced concrete material tests	101
5.3. Results and discussion	103
5.3.1 Compressive strength.....	104
5.3.2 Post-cracking behaviour of fibre-reinforced concrete	104
5.3.3 Flexural performance of fibre-reinforced concrete.....	106
5.3.4 Responses of ground slabs	108
5.3.5 Flexural and punching shear strength of ground slab	113
5.4. Conclusion	117
Chapter 6. Conclusions and future work	119
6.1 Main findings	119
6.2 Recommendations for future work	121
Reference	123
Appendix I	132
Appendix II.....	134
Bibliography disclaimer.....	136

1. Introduction

1.1 Preamble

Concrete is one of the most popular construction materials because of the low cost and easily obtained raw materials. Concrete is strong in compression but has a low tensile strength. Besides, concrete is a quasi-brittle material, which means it breaks with small plastic deformation and absorbs relatively little energy during fracture. These weaknesses can be counteracted by the inclusion of reinforcements with higher tensile strength and ductility. The use of embedded steel bars can resist the tensile stresses in the tension side of the beam section. Ductile steel bars provide structural members with adequate ductility, thereby reducing the possibility of sudden brittle failure, which enhances the safety of a structure. Steel reinforced concrete is effective and popular for more than a century while there are still some drawbacks. Due to chloride corrosion of steel, there is a thickness requirement for concrete cover in reinforced concrete [1]. This requirement affects the thickness of steel bar reinforced concrete due to the deep location of steel reinforcements. Therefore, using steel bars for crack control is very difficult, especially surface shrinkage cracks, which may happen both in the early-age and hardened stage. When cracks occur, the tensile stress in concrete is not fully distributed to steel bars until cracks have developed to the depth of reinforcements. Therefore, a reinforced concrete structure often works with relatively large cracks.

To solve these problems, dispersed fibre reinforcement offers another approach to reinforce concrete as stress-transfer bridges. The schematic diagram in Figure 1-1 illustrates the mechanism of crack growth during concrete cracking [2]. Energy can be effectively absorbed during fibre failure (1) and fibre pullout (2) and fibre debonding from the matrix (4). The propagation of crack can be slowed or even restrained due to fibre bridging (3). Besides, fibres can release the stress concentration at tips and redistribute small cracks to other locations in

the cracked matrix (5). The overall effects of fibre reinforcement are cumulative from individual fibres. Thus, fibres are effective in controlling the crack growth, hence preventing both plastic and dry shrinkage cracks [3], improving post-cracking performance and maintain the integrity of concrete after it cracks [4], and converting brittle concrete matrix into a material with ductility and improved crack resistance [5]. The fibre-reinforced method can partially or fully replace steel bars in concrete according to different requirements. Over the past decades, fibre-reinforced concrete has been widely used in various structural and non-structural applications such as ground slabs [6], shotcrete tunnel linings [7] and precast elements [8].

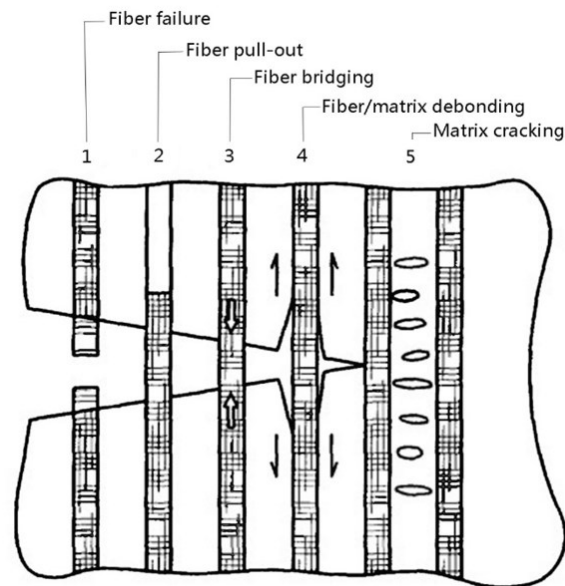


Figure 1-1. Failure mechanisms in fibre-reinforced concrete [2]

In recent years, macro PP fibres have become increasingly popular and widely used in different concrete structures. Macro PP fibres normally have a length between 30-60 mm and a diameter between 0.5-1 mm. Their tensile strength and Young's modulus can reach 700 MPa and 12 GPa, respectively. Randomly distributed fibres can effectively control dry shrinkage by acting as stress-transfer. Also, they can offer comparable post-cracking strength with steel fibres. However, sole macro PP fibres still have some shortcomings. Their low Young's modulus weakens their contribution on the peak compressive and tensile strengths of concrete. This

shortcoming can be overcome by hybridization with other fibres with high Young's modulus to help improve the concrete strength efficiently. Another problem of macro PP fibres is that their hydrophilic surface causes weak bonding at the hydrophobic concrete interface, which limits their application, especially in ultra-high performance concrete (UHPC). In addition, the performance of macro PP fibre-reinforced concrete (PFRC) has not been investigated under dynamic loads. Since concrete is a strain rate sensitive material, it is necessary to investigate the influence of macro PP fibres on the mechanical properties of concrete under dynamic loads. Also the structural performance of macro PFRC as compared to traditional steel-reinforced concrete or steel FRC has not been well investigated. Therefore, this dissertation studied (1) the material properties of hybrid fibre-reinforced concrete under static and dynamic loads, (2) effectiveness of surface modification techniques on enhancing the bonding between fibre and matrix, and (3) structural performance of macro PFRC ground slabs.

1.2 Objectives

The objective of this dissertation is to investigate the material properties of macro polypropylene fibre-reinforced concrete subjected to static and dynamic loading, which can be used to replace traditional steel reinforcements in pavements, shotcrete tunnel linings and precast elements. Concept of hybrid FRC was adopted by using high Young's modulus basalt fibres and macro PP fibres. Influences of fibre volume fractions and concrete grade (C30 and C60) on the slump, compressive strength and flexural capacity were examined. Besides, methods of modifying the fibre surface by grafting silane groups and hydrophilic groups were adopted to improve the bonding strength between PP fibres and concrete. To achieve the objective, the following investigations were carried out:

- The post-cracking behaviour of hybrid FRC under quasi-static loads was investigated by using four-point bending tests. The compressive strength, flexural strength, failure

mode, energy absorption, and post-peak behaviour of hybrid FRC was examined and compared to those of corresponding plain concrete.

- Performance of hybrid FRC under dynamic loadings was studied by using the split Hopkinson bar (SHPB) equipment. Stress-strain curves and failure progress of specimens under dynamic compressive loadings were studied. The crack development and failure pattern of specimens under dynamic splitting tensile loadings were also examined and discussed. Additionally, the empirical relationships between the dynamic increase factor (DIF) and strain rate were proposed for practical use.
- To improve the bonding behaviour of macro PP fibres, different surface treatment techniques were adopted including grafting silane groups and hydrophilic groups. The pull-out tests were then carried out to examine the enhancement of the surface modification techniques.
- To evaluate structural performance, tests of ground slabs reinforced with macro PP fibres and other reinforcing materials were conducted. The applicability of the design procedure for ground slabs with various reinforcement type was also evaluated.

1.3 Research Outline

This dissertation comprises six chapters. The contents of the five chapters following the introduction are presented as follows:

Chapter 2 presents an experimental investigation on the slump, static compressive strength and flexural strength, post-cracking behaviour of concrete reinforced by hybrid fibres and sole fibres. Influences of concrete grade (C30 and C60 concrete), volume fractions of macro PP fibres (0.3%, 0.7% and 1%) and volume fraction of basalt fibres (0.1%) on the mechanical properties of concrete were studied. This chapter aimed to investigate the improvement in the mechanical properties of adding basalt fibres to macro PFRC.

Chapter 3 examined the enhancement of the bonding behaviour of macro PP fibre and concrete matrix when using different surface modification techniques including silane groups and hydrophilic groups grafted macro PP fibres. Fourier transform infrared and water contact angle measurements were used to characterize the results of grafting. Results of single fibre pull-out tests and flexural tests were presented and discussed.

Chapter 4 investigated the dynamic compressive and splitting tensile behaviour of hybrid FRC (1% macro PP fibres + 0.1% basalt fibres and 2% macro PP fibres + 0.1% basalt fibres). The crack development and crack mouth opening displacement (CMOD) on concrete specimens under dynamic loads were evaluated with the help of digital image correlation (DIC) technique. Experimental results including the compressive strain-stress curve, concrete failure modes, dynamic compressive and splitting tensile increase factor were evaluated and discussed.

Chapter 5 presents experimental and analytical analyses of the ground slabs reinforced with macro PP fibres, steel fibres and steel mesh, respectively. Load-strain responses at bottom of slabs, load-deflection response of slab centre and slab deflection profile were studied. The applicability of current design procedure for traditional ground slabs to the tested slabs was evaluated and discussed.

Chapter 6 summarizes the main findings from this dissertation. Suggestions for possible future works are also given in this chapter.

Chapter 2. Post-cracking behaviour of basalt and macro polypropylene hybrid fibre-reinforced concrete

Abstract¹

This chapter experimentally investigated the mechanical properties of basalt-macro PP hybrid fibre-reinforced concrete. Three macro PP fibre volume fractions (0.3%, 0.7% and 1%), two concrete compressive strengths (30 MPa and 60 MPa) and basalt fibre volume fraction 0.1%, were used to study their influences on the slump, compressive strength and flexural capacity of fibre-reinforced concrete. A new failure mode was observed and a new behaviour classification was introduced for hybrid fibre-reinforced concrete. The hybrid fibre-reinforced concrete containing 0.1% basalt fibres and 1% macro PP fibres showed excellent flexural strength, initial post-cracking strength and energy absorption as compared to plain concrete. The fracture energy of concrete had a significant influence on the post-cracking response of fibre-reinforced concrete and thus concrete with different strengths showed distinguished behaviours. Both the C30 and C60 grade concrete showed that using hybrid basalt and macro PP fibres could achieve approximately 10% and 20% improvement of the compressive strength and flexural strength, respectively.

2.1. Introduction

Concrete is one of the most popular construction materials because of the low cost and easily-obtained raw materials. Concrete is strong in compression but has a low tensile strength. Besides, concrete is a quasi-brittle material, which means it breaks with small plastic deformation and absorbs relatively little energy during fracture. These weaknesses can be counteracted by the inclusion of reinforcements with higher tensile strength and ductility. The use of steel bars embedded can resist the tensile stresses in the tension side of the beam section. Ductile steel bars provide structural members with adequate ductility, thereby reducing the

¹ This chapter was extracted from the paper published in *Construction and Building Materials*, but the subsections were modified to follow the flow of the thesis. The full bibliographic citation of the paper is as follows:

Feng Shi, Thong M. Pham, Hong Hao, Yifei Hao. Post-cracking behaviour of basalt and macro polypropylene hybrid fibre reinforced concrete with different compressive strengths. *Construction and Building Materials*, 2020, 262: 120108.

<https://doi.org/10.1016/j.conbuildmat.2020.120108>

possibility of sudden brittle failure, which enhances the safety of a structure. This system is effective and popular for more than a century while there are still some drawbacks. Due to chloride corrosion of steel, there is a thickness requirement for concrete cover in reinforced concrete [9]. This requirement limits the thickness of steel bar reinforced concrete due to the deep location of steel reinforcements. Therefore, using steel bars for crack control purposes is very difficult, especially surface shrinkage cracks, which may happen both in the early-age and hardened stage. When cracks occur, the tensile stress in concrete is not fully distributed to steel bars until cracks have developed to the depth of reinforcements. Therefore, a reinforced concrete structure often works with relatively large cracks.

To solve these problems, dispersed fibre reinforcement offers secondary reinforcement to concrete as stress-transfer bridges [10]. The addition of fibres into concrete matrix can enhance the flexural strength and post-cracking properties of concrete, which improve the ability of concrete to resist cracking. The fibre-reinforced method can partially or fully replace steel bars in concrete according to different requirements. Over the past decades, fibre-reinforced concrete has been widely used in various structural and non-structural applications such as ground slabs [6], shotcrete tunnel linings [7], and precast elements [8].

ACI Committee classifies fibres into steel, glass, synthetic and natural fibres [11]. Steel fibres are the most popular type both in research and practical applications due to their high efficiency. However, steel fibres have problems such as a large reduction of workability, easily rust, and basset [12]. Glass, synthetic and natural fibres also have their shorting comings including low alkaline-resistance [13], relatively low mechanical properties, and uncertainty in long-term performance.

According to size, fibres are classified into two categories: micro fibres and macro fibres. Micro fibres are usually 6 to 20 mm in length and tens of microns in diameter. They have been widely accepted as an effective method for controlling plastic shrinkage. However, since micro fibres are short in size, they offer little structural benefits to concrete if structures enter the large-deformation region. Besides, macro fibres, which are normally 30 to 60 mm long and more than 0.3 mm in diameter, can carry loads and arrest propagation of visible cracks like steel bar reinforcements after concrete matrix breaks.

As can be seen, there is no single type of fibre that can provide all-sided reinforcement on the strength, ductility, and durability. The methods of combining different types and sizes of fibres to provide improvements on multiple properties of fibre-reinforced concrete have been proven

successful [14-16]. In a hybrid fibre-reinforced concrete, micro fibres are used to bridge microcracks and lead to higher first cracking strength and less shrinkage, while macro fibres can arrest the macrocrack propagation, thus improve the toughness and post-cracking performance Figure 2-1. Sivakumar and Santhanam [17] investigated the mechanical properties of high strength concrete reinforced with steel fibres (30 mm) and non-metallic fibres (6-20 mm) including micro PP fibres, polyester fibres, and glass fibres. The results showed that among all hybrid fibre combinations, steel-PP fibres combination performed better than others in all aspects. Qian and Stroeven [18] studied mechanical properties of concrete reinforced with hybrid fibres including micro PP fibres and different types of steel fibres. The results showed that the small size of steel fibres (6 mm) was more effective on improving the compressive strength than the tensile strength of concrete while large ones (30 and 40 mm) mainly improved the post-cracking strength in the hybrid fibre matrix. Besides, the optimum dosage of micro PP fibres in the hybrid fibre matrix was found at approximately 0.15%. Afroughsabet and Ozbakkaloglu [19] mixed steel and PP fibres in concrete and found that steel-PP hybrid fibre-reinforced concrete combined advantages of high cracking strength from steel fibres (60 mm) and improved the post-cracking toughness from PP (12 mm) fibres. Similar findings were also reported in previous studies [20, 21]. These previous studies used macro steel fibres in the hybrid FRC while long macro PP fibres can also be utilised in hybrid FRC to improve the post-peak performance. Hsie, et al. [22] investigated the performance of hybrid FRC, which had 0.1% micro PP fibres (12-25mm) and 0.3-1% macro PP fibres (60 mm). The experimental results showed that the compressive strength, modulus of rupture, and post-cracking strength of hybrid FRC were better than single fibre-reinforced concrete using the same volume fraction of macro PP fibres.

As shown above, the PP-steel hybrid system is effective to improve the comprehensive properties of concrete. Using macro PP fibres is an alternative to steel fibres and it is increasingly becoming popular due to its advantages, such as eco-friendly material, lightweight, high corrosion resistance, and well distribution in concrete. However, macro PP fibre has low Young's modulus, leading to less efficient reinforcement than steel fibres. Besides, due to the large volume of individual macro PP fibre, it has much less number in the same volume of micro fibres, leading to weaker shrinkage control ability.

Basalt fibres are a new type of inorganic micro fibres extruded from melted basalt rock and have been used in many civil engineering projects. They have many advantages, including high Young's modulus, better resistance to chemicals than glass fibres, and better shrinkage control

than micro PP fibres [23]. Therefore, basalt fibres can be a great supplement to macro PP fibres in terms of improving peak flexural strength and post-cracking strength of concrete due to the high Young's modulus of basalt fibres.

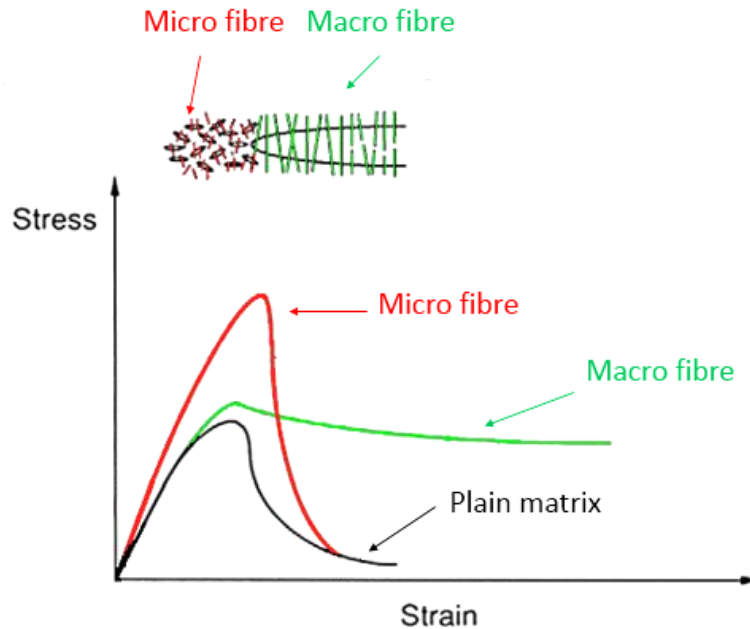


Figure 2-1. Mechanism of different size of fibre reinforcement

This research proposed the method of combination of high Young's modulus micro fibre and low Young's modulus macro fibre as a hybrid fibre reinforcement system. macro PP fibres and basalt fibres were used to improve the concrete properties including both the peak response and post-peak behaviour. Influences of volume fractions of macro PP fibres on the concrete strength and basalt on workability, compressive strength, and flexural performance of concrete were examined and discussed.

2.2. Experimental program

2.2.1 Concrete mix design and fibre properties

This chapter performed on concrete with the target compressive strengths of 30 MPa and 60 MPa. Mix design for 30 MPa and 60 MPa concrete used in this dissertation is showed in Table 2-1. Type 1 Portland cement was used as cementitious materials with specific gravity from 2.5 to 3.2. Silica sand with a specific gravity between 2.0-2.7 was utilised as fine aggregates. Size of 78% of silica sand was between 0.125 mm and 0.25 mm. As suggested in the previous study by Swamy [24], using a relatively small size of coarse aggregates can improve the effectiveness of fibres in concrete. So the maximum size of coarse aggregates was limited to 10 mm. Before

mixing, coarse aggregates were washed to remove clay and silt. In order to minimise the influences of moisture changes of aggregates in different mix batches, all aggregates were in a saturated-surface-dry state before mixing. A pan mixer of 70L capacity was used for all the mixes. Coarse aggregates were placed first in the mixing drum, followed by sand, cement, and fibres. Water was then added until fibres were distributed uniformly. Three minutes of further mixing was considered enough before concrete was poured into moulds. All the samples were vibrated by a machine during the casting until entrapped air bubbles were no longer observed rising to the surface of the specimens. The specimens were demoulded after 24 hours and cured in a 23 °C water storage tank in a curing room until they were tested at 28 days.

Table 2-1. C30 and C60 concrete mix design

Material	C30 (kg/m ³)	C60 (kg/m ³)
Portland cement	338	521
Sand	790	500
Coarse aggregates	1044	1151
Water	230	229

The dimension and shape of the fibres also influence their performance due to various effects. When macro fibres are pulled out from the concrete matrix, damaging and scratching of fibre surface will increase the surface roughness and thus improving the pull-out resistance as reported in the previous study [25]. This phenomenon is more obvious in macro PP fibres due to its low surface hardness. Accordingly, longer macro PP fibres can make more contributions to the post-cracking strength of concrete [26]. Thus, the length of macro PP fibres was chosen as 60 mm for better post-cracking performance. MACRO PP fibres in this research were supplied by BarChip [27]. The purpose of using short fibres is to increase the tensile strength and initial post-cracking strength as well as to provide enough shrinkage control ability. Therefore, basalt fibres with 0.1% volume fraction, 20 mm in length and 21 µm in diameter (RLD=950) were chosen to get better reinforcement results [28]. The properties of the two types of fibres are summarised in Table 2-2.

For each mix design, three identical cylinders for the compressive tests and three beams were tested. In total, 48 cylinders and 48 beam specimens were tested.

Table 2-2. Properties of basalt and macro PP fibre

Fibre type	Diameter (μm)	Length (mm)	Density (kg/m^3)	Tensile strength (MPa)	Elastic modulus (GPa)
Basalt	21	20	2.7	4200	91
Macro PP	580	60	0.9	640	12

Table 2-3 shows the specimen names according to the different compressive strengths of concrete and the corresponding fractions of fibres.

Table 2-3. Specimen names and fibre content

Name	Target compressive strength	Basalt fibre volume fraction	Macro PP fibre volume fraction
C30 Plain	30	0	0
C30B00P03	30	0	0.3%
C30B00P07	30	0	0.7%
C30B00P10	30	0	1%
C30B01P0	30	0.1%	0
C30B01P03	30	0.1%	0.3%
C30B01P07	30	0.1%	0.7%
C30B01P10	30	0.1%	1%
C60 Plain	60	0	0
C60B00P03	60	0	0.3%
C60B00P07	60	0	0.7%
C60B00P10	60	0	1%
C60B01P0	60	0.1%	0
C60B01P03	60	0.1%	0.3%

C60B01P07	60	0.1%	0.7%
C60B01P10	60	0.1%	1%

2.2.2 Test setup and procedure

2.2.2.1 Slump tests

The slump tests were performed according to ASTM C143 [29] to characterise workability of fresh concrete. After sufficient mix, fresh concrete was filled in a cone mould in three equal layers with 25 times rodding in each layer. Then excessive concrete on the top was removed and the cone mould was lifted vertically. The distance between the height of the cone mould and displaced original centre of the top surface of the fresh concrete was measured and defined as slump (see Figure 2-2).

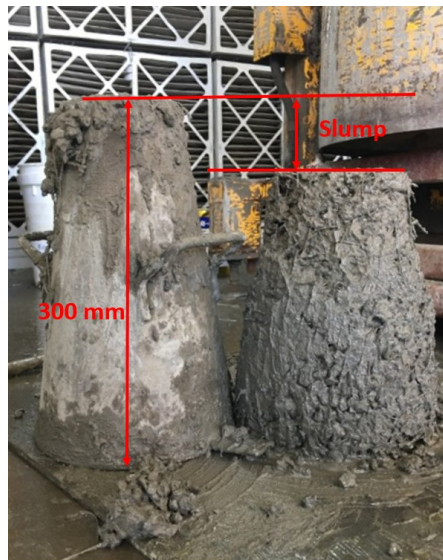


Figure 2-2. Slump test for fresh concrete

2.2.2.2 Compressive tests

A few compressive tests were performed according to ASTM C39 [30] after specimens being cured for 28 days. Large cylinder specimen size (150 mm diameter and 300 mm height) was chosen for better fibre distribution since the maximum fibre length was 58 mm. One day before testing, both ends of the cylinder was capped with sulphur mortar to get flat loading surfaces and constant height for all cylinders. The axial loading was applied at 0.1 MPa/s by a servo-hydraulic material test machine.

2.2.2.3 Flexural tests

The flexural tests were conducted in accordance with ASTM C1609 [31]. The size of beam specimens was 550 mm × 150 mm × 150mm. The span length between supports was 450 mm, which was three times of depth of specimen. The distance of loading points was 150 mm. To avoid stress concentration in the contact surface between specimens and a test machine, a rubber plate was used. A rectangular jig was used to mount linear variable differential transducers (LVDTs), as shown in Figure 2-3. Two LVDTs were installed at both sides of the rectangular jig to measure the vertical displacement. The purpose of using rectangular jig was to ensure accurate measurement of the mid-span deflection and minimises errors due to concrete specimen twisting during tests [32]. The load was applied at a rate at 0.1 mm/min up to mid-span deflection of 0.5 mm and increased to 0.2 mm/min until failure by using Instron testing machine.

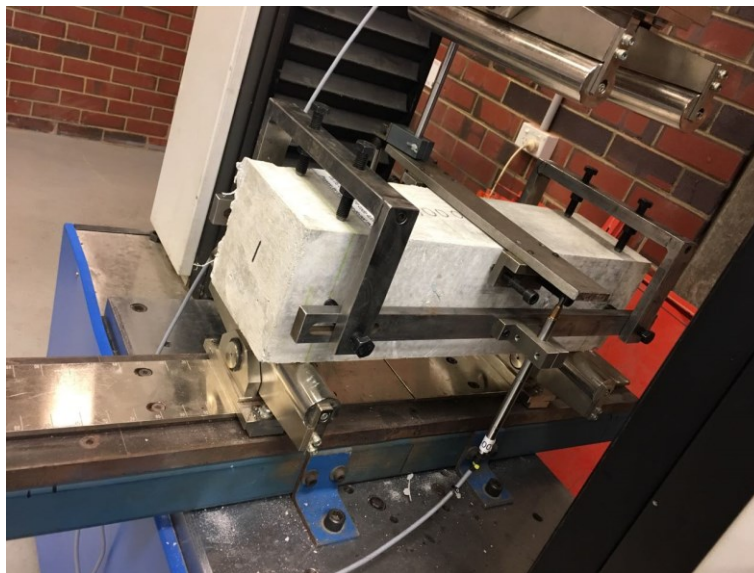


Figure 2-3. Experimental set up of a flexural test

2.3. Results and discussion

2.3.1 Slump of hybrid fibre-reinforced concrete

Figure 2-4 shows the slump result of concrete with different fibre types and volume fractions. In order to achieve good workability after adding fibres, water/cement ratio of C30 and C60 concrete was designed to be relatively high (0.68 and 0.44, respectively) and kept constant when the fibre volume fraction was changed. Due to different water/cement ratio and mix design, the influence of fibres on C30 and C60 was quite similar. The slump of these mixes

decreased about 110 mm and 12 mm by adding 1% macro PP fibres and 0.1% basalt fibres, respectively. Compared with results from previous studies as presented in Table 2-4, it can be seen that 1% macro PP fibres normally reduce about 60 mm in the slump with the help of superplasticiser while the slump reduction after adding 0.1% basalt fibres is usually approximately 13 mm. Test results of this dissertation were slightly lower than other researchers' results given in Table 2-4 because no plasticiser was used in these mixes. Accordingly, greater slump reduction for these mixes would be expected if superplasticiser was used. The experimental results have shown that slump decreased approximately 36 mm corresponding to every addition of 0.3% macro PP fibre in volume fraction in both the C30 and C60 concrete. When it came to the influence of hybrid fibres, the average reduction in the slump increased to 44 mm. Based on test results, empirical equations were proposed to predict the slumps with consideration of fibre volume fraction. They are given as:

For C30 FRC,

$$Slump = \begin{cases} Slump_{(0)} - 111 \times VF_P & \text{For FRC with macro PP fibres} \\ Slump_{(0)} - 100 \times VF_B & \text{For FRC with basalt fibres} \\ Slump_{(0)} - 100 \times VF_B - 111 \times VF_P & \text{For FRC with hybrid fibres} \end{cases} \quad (2-1)$$

For C60 FRC,

$$Slump = \begin{cases} Slump_{(0)} - 102 \times VF_P & \text{For FRC with macro PP fibres} \\ Slump_{(0)} - 130 \times VF_B & \text{For FRC with basalt fibres} \\ Slump_{(0)} - 130 \times VF_B - 129 \times VF_P & \text{For FRC with hybrid fibres} \end{cases} \quad (2-2)$$

where $Slump_{(0)}$ is the slump of plain concrete in mm, VF_P is macro PP fibre volume fraction and VF_B is basalt fibre volume fraction.

Table 2-4. Summary of the concrete slump from previous studies

Authors	Fibre type	Fibre dimension	Fibre volumetric content (%)	Slump (mm)	Compressive strength (MPa)
Iyer [33]	Basalt	12 mm in length	0	200	31.0
	fibre	16 mm in diameter	0.15%	180	36.0
Jiang [34]	Basalt	22 mm in length	0	185	45.1
	fibre	20 μ m in diameter	0.05%	170	47.0

			0.1%	155	47.7
Babafemi [35]	Macro		0	160	43.8
	PP fibre	40 mm in length 0.8 mm in diameter	1%	100	40.2
Yin [36]	Macro		0	102	35.0
	PP fibre	50 mm in length 0.9 mm in diameter	1	38	35.4
			1.5	6.5	30.7

It can be seen from Figure 2-4 that the low volume fraction of basalt fibres (0.1%) had a little influence on the slump while macro PP fibres had an obvious influence on the slump value of both the C30 and C60 concrete. The effect of macro PP fibres on slump became more significant when 0.1% basalt fibres were further added to the mixes. Basalt and macro PP fibres decreased slump value through the influence of different particle sizes of concrete. Macro PP fibres could form a network structure in fresh concrete, increase the difficulty of relative movement of coarse aggregates and therefore reduce the mobility of the mixture. Compared with macro PP fibres, basalt fibres had nearly no influence on the movement of coarse aggregates due to their low flexural force, but the much larger surface area of basalt fibres can easily absorb cement paste to wrap around and largely increase the viscosity of mortar even in low volume fractions, thus reducing slump of concrete. Due to different mechanisms and interaction, when basalt and macro PP fibres were used together, the total level of slump reduction would be more than simply summing the decrease in the slump of these two individual types of fibres. Accordingly, with the increase of volume fraction of macro PP fibres, the slump difference between hybrid fibre FRC and macro PFRC would also become more significant. Therefore, different methods such as introducing super plasticiser, adjusting grading of aggregate could be used to minimise the influence of basalt -macro PP hybrid fibres to the slump.

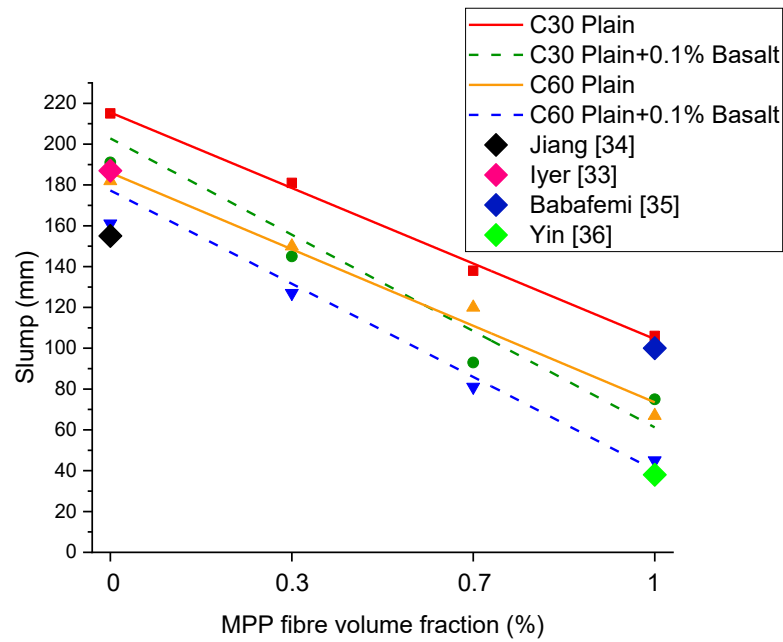


Figure 2-4. Effect of fibre volume fraction on the slump of concretes with different compressive strengths

2.3.2 Compressive strength of hybrid fibre-reinforced concrete

According to ASTM C39 standard [30], there are four types of well-defined fracture patterns under the compression test as described in Figure 2-5. Through the tests, all these four types of fracture patterns were observed in Figure 2-6. Among these four types, plain and basalt FRC showed more fracture in pattern 1 and pattern 2, while macro PFRC and hybrid FRC were more likely to fracture in pattern 3 and pattern 4. Due to the unavoidable friction between the concrete and the steel plates, specimen fracture with core segments (type 1 and type 2) was more likely to be observed during the tests. Apart from these four fracture patterns, the new one was also observed in macro PFRC. The newly observed fibre-reinforced concrete fracture pattern was illustrated in Figure 2-7. When plain concrete and 0.1% basalt fibre-reinforced concrete reached their maximum compressive strength, they broke into segments suddenly with a loud sound. On the other hand, macro PP fibre-reinforced concrete still remained relatively intact, namely bulging failure, after fracture with a small sound. This bulging failure showed damage of concrete at the mid-height while concrete at the two ends still intact and in an undamaged condition. Although only limited improvement of compressive strength macro PP fibres can provide, it would play a more important role in the post-cracking part and prevent complete brittle concrete fracture.

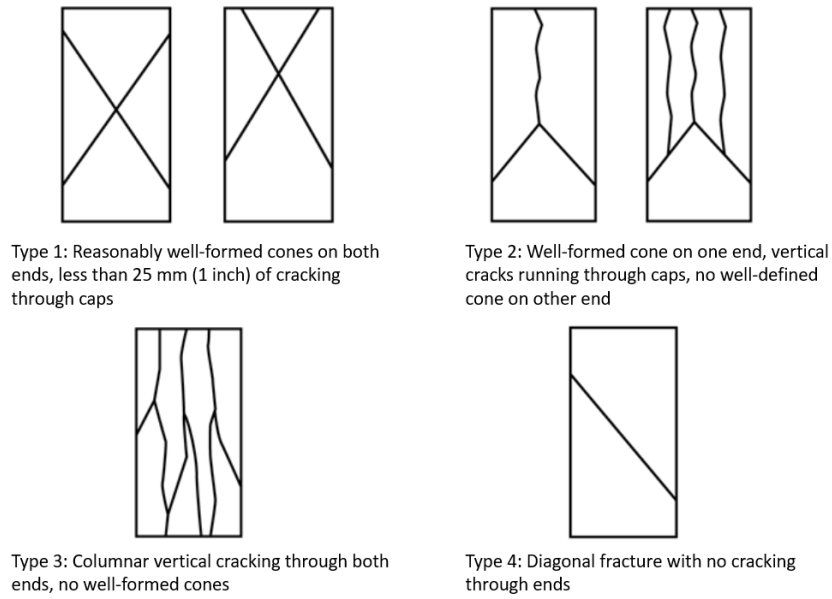


Figure 2-5. Schematic of typical well-defined fracture patterns [30]

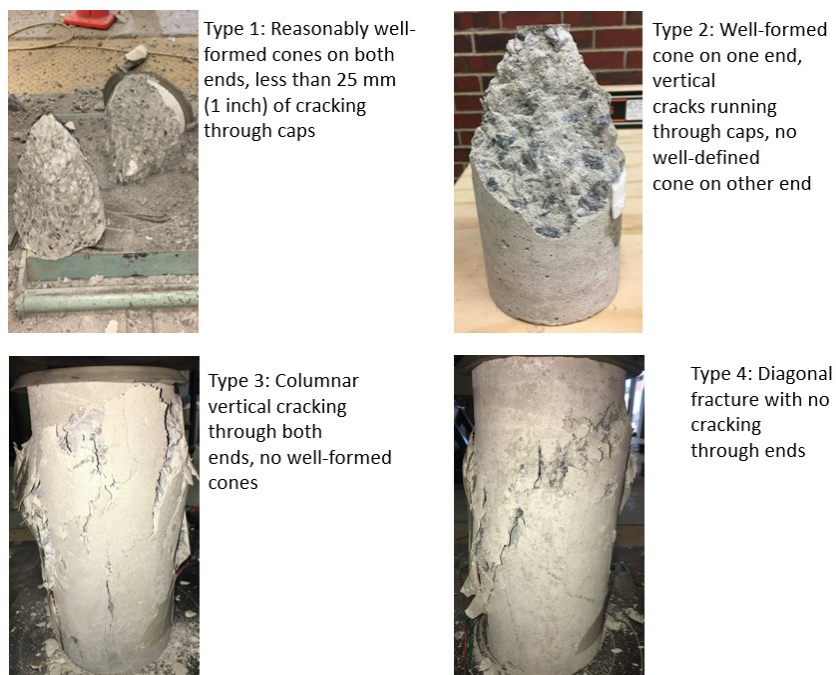


Figure 2-6. Representative fracture patterns from this test

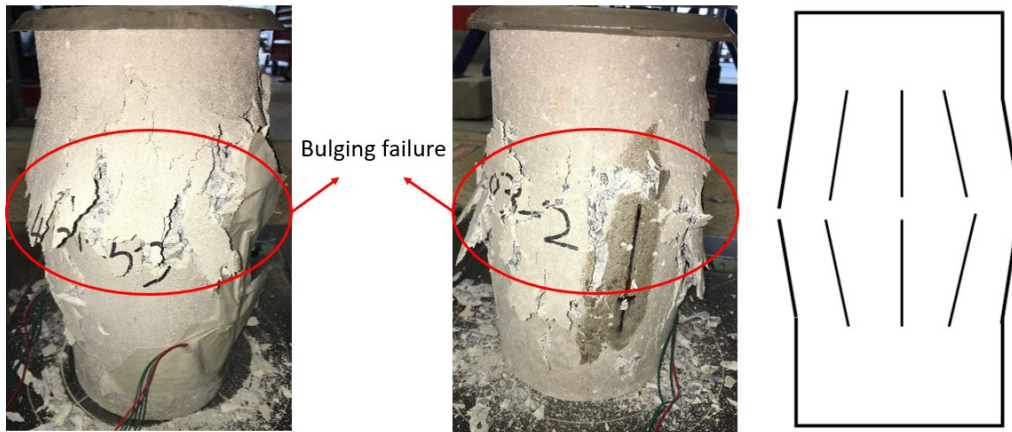


Figure 2-7. Observed typical macro fibre-reinforced concrete fracture pattern

Figure 2-8 shows the compressive strength of hybrid fibre-reinforced concrete. There are four groups in Figure 2-8 according to the contents of macro PP fibres. It could be found that basalt fibre could increase compressive strength effectively in both C30 and C60 concrete. Adding solely macro PP fibres to C30 plain concrete at 0.3%, 0.7% and 1% in volume fraction increased the compressive strength by 9.8%, 5.8% and 5.8%, respectively. After 0.1% of basalt fibres were used solely to reinforce C30 concrete, its compressive strength increased by 11.4% from 30.6 MPa to 34.1 MPa. When combining 0.1% basalt fibres with macro PP fibres at 0.3%, 0.7%, and 1% for reinforcement in C30 concrete matrix, the increment of the compressive strength ranges from 9.5% to 12.7% as compared to 30.6 MPa of C30 plain concrete. These results indicate that combining 0.1% basalt fibres with macro PP fibres do not necessarily lead to higher compressive strength as compared to the case with 0.1% basalt fibre reinforcement only. Similarly, the compressive strength of C60 concrete reinforced with 0.1% basalt fibre was 11% higher than the plain concrete. Those with macro PP fibre reinforcement only of C60 concrete were 5.5% to 7.9% higher than plain C60 concrete (57.8 MPa and 59.1 MPa versus 54.8 MPa). When using hybrid fibre to reinforce C60 concrete, the compressive strength increased by 9.1% to 11.0% compared with plain C60 concrete (59.8 MPa and 60.8 MPa versus 54.8 MPa), but the increment in the compressive strength was not necessarily higher than that with 0.1% basalt fibre reinforcement only. The Young's moduli of C30 and C60 were 29.6 GPa and 34.2 GPa, respectively. Due to marginal effects of fibres on Young's modulus of concrete, the influence of different fibre volume fraction on the Young's modulus of concrete is not discussed in this chapter.

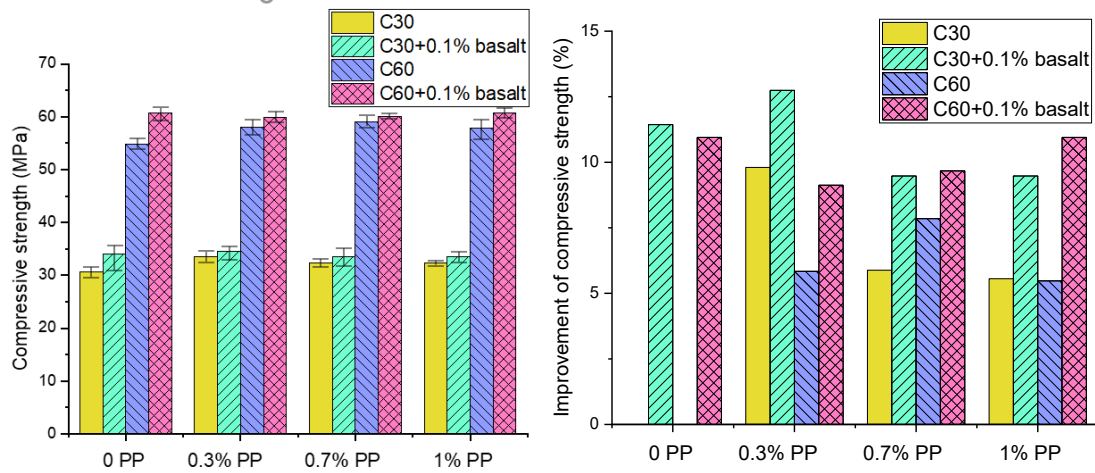


Figure 2-8. Compressive strength of plain and fibre-reinforced concrete

As can be seen, the addition of both the two types of fibres could improve the compressive strength of FRC. This is because concrete cylinder specimens developed lateral expansion and gradually generated micro cracks in the weakest zone with increasing compression loads. When these cracks reached fibres, fibres began to be stretched and even debonded at fibre-matrix interfaces. These processes reduced crack-tip stress concentration by fibre acting as stress-transfer bridges. As a result, local crack propagation was slowed or even blocked. Therefore, there would be less sudden collapse due to stress concentration in fibre-reinforced concrete. As a result, more evenly distributed lateral expansion in the middle region could be achieved. So from the perspective of relief stress concentration in concrete, adding fibres could slightly improve the compressive strength of concrete. On the other hand, the number of fibres and relative Young's modulus to concrete also affect their performance on the compressive strength of concrete. Fibres with higher Young's modulus than concrete will sustain more stress during compression deformation. Therefore, basalt fibres also can improve the compressive strength of concrete through their high Young's modulus while macro PP fibres only have little influence due to low Young's modulus. Besides, the compressive strength of basalt fibre concrete topped that of macro PP fibre concrete. This phenomenon stemmed from that basalt fibre had higher tensile strength and Young's modulus and the number of fibres than macro PP fibre, which resulted in more tensile stresses being transferred from the matrix to fibres. However, the combination of both types of fibres did not always lead to higher compressive strength than sole basalt fibres. The compressive strength of hybrid fibre-reinforced concrete is basically the same with basalt fibre-reinforced concrete.

2.3.3 Flexural performance of hybrid fibre-reinforced concrete

Flexural tests are usually utilised to characterise the flexural behaviour of FRC. Traditionally, the two distinctive responses in a simply supported beam in flexural performance tests include (1) deflection-hardening or (2) deflection-softening. If fibre-reinforced concrete can carry higher loads after first cracking, it is commonly known as deflection hardening and the other is known as deflection softening. However, this classification only focuses on whether the first peak strength is the highest point during the whole test while the different trends after cracking cannot be distinguished as observed in this dissertation. Therefore, combined with results of different fibre types and dosage, the new classification is proposed to distinguish the trend of fibre-reinforced concrete. There are four types of responses according to relative values of the first-peak stress, second-peak stress, and initial post-cracking stress as shown in Figure 2-9. Type 1 is often found in Engineered Cementitious Composite (ECC) or ultra-high strength concrete (UHPC) with multiple cracks after concrete matrix cracking. In Type 2, after matrix cracking, there is a sudden drop of load, but the applied load will increase and overtake the first-peak load. The typical response of a high volume fraction of steel fibre-reinforced concrete belongs to type 2. If volume fraction of fibres is low or Young's modulus of fibres is not high enough, its response in load-deflection will fall into Type 3 or Type 4. The difference between Type 3 and Type 4 is that there is still an increase in load after an initial post-cracking deflection in Type 3 while the load remains flat or continues to decrease in Type 4. In this dissertation, Type 3 and Type 4 were observed in different groups of FRC. In order to distinguish them, the term deflection-increase was used to describe the load increment after cracking in Type 3.

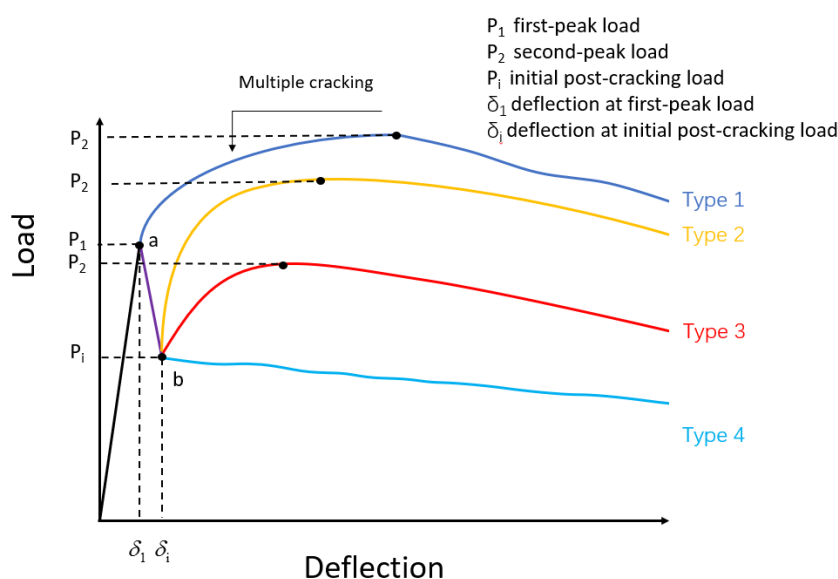


Figure 2-9. Load-deflection curves of different fibre-reinforced concrete

2.3.3.1 Peak load

In the region prior to cracking, load and deflection showed a linear elastic behaviour. The first-peak load is defined as the first point on the load-deflection curve where the slope is zero in ASTM C1609 standard [31]. In this chapter, the first peak load coincides with the maximum load while the maximum load by the bridging effect of fibres in the post-cracking region could not overtake the first peak load.

The peak stress was calculated from the peak load according to the following equation:

$$f = \frac{PL}{bd^2} \quad (2-3)$$

where f is peak strength in MPa, P is peak load in N, L is the span length of specimens in mm, which is 450 mm in this case, and b and d are the width and depth of specimens in mm respectively, which are both 150 mm.

Table 2-5. Flexural experimental results

Specimen	Peak load (kN)	Peak stress (MPa)	Peak stress Improvement (%)	Initial post-cracking load (kN)	Initial post-cracking deflection (mm)	f^D_{600} (MPa)	f^D_{300} (MPa)	f^D_{150} (MPa)
C30 Plain	23.17	3.09	-	-	-	-	-	-
C30B0P03	22.08	2.94	-4.7	6.4	0.85	6.44	6.99	6.00
C30B0P07	25.78	3.44	11.3	10.5	0.62	10.67	12.14	10.90
C30B00P10	25.54	3.4	10.2	16.2	0.48	17.29	18.47	13.95
C30B01P00	23.96	3.19	3.4	-	-	-	-	-
C30B01P03	24.39	3.25	5.3	9.0	0.63	9.06	10.04	9.01
C30B01P07	28.36	3.78	22.4	12.9	0.51	13.59	15.97	15.26
C30B01P10	27.70	3.69	19.6	18.54	0.35	21.34	23.66	19.18
C60 Plain	28.40	3.79	-	-	-	-	-	-
C60B00P03	26.10	3.48	-8.1	6.4	0.73	6.42	6.25	2.62
C60B00P07	30.81	4.11	8.5	12.5	0.66	12.39	13.29	9.54
C60B00P10	32.39	4.32	14.0	21.2	0.38	23.89	28.07	21.22
C60B01P0	29.87	3.98	5.2	-	-	-	-	-
C60B01P03	27.89	3.72	-1.8	7.4	0.69	7.47	8.35	4.42
C60B01P07	34.35	4.58	21.0	16.3	0.57	16.63	18.80	13.50
C60B01P10	35.99	4.80	26.7	23.4	0.35	26.27	31.47	27.08

Table 2-5 and Figure 2-10 show the mean peak stresses of all the specimens. Compared with plain concrete, the peak stress of C30 concrete reinforced by 0.3% macro PP decreased 4.7% from 3.09 MPa to 2.94 MPa. After increasing the volume fraction of macro PP fibre to 0.7% and 1%, the peak stress of C30 concrete improved by 11.3% and 10.2%, respectively. The tendency was similar for C60 concrete. With an increase of macro PP fibre contents from 0.3%

to 1%, the peak stress of FRC initially decreased to 91.9% of plain concrete and then increased to 108.5% and 114% of C60 plain concrete from 3.79 MPa, respectively. It can be concluded that the low content of macro PP fibres did not improve the peak stress but even reduced the peak stress in the flexural tests. When the volume fraction of macro PP fibres increased to more than 0.7%, the peak stress of FRC was about 10% higher than plain concrete. In contrast, basalt reinforced concrete had higher peak stress than plain concrete by 3.4% to 5.2% with 0.1% fibre contents. In general, the use of lower volume fraction (approximately 0.3%) of macro PP fibres did not enhance but even reduce the peak stress. This finding is reasonable since a low content of the macro PP fibres did not help to improve the first peak response due to negative effects caused by lacunas or holes, as also observed in a previous study [37].

For hybrid fibre-reinforced concrete, it could be observed that all the hybrid fibre had better performance than corresponding macro PP solely reinforced ones. The C30B01P07 batch produced the highest peak stress of 3.78 MPa. After continuing to increase the content of macro PP to 1%, the peak stress of hybrid reinforced C30 concrete reduced slightly to 3.69 MPa. It is again caused by the negative effect by lacunas or holes mentioned previously together with the less efficiency of macro fibre in improving the peak behaviour. For C60 hybrid reinforced concrete, with increasing of macro PP fibres from 0.3% to 0.7 and 1% in hybrid FRC, the stress firstly decreased to 3.72 MPa and then increased to 4.58 MPa and 4.53 MPa, respectively.

In general, the addition of macro PP fibres showed a marginal influence on the peak stress in four-point flexural tests due to its mechanical properties and the smaller number of fibres. Similar to the influences in the compression tests, macro PP with low Young's modulus only can bear little stress from concrete matrix before concrete cracks. Low content of macro PP such as 0.3% even reduced the peak stress by 4.7%-8.1%. Because there were not enough fibres to make a positive effect on the peak stress while lacunas or holes induced by macro PP fibres might lead to lower peak stresses. Using 0.7% to 1% volume fraction of macro PP fibres could improve about 10% of the peak stress. This is because it can provide a sufficient bridging effect with the concrete matrix. Through transferring stress in stress concentration parts, higher stress could be achieved when concrete breaks in the flexural tests. However, it could be found that the further increase of macro PP fibres from 0.7% to 1% only offer limited improvement to the peak stress. Meanwhile, with the addition of a low amount of short basalt fibres, the enhancement effect of fibre on the peak stress could be further improved. Approximately 20% improvement of peak stress was found by using 0.7% to 1% volume fraction of macro PP fibres accompanied with 0.1% basalt fibres. Through micro and macro hybrid fibre reinforcements,

higher stress can be transferred from concrete interfaces to fibres and consequently a higher load can be resisted before failure. Reduction of the peak stress due to fibre addition, such as C30B00P3, C60B00P3, and C60B01P3 can be attributed to non-uniform distribution of fibres, lacunas or holes in concrete as also reported in the previous study [37].

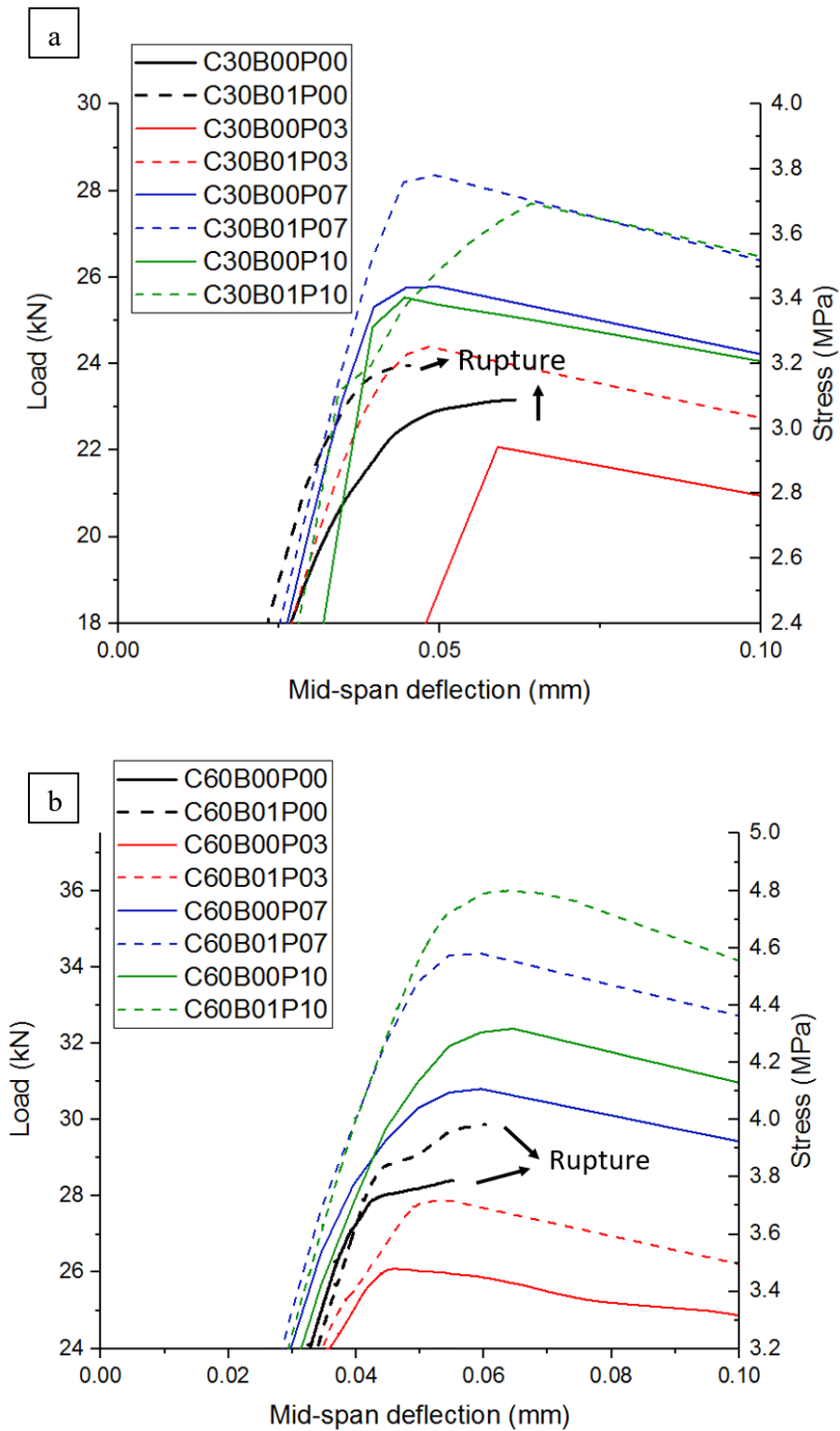


Figure 2-10. Peak stress in (a) C30 concrete, (b) C60 concrete

2.3.3.2 Load-deflection relationships

The loading-deflection curves obtained from the flexural tests of fibre-reinforced concrete samples with the compressive strengths of 30 and 60 MPa are shown in Figure 2-11. The deflection was derived as the average from the two LVDTs fixed to the testing frame.

After concrete specimens cracked, the applied load had dropped suddenly from point a to point b, shown in Figure 2-9. The corresponding load and deflection are called the initial post-cracking load and the initial post-cracking deflection in this chapter. The experimental results have shown that both the initial post-cracking load and the initial post-cracking deflection were influenced by the fibre volume fraction and compressive strength of the concrete matrix. The higher macro PP fibre volume fraction, the higher initial post-cracking load that specimen can bear. It can be seen from Figure 2-11 and Table 2-5, with the increase of macro PP fibre volume fraction (0.3%, 0.7% and 1%), the initial cracking load increased from 6.4 to 10.5 and reached 16.2 kN in C30 macro PP fibre-reinforced concrete, from 6.4 to 12.5 and reached 21.2 kN in C60 macro PP fibre-reinforced concrete, respectively. High strength concrete matrix exhibited a greater degree of improvement in the initial cracking load with an increase of macro PP fibre content. Meanwhile, the initial post-cracking deflection became smaller with the increase of volume fraction of macro PP fibre. Unlike its influence on load, the compressive strength of concrete had little influence on the initial post-cracking deflection. Besides, the addition of basalt fibres could improve the initial post-cracking load and reduce the initial post-cracking deflection more efficiently due to its high Young's modulus, which made them efficient with microcracks.

The addition of macro PP fibres exhibited very effectively in improving the post-peak behaviour. Overall, the higher the macro PP fibre content, the higher the residual stress. Subsequently, with an increase of deflection, trends of post-cracking of concrete with different matrix strengths and fibre contents were different. After the first peak, the applied load of C30B00P03 remained horizontal up to deflection of 3 mm while the applied load of C30B07P10 and C30B00P10 exhibited a slight increase. Due to low Young's modulus of macro PP fibres, a slight increase of the applied load could be observed only when a relatively high volume fraction macro PP fibres were added. Apart from increasing the post-cracking strength, the addition of basalt fibres made the trend of increase of the applied load of C30 reinforced with 0.7% or 1% macro PP fibre more obviously. The influence of the macro PP fibre content on C60 concrete was more distinguished. With increasing of the macro PP content,

the trend of post-cracking stress changed from flat to rapidly increase until a deflection of 1.5 mm. After deflection of about 1.5 mm, all C60 concrete specimens showed a decreasing trend.

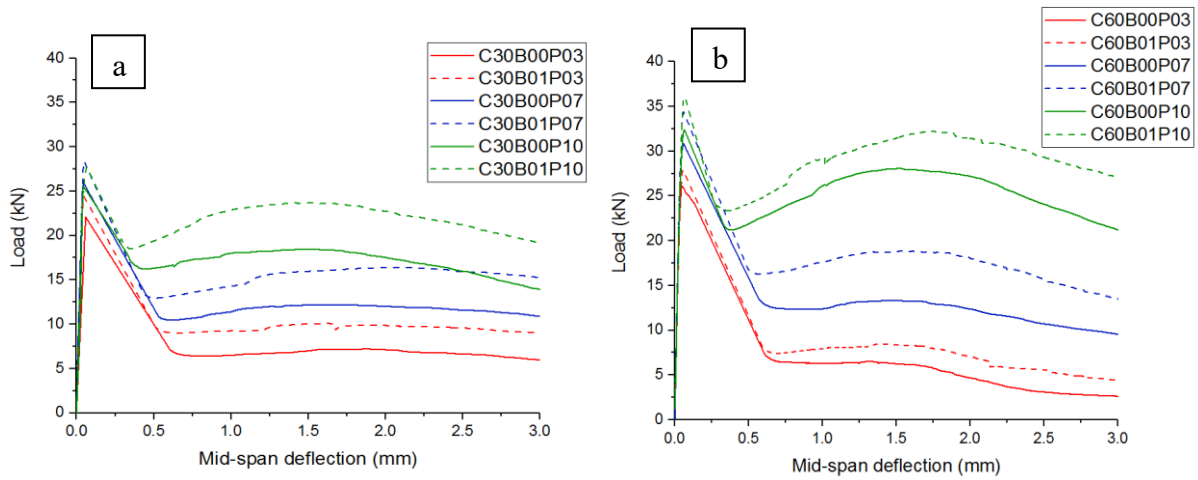


Figure 2-11. Load-deflection curves for (a) C30 concrete, (b) C60 concrete

Figure 2-12 shows the fracture surface of a typical macro PP fibre-reinforced concrete beam. On the fracture surface, there were two types of remaining fibres in concrete. Nearly all the macro PP fibres fractured, which indicated excellent bonding of fibres with the concrete matrix. Good reinforcement had been achieved because the tensile capacity of fractured fibres was fully utilised. Among fractured fibres, most fibres went through abrasion-rupture procedures, which had been proven in fibre pull-out tests [38]. These procedures showed how adequate properties of macro PP fibres including soft hardness and high elongation at break helped to improve the reinforcing efficiency. There were also some macro PP fibres being pulled out. It could be seen that there were some pieces of concrete debris on pulled-out macro PP fibres. Due to special surface scotch, bonding between macro PP fibres and concrete sometimes was even stronger than the interfacial transition zone of concrete and aggregates.

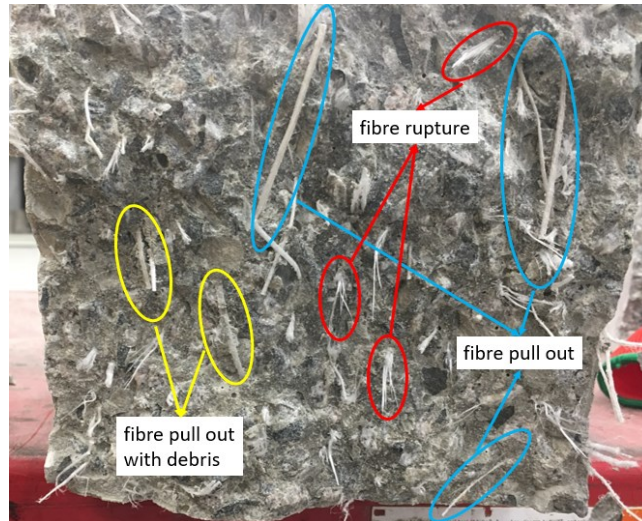


Figure 2-12. The fracture surface of a typical macro PP fibre-reinforced concrete beam

2.3.3.3 Residual stress

Before cracks occur in concrete, concrete matrix primarily resists loads while the role of fibres is limited. After concrete cracks, fibres mixed in concrete could impede the propagation of tensile cracks by the bridging effect. One common way to evaluate the effect of fibre on the flexural strength is based on the residual strength, which is also referred as the post-cracking strength. ASTM C1609 Standards [31] suggest two indices f^D_{600} and f^D_{150} to evaluate the residual strength of fibre-reinforced concrete. f^D_{600} and f^D_{150} refer stress at the deflection of $L/600$ (0.75 mm) and $L/150$ (3 mm), respectively. f^D_{600} reflects the capacity of fibre-reinforced concrete in the initial cracking stage while f^D_{150} can be defined as the residual strength at the allowable maximum deflection of concrete in practice. However, stress at these two deflection points cannot fully represent the post-cracking characteristics of FRC, especially for deflection-increase types as observed above. Based on the observations in this dissertation, an additional parameter, f^D_{300} , is proposed to quantify the stress at the deflection of $L/300$ (1.5 mm) between f^D_{600} and f^D_{150} . Deflection of 0.75 mm can be regarded as an early stage in the post-cracking response of FRC.

In sole macro PP fibre-reinforced concrete (0.3% macro PP), the residual stress f^D_{600} was the same for C30 and C60 FRC, which indicated C60 FRC exhibited greater stress reduction than that of C30 FRC (Figure 2-13). The residual stress f^D_{600} was more sensitive to the increase of macro PP fibre volume fraction in C60 FRC than in C30 FRC. For the macro PP fibre volume fraction of 1%, the residual stress f^D_{600} of C60 FRC was 1.4 times higher than C30 FRC. When the fibre volume fraction was smaller than or equal to 0.7%, after the initial peak stress, the

stress reduction of C60 FRC was more significant than that of C30 FRC due to its greater fracture energy. When specimens fractured, more energy was released in high strength concrete, thus lower residual stress in hybrid FRC with the volume fraction of 0.3% and 0.7% was observed. When the volume fraction of macro PP fibres increased to 1%, the influence of fibres would be greater than the influence of energy release from the concrete of different strengths. Therefore, with the increase of volume fraction of macro PP fibres, the residual stress of C60 overtook that of C30 concrete.

The residual stress f^D_{300} (deflection at 1.5 mm) was the highest in the post-cracking stage of FRC in this dissertation. When the fibre volume of macro PP was 0.3% or 0.7%, the difference in the residual stress f^D_{300} between C30 and C60 FRC was marginal (less than 0.5 MPa). However, residual stress f^D_{300} of C60 FRC with 1% macro PP fibres was much higher (more than 1 MPa) than that of C30 FRC. This means deflection-increase phenomenon becomes more distinctive in C60 than C30 with the increase of macro PP fibre content. This is because the bond between macro PP fibres and concrete with higher compressive strength is stronger, thus more stress can be transferred from the concrete matrix to macro PP fibres.

After reaching the peak value in the post-cracking stage, the residual stress of C60 FRC decreased faster than that of C30 FRC. So the residual stress f^D_{150} of C60 FRC was lower than that of C30 FRC when the volume fraction of macro PP was less than 1%. However, the residual stress of C60 FRC with 1% macro PP is higher than the corresponding of C30 FRC because the effect of fibre is more prominent when the fibre volume fraction is large (i.e. 1%). In conclusion, the improvement of the residual stress from basalt fibres in hybrid fibre-reinforced concrete increased with the increase of the volume fraction of macro PP fibres. Due to more energy was released during specimen fracture in C60 concrete, the residual stress of C60 FRC was lower than that of C30 in the low volume fraction of 0.3% macro PP. This problem could be solved by increasing macro PP volume fraction to 0.7% and 1% as shown in Figure 2-13.

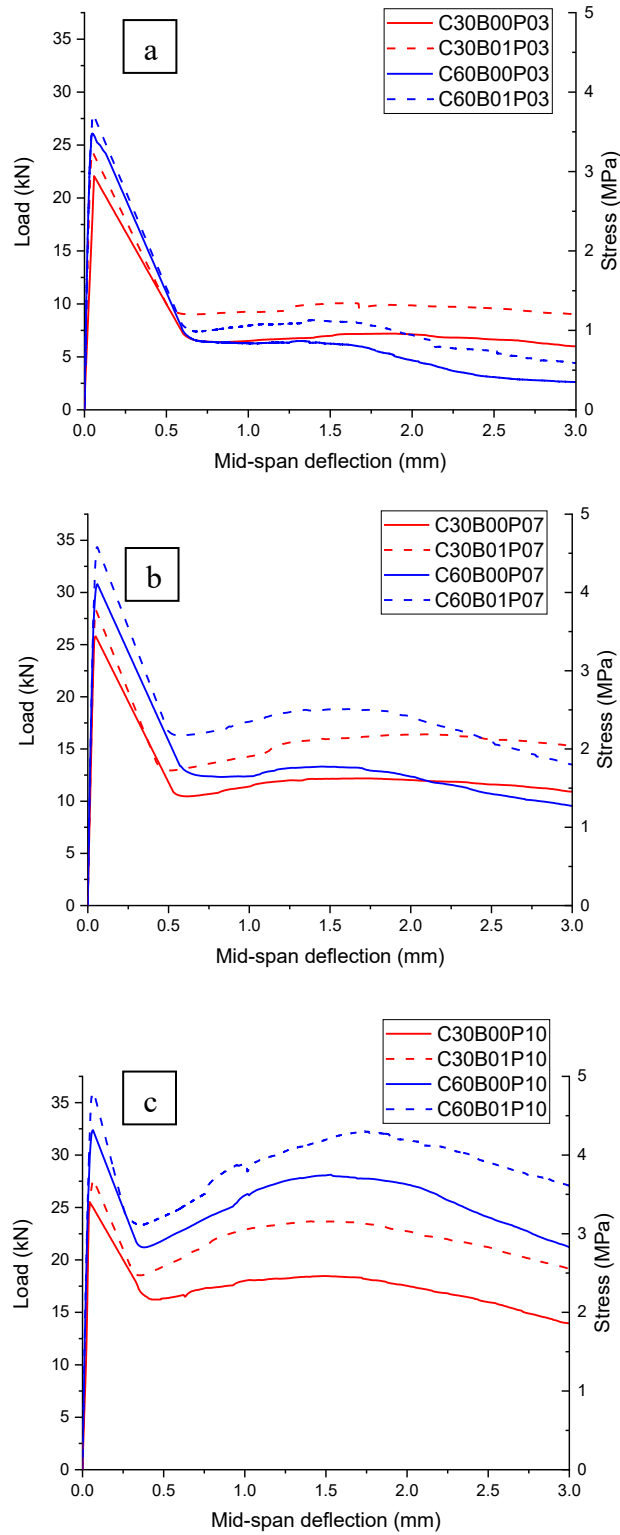
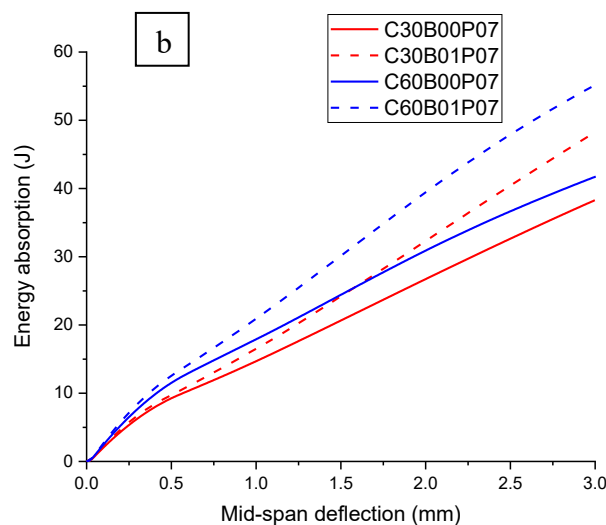
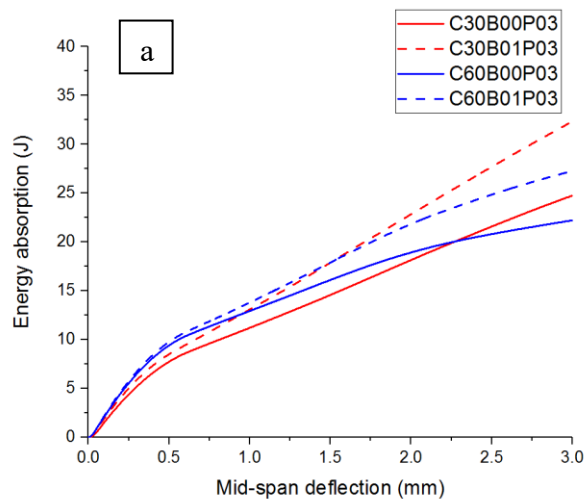


Figure 2-13. Load-deflection curves of specimens with various macro PP volume fractions (a)0.3%, (b)0.7%, and (c)1%

2.3.3.4 Flexural toughness

Flexural toughness represents the energy absorption capacity of fibre-reinforced concrete. It is defined as the enclosed area under the load-deflection curve up to net deflection at 1/150 of the span length, which corresponds to 3 mm for 450 mm span used in this dissertation.

The energy absorption of unreinforced and sole basalt fibre-reinforced concrete beams of different compressive strength was less than 2 J because they cracked at about 0.05 mm and exhibited no post-cracking stress. Figure 2-14 shows the relationship between the energy absorption and deflection of the specimens. In all the figures, it could be found that hybrid fibre-reinforced concrete beams possessed higher energy absorption than the corresponding macro PP fibre-reinforced ones. However, there were also some differences in concrete reinforced by different macro PP fibre volume fractions.



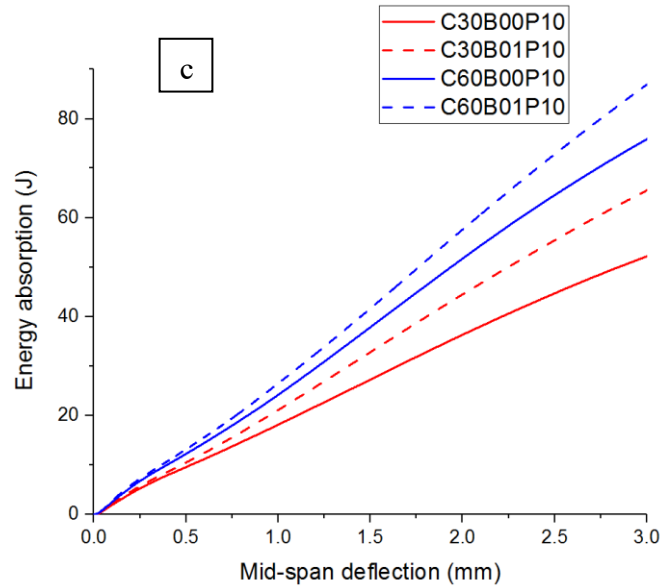


Figure 2-14. Energy absorption capacity-deflection curve for macro PP fibre volume fraction of (a)0.3%, (b)0.7%, and (c)1%

As shown in Figure 2-14(a), with 0.3% macro PP fibre, there was an inflection point at 0.5 mm for all the groups. After this point, the growth of each group became slower, especially for C60 FRC. Hybrid fibre-reinforced beams had higher total energy absorption than the corresponding macro PP sole fibre-reinforced concrete at 3 mm deflection. It also can be concluded that the energy absorption was more sensitive to the addition of basalt fibres than the compressive strength, i.e. the energy absorption of C30B01P03 was higher than that of C60B00P03 after the deflection of about 1 mm. The C60 FRC beams reinforced with 0.3% macro PP fibres absorbed less energy than the C30 FRC beams reinforced only with 0.3% macro PP fibres at 3 mm deflection. This phenomenon was due to higher fracture energy of high strength concrete and less effectiveness of low volume fraction of macro PP fibres as mentioned previously.

The energy absorption capacity of concrete reinforced by 1% macro PP fibre outperforms other mixes as shown in Figure 2-14(c). The energy absorption increased near linearly with deflection. Different from other groups, the energy absorption was more sensitive to the concrete matrix strength than the existence of basalt fibres, i.e. the energy absorption of C30B01P10 was lower than that of C60B00P10 due to the better bond effectiveness between macro PP fibres and high strength concrete matrix.

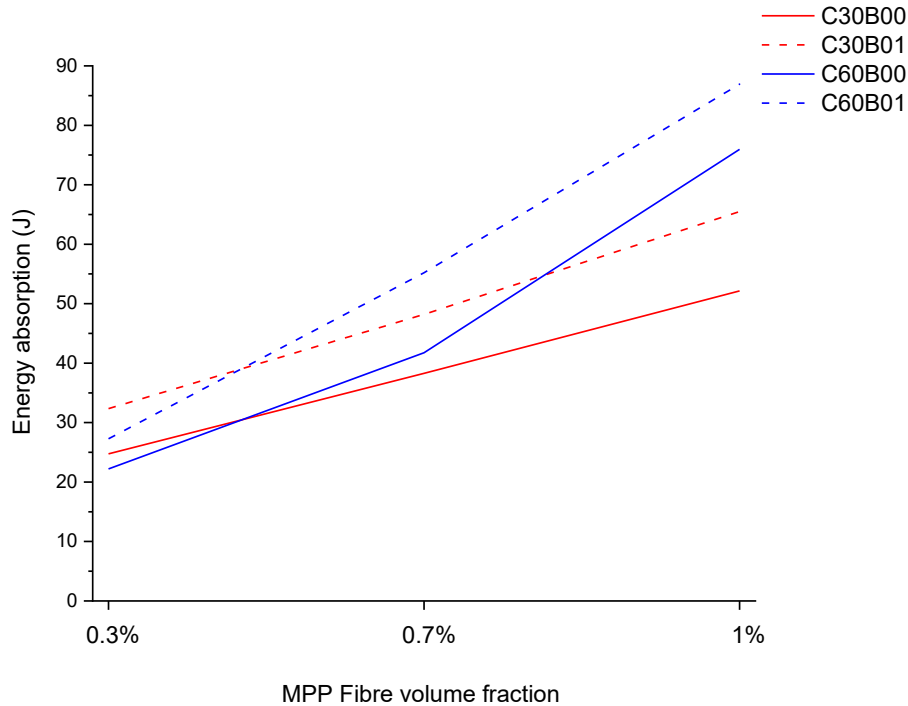


Figure 2-15. The energy absorption capacity of specimens with different concrete strengths and basalt fibre contents

Figure 2-15 shows the trend of energy absorption of specimens of two concrete strengths with or without 0.1% basalt fibre and different volumes of macro PP fibres. It could be found that with the increase of volume fraction of macro PP fibres from 0.3% to 1%, the growth of energy absorption was nearly linear except the beams with C60 and no basalt fibre reinforcement. It is recommended that greater than 0.7% macro PP should be used to achieve higher effectiveness of macro PP and high strength concrete.

2.4. Conclusion

In this chapter, an experimental investigation was performed to evaluate the mechanical properties of hybrid basalt-macro PP fibre-reinforced concrete. It can be concluded that the addition of 0.1% basalt fibres and 1% macro PP fibres significantly enhanced the mechanical properties of concrete, especially the flexural capacity. The following conclusions were drawn:

- The inclusion of macro PP fibres and basalt fibres reduced the workability of fresh concrete. Hybrid fibres showed a larger reduction extent than macro PP fibres when the fibre volume fraction increases.

- Both basalt and macro PP fibres could increase the compressive strength of concrete, and basalt fibres were more effective than macro PP fibres. About 10% improvement on compressive strength was found in hybrid fibre-reinforced concrete. Adding macro fibres changed the failure of concrete from brittle to ductile.
- The addition of 0.1% basalt fibres into traditional macro PP fibre-reinforced concrete could increase the peak stress in the flexural tests. There was about 20% improvement to the peak stress when the macro PP fibre content was 1%.
- The use of 0.1% basalt fibres improved the low initial post-cracking strength of macro PP fibre-reinforced concrete.
- The obvious increase of the applied load trend in high content macro PP fibre-reinforced concrete was observed, hybrid fibres reinforcement further improved this trend and increased the energy absorption ability of FRC.

Chapter 3. Pullout and flexural performance of silane groups and hydrophilic groups grafted polypropylene fibre-reinforced UHPC

Abstract²

To improve the bonding strength between PP fibres and concrete, this dissertation investigates a new method of modifying the surface by grafting hydrophilic groups and silane groups on PP fibres. Characterisation of fibre modification, fibre pullout performance from concrete, and flexural behaviour of fibre-reinforced UHPC were studied. From the Fourier transform infrared and water contact angle measurements, both the hydrophilic groups and silane groups demonstrated successful and efficient surface grafting on the PP fibres, which helped to improve the bonding behaviour of the grafted fibres. The silane groups and hydrophilic groups grafted PP fibres showed significant improvement in the bond behaviour, in which the pullout forces were approximately 3.0 and 1.6 times of unmodified PP fibres, respectively. The energy absorption of the modified fibres, estimated from the pullout tests, showed an increase by 121% and 80% for silane groups and hydrophilic groups, respectively. The silane groups grafted PP fibre-reinforced UHPC showed outstanding toughness and deflection-hardening performance, which increased by 97% as compared to those of unmodified fibres. The flexural performance of 27 kg/m³ silane groups grafted PP fibre-reinforced UHPC was comparable with the 78 kg/m³ steel fibre-reinforced UHPC.

3.1. Introduction

With the development of modern concrete technology, strength, ductility and durability of concrete have been the focus of many researchers. High strength concrete provides additional

² This chapter was extracted from the paper **published** in Construction and Building Materials. The subsections were modified to follow the flow of the thesis. The full bibliographic citation of the paper is as follows:

Feng Shi, Shi Yin, Thong M. Pham, Rabin Tuladhar, Hong Hao. Pullout and Flexural Performance of Silane Groups and Hydrophilic Groups Grafted Polypropylene Fibre-reinforced UHPC. Construction and Building Materials, 2021, 277: 122335.

<https://doi.org/10.1016/j.conbuildmat.2021.122335>

safety margins and reduces the dead load and the cost of structures [39]. On the other hand, ductile response prevents catastrophic collapse of structures by absorbing energy induced by excessive loading conditions such as earthquakes, impact and blast. Enhancing the durability of concrete structures will increase the service life of a structure, reduce the maintenance cost and hence, improve the sustainability of the structure.

There have been a few different opinions on the definition of UHPC. Of these, concrete can be classified as UHPC if it has a compressive strength of over 120 MPa [40]. Besides, a high compressive strength, UHPC has other outstanding mechanical properties [41-44], such as high tensile strength, the exhibition of strain-hardening behaviour, high ductility, extremely low permeability, and great durability. UHPC has been widely used for structural members, such as beams, columns, waterproofing layers, bridge decks, precast curtain walls and so on due to its many advantages [45, 46].

In general, UHPC comprises of over 800 kg/m³ cement and very fine powders, such as crushed quartzite and silica fume [47, 48]. Since the water/binder ratio in UHPC is lower than 0.2, high-range water-reducing admixture is required to improve the workability of concrete [49]. The simultaneous characters of UHPC including high amount of cement and powder and low water/binder ratio lead to the fact that plain UHPC is very brittle and easy to crack, which is the main limitation of plain UHPC. Therefore, fibres are often used in UHPC to enhance its strength, ductility, and durability [50].

Among many different types of fibres, steel fibres are normally used to reinforce UHPC for most structural purposes. Many previous studies have revealed that steel fibres can effectively improve the compressive strength, tensile strength, flexural strength and toughness [51-53]. Steel fibres can bridge cracks, thus improve the interfacial transition zone between cement paste and aggregates. Therefore, steel fibre-reinforced UHPC has high energy absorption capacity and toughness [54]. However, there are still some disadvantages of using steel fibres in concrete. The use of steel fibres significantly decreases the workability of UHPC mixtures. Steel fibres are hard to disperse in concrete when used in high dosage. Furthermore, steel fibres may cause health and safety threats. Steel fibres are also vulnerable to corrosion [55]. Therefore, researchers have been seeking alternative types of fibres to reinforce UHPC, for example synthetic fibres, since they have high durability and are safe to handle [56].

There are many kinds of synthetic fibres used to reinforce UHPC, including polyvinyl alcohol (PVA) fibres, ultra-high-molecular-weight polyethylene (UHMWPE) fibres,

polyoxymethylene fibres and PP fibres. Yu et al. [57] used 20 kg/m³ UHMWPE fibres to reinforce UHPC and found that the fibres provided obvious strain-hardening behaviour and multiple crack characteristics for UHPC. The UHPC had a tensile strength of 20 MPa and elongation of 8.7%. Hannawi et al. [58] compared the effect of adding different types of fibers to the microstructure and the mechanical behaviour of UHPC. They found that the unsteady cracking threshold of PVA fibre-reinforced UHPC was 134.5 MPa, which is comparable with the steel fibre-reinforced UHPC (166.3 MPa) and higher than that reinforced with wollastonite fibres (127.7 MPa), basalt fibres (124 MPa) and plain UHPC (109.5 MPa). They also found that PP fibre-reinforced UHPC has the lowest unsteady cracking threshold (92.9 MPa) since PP fibres have porous fiber/matrix interfacial zones due to its hydrophobic property. PP fibres, however, have the most reasonable cost compared to the other types of fibres.

However, thermodynamic incompatibility between hydrophobic concrete and hydrophilic PP fibres always causes weak bonding at the interface. In order to further improve the reinforcing effects of PP fibres, many researchers have focused on modified PP fibres, including plasma treatment modification [59], surface oxidation modification [60], surface grafting hydrophilic groups [61], silane coupling agent modification [62], modification by using surfactant [62], modification by changing the cross-section shape [63], treatments with HCl or NaOH [64] and so on. Majority of these studies have focused on the modification techniques and proven that PP fibres have been successfully modified without comprehensive investigations on the bond behaviour. Among these methods, hydrophilic groups and surface grafting silane groups are considered the two most efficient techniques which can be applied at the industrial scale [65].

Feng et al. [60] grafted acrylic acid (AA) and graphene oxide (GO) onto the surface of PP fibres. They found that the static water contact angle of un-modified PP fibres was 77° while the water contact angle of modified PP-g-AA and PP-g-AA-GO fibres significantly decreased to 64.1° and 29.2°, respectively. Compared with the flexural strength of un-modified PP fibre-reinforced concrete, the flexural strength of PP-g-AA and PP-g-AA-GO fibre-reinforced concrete increased by 3.3% and 25.6%, respectively. Yang et al. [66] proposed two kinds of nano-silica modified PP fibres by direct blend-spinning and by surface chemical deposition of the silica particles through the sol-gel method. They found that 0.9 kg/m³ unmodified PP fibre-reinforced concrete had a crack area of 342.7 mm² and average crack width of 1.12 mm. The crack area decreased to 250.1 mm² and the average crack width decreased to 0.51 mm when using nano-silica modified PP fibres by direct blend-spinning. The crack area decreased to 137.3 mm² and the average crack width decreased to 0.37 mm when using PP fibres modified

by surface chemical deposition of silica particles through the sol-gel method. These two methods have been shown very effective in improving the performance of modified PP fibres.

As can be seen, surface grafting either with hydrophilic groups or silane groups on PP fibres showed a significant improvement in the performance. These two modification methods improve the performance of the modified fibres through different mechanisms. PP fibres have hydrophobic and smooth surfaces which result in their poor bonding strength with concrete. The surface grafting with hydrophilic groups results in better bonding between concrete and fibres due to thermodynamic compatibility between their interfaces. Silane groups, on the other hand, can take part in the hydration reaction of concrete which improves the bonding between concrete and fibres. Currently, there has been no study in the literature to compare the effects of these two modification methods and investigate their different reinforcing mechanisms. This dissertation has adopted surface grafting with hydrophilic groups and silane groups. Fourier transform infrared (FTIR) spectrometer measurement and water contact angle were also performed to study the modification effectiveness of modified PP fibres. The Pullout behaviour of these two modified PP fibres in concrete was studied while their bonding strength with concrete was also compared and analysed. Finally, the reinforcing effects of the modified PP fibres in the UHPC are presented.

3.2. Experimental investigation

3.2.1 Material properties

Steel and PP fibres used in this dissertation are shown in Figure 3-1. PP fibres were provided by Ningbo Shike New Material Technology Co., Ltd. [67]. PP fibres had a diameter of 0.18 mm, length of 20 mm used in flexural tests and macro PP fibres had a diameter of 0.8 mm used in pullout tests, which had the tensile strength of 700 MPa and Young's modulus of 7 GPa. Copper coated steel fibres with a diameter of 0.17 mm and length of 13 mm were provided by Sobute New Materials Co., Ltd. [68]. The tensile strength and Young's modulus of the steel fibres were 1200 MPa and 200 GPa, respectively. UHPC modified admixture and high range water-reducing admixture were provided by Sika (Jiangsu) Building Materials Co., Ltd. [69]. Based on the previous studies [48, 70] and industry practice, standard concrete mix design for 120 MPa UHPC used in this dissertation is shown in Table 3-1.

Table 3-1. UHPC mixture design

Material	Mix 1	Mix 2
	kg/m ³	kg/m ³
Portland cement	814	814
UHPC modified admixture	236	236
Silica fume	70	70
0.075-0.6 mm fine sand	1200	1200
Water	160	160
High range water-reducing admixture	20	20
Unmodified or modified PP fibre	27	0
Copper coated steel fibre	0	78

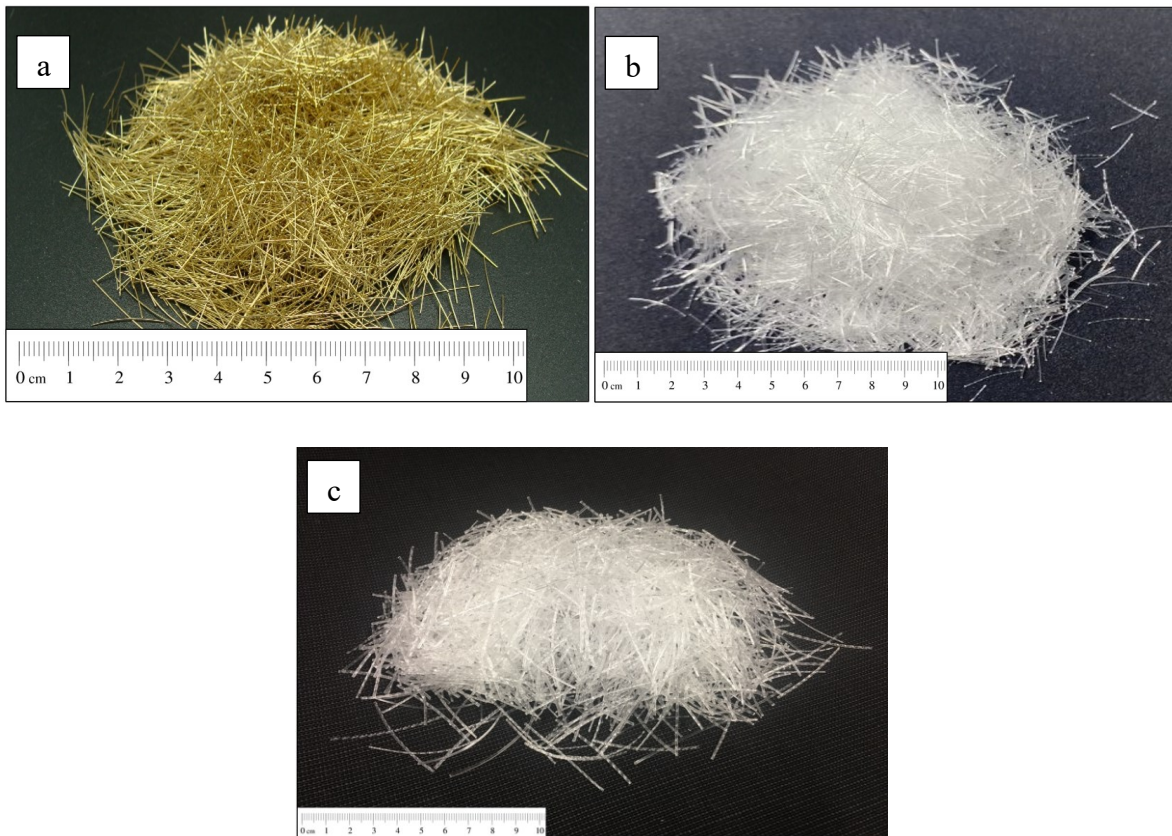


Figure 3-1. Steel (a), PP (b) and macro PP (c) fibres used in this test

3.2.2 Modification of fibres

3.2.2.1 Surface grafting hydrophilic groups

The first modified PP fibres were produced by using surface grafting hydrophilic groups. Firstly, 40 g maleic anhydride (MA), 40 g Butyl Methacrylate (BMA), 0.5 g dicumyl peroxide (DCP), and 1 g antioxidant were added and fully dissolved in 10% acetone. Secondly, the solution was sprayed on the 1000 g PP powder and mixed evenly. Thirdly, the PP mixture was put in a fume cupboard and stirred continuously until all the solution was volatilised. The dried PP mixture was then added into a twin-screw extruder, and then the modified PP granule was produced. The modified PP granule was added into a single screw extruder, followed by a high-rate drawing process, finally producing the modified PP fibres with surface grafting hydrophilic groups. The schematic illustration of the fabrication process of hydrophilic groups grafted PP fibres is shown in Figure 3-2.

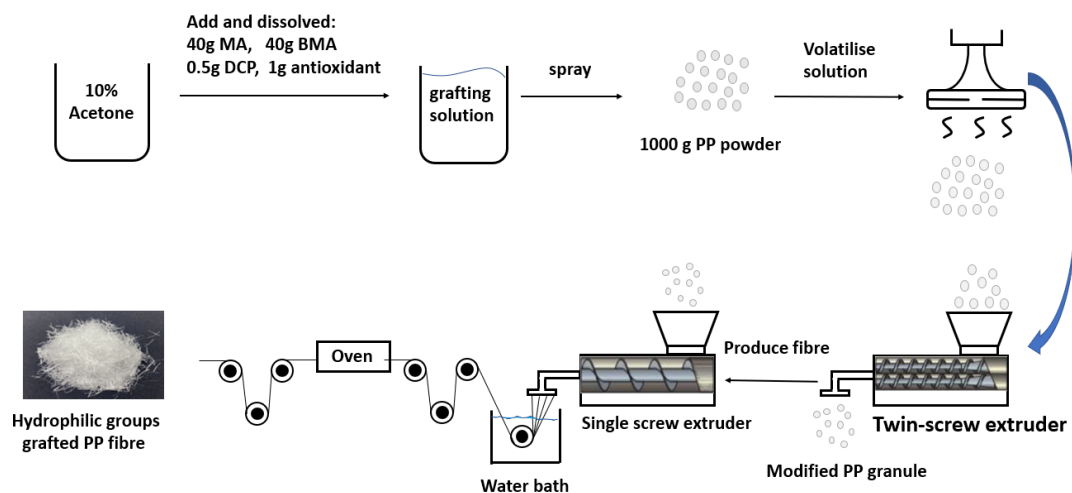


Figure 3-2. Schematic illustration of the fabrication process of hydrophilic groups grafted PP fibres

3.2.2.2 Surface grafting silane groups

The second type of modified PP fibres was made by adopting the technique of surface grafting silane groups. In this method, the unmodified PP fibres were first produced through the single screw extruder, followed by a high-rate drawing process. Secondly, the PP fibres were immersed in xylene. Xylene was heated to 80 °C for 2 hours until the soluble inflation phenomenon on the PP fibres was observed. The whole heating process was protected under the nitrogen environment in case of fire. Fibres were taken out and washed by acetone. After that, the washed PP fibres were put into the 60 °C oven for 8 hours, until acetone was fully

volatilised. A mixture solution was then produced by adding silane coupling agent KH570: ethyl alcohol: water at the rate of 5: 4: 1. Finally, the PP fibres were immersed in the KH570 mixture solution for 3 hours, getting the modified PP fibre with surface grafting silane groups. Schematic illustration of the fabrication process of silane groups grafted PP fibre was shown in Figure 3-3.

3.2.3. Characterisation of fibres

3.2.4.1 Fourier transform infrared measurement

Fourier transform infrared (FTIR) spectrometer measurement was carried out with a Perkin-Elmer spectrum 100 FTIR Spectrometer. The type and content of hydrophilic groups and silane groups grafting can be determined in terms of intensity of the absorption bands in the FTIR. Different PP fibre samples were heated to 200°C and pressed into a thin film with 15 mm diameter by a spectrometer filmmaker kit. Before the tests, FTIR spectrometer was re-initialized and background scanned to eliminate noise signals. The scan range was set between 400-4000 cm^{-1} and the scan mode was percentage transmittance.

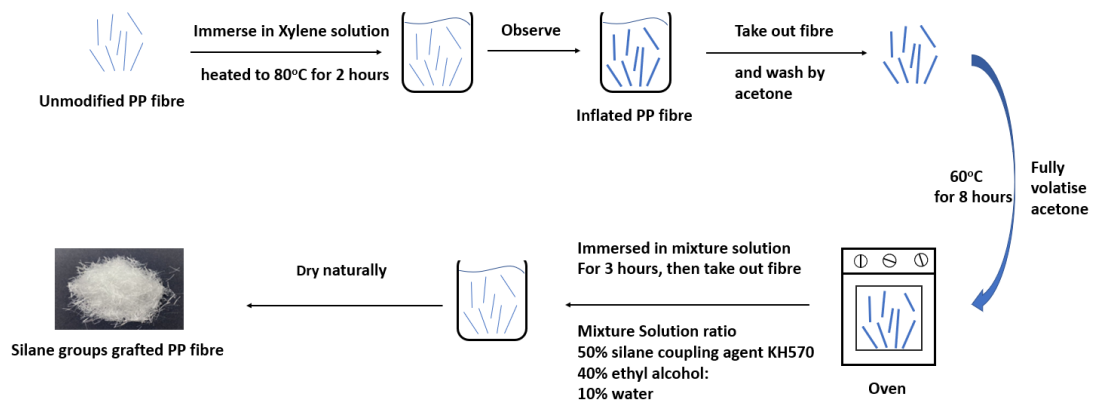


Figure 3-3. Schematic illustration of the fabrication process of silane groups grafted PP fibres

3.2.4.2 Water contact angle measurement

Water contact angle measurement was carried out to study the improvement of wettability of modified fibre's surface. This test can be used to evaluate the effectiveness of fibre modification by comparing the angle between the fibre surface and a water droplet. Reducing the contact angle illustrates better wettability of fiber resulting from the fibre modification. The test was performed on a PAT-1 surface tensiometer, accompanied with a digital camera. 0.1 μl

of deionized water with a microsyringe was dropped onto dry fibre membrane in air and the contact angle was measured by using a digital camera.

3.2.4. Mechanical properties of fibre-reinforced UHPC

3.2.4.1 Pullout tests

The bonding strength between fibre and concrete can be characterised by pullout tests. When fibres were pulled out from UHPC, the fibre would experience fibre deformation, fibre debonding, and fibre slip and friction with concrete. Therefore, the pullout tests are efficient methods which can reflect the effectiveness of fibre modification [51]. However, there were no standards currently available for the pullout tests. It is reasonable to assume that the macro PP fibres with the same mechanical properties and the same chemical treatments as small PP fibres would have similar bond strength in UHPC although the pullout force would be different, and the pullout force is linearly proportional to the contact surface area between fibre and UHPC. Furthermore, the primary objective of this dissertation is to verify the effectiveness of the two modification methods as described above to enhance the bond strength of PP fibre in UHPC, therefore, only macro fibres were used in pullout tests for better visualization of the progress of the fibre pullout and better quality control of the tests as it is rather difficult to perform pullout tests on 0.18 mm fibres. As shown in Figure 3-4, macro PP fibres were vertically embedded in a concrete beam of $150 \times 150 \times 550 \text{ mm}^3$. The distance between two macro PP fibres in horizontal directions was about 78 mm. The macro PP fibres had a diameter of 0.8 mm, and the embedded depth of fibre in the concrete was 100 mm. It has been proved in a previous study that during fibres being pulled out, the affected zone of concrete was about five times the diameter of fibres [71], which is 4 mm in this test. Therefore the pullout test of one fibre would not affect the adjacent fibres as shown in Figure 3-8. One side of macro PP fibres was embedded vertically into concrete while the other side was gripped on the tensile test machine. United STM ‘Smart’ Test System (STM-50KN) from United Calibration Corporation with a 2 kN load cell and data acquisition software was used for the pullout tests. The pullout load would remain flat or decrease when fibres were in the fully-slip stage so that the tests were stopped when the pull-out displacement was about 14 mm. The concrete base was cured in water for 28 days before testing. There were seven samples for each type of fibre.

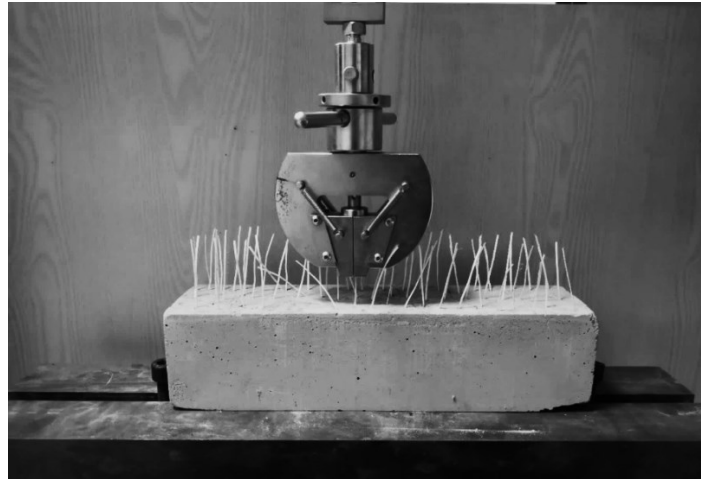


Figure 3-4. Pullout test setup

3.2.4.2. Flexural performance measurement

The flexural performance of different modified PP fibre-reinforced UHPC was studied on concrete beams with a square cross-section of $100 \times 100 \text{ mm}^2$ and length of 400 mm as per ASTM C1609 [31], as shown in Figure 3-5. The distance between the supports was 300 mm while the distance between the two loading points was 100 mm. The loading rate was 0.2 mm/min as recommended by ASTM C1609 [31]. The applied load was measured by using a load cell which was embedded in the machine while the midspan displacement of the beams was monitored via two linear variable differential transformers (LVDTs) as shown in Figure 3-5. The reported displacement was averaged between the two LVDTs. All the concrete beams were cured in water for 28 days before testing. To improve the reliability of testing, three identical concrete beams were tested for each case of fibre-reinforced UHPC. The mix designs are shown in Table 1.

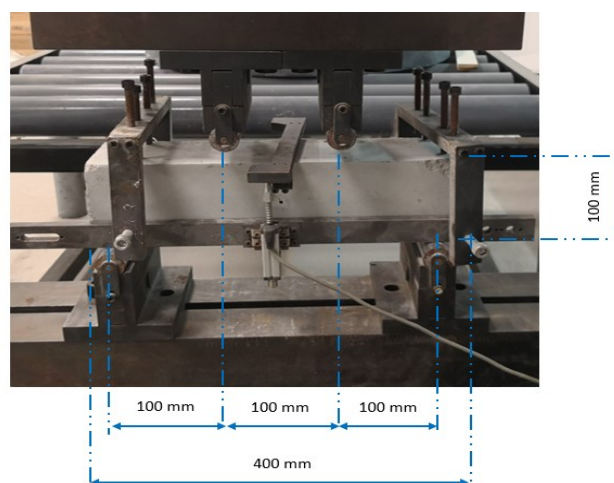


Figure 3-5. Setup of the flexural tests on fibre-reinforced UHPC

3.3. Results and discussion

3.3.1. Characterisation of PP fibres

FTIR results of PP fibres are presented in Figure 3-6, which reflected the grafting condition of the modified PP fibre. Compared with the unmodified PP fibres, the silane groups grafted PP fibres displayed three different absorption bands at 1093, 1043 and 893 cm^{-1} (see Figure 3-6a), which present -Si-O-Si-, -C-O- and -Si-C-, respectively [72-75]. It proved that the silane groups were successfully grafted on the PP fibres. Moreover, hydrophilic groups of -C-O- were also grafted by finding -C-O- absorption band at 1043 cm^{-1} [76], which improved hydrophilicity and dispersibility of fibres. Through the water contact angle measurement, the water contact angle of silane groups grafted PP fibre was 81°, which is lower than that of unmodified PP fibre (90°).

For the hydrophilic groups grafted PP fibre (see Figure 3-6b), there were two absorption bands at 1770 and 1704 cm^{-1} , which relate to -C=O [77-79]. Three absorption bands at 1295, 1244 and 1204 cm^{-1} were also observed and all of them represent -C-O- [79]. It proved that the hydrophilic groups were successfully grafted on the PP fibres. The water contact angle of hydrophilic groups grafted PP fibre was 69°. This significant reduction (21 °) in the water contact angle proved that the hydrophilic modification was as efficient as corona treatment method (18 °) [80], γ -ray induced graft copolymerization with hydroxyethyl methacrylate method (25 °) [81] and atmospheric nitrogen dielectric barrier discharge plasma method (26 °) [82].

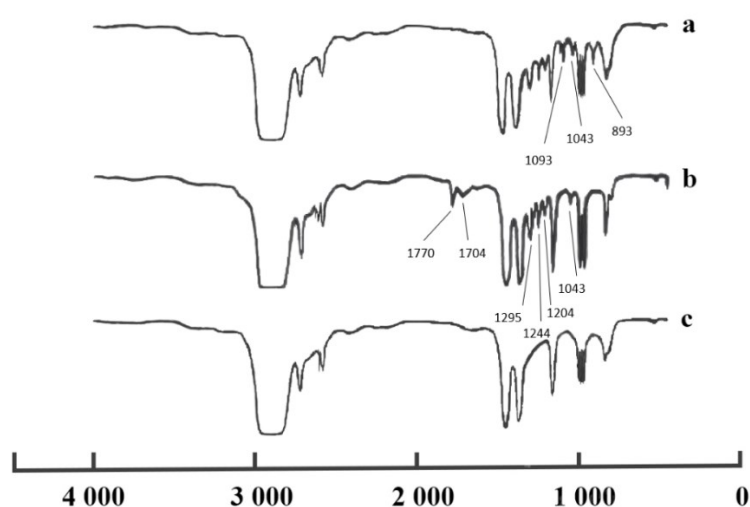


Figure 3-6. FTIR results of PP fibres: (a) silane groups grafted PP fibres; (b) hydrophilic groups grafted PP fibres; and (c) unmodified PP fibres

3.3.2 Pullout performance of fibres

All the load-displacement curves of the pullout tests are shown in Figure 3-7. The whole pullout process experienced fibre elongation, fibre debonding, fibre slip and friction with concrete. There was no fibre rupture observed during the pullout tests because the pull-out force, required to achieve fibre rupture, is estimated as 350 N, which is much greater than the bonding forces as shown in Fig.7. When the displacement is over 14 mm, only the phenomenon of fibre slip and friction with concrete was observed so that the tests were stopped at the displacement of 14 mm.

For unmodified PP fibres, the pullout load increased nearly linearly until the maximum load (90 N) at approximately 1.7 mm. The bonding of the fibre is the primary resistance to the pullout force as also reported in the previous study [83]. After that, the load drastically decreased to less than 50 N before it steadily increased again to 93 N at approximately 14 mm. The sudden drop after the first peak load indicated that a total bond loss between fibre and matrix [84]. This process was associated with the slip, elongation, and friction action of fibres. This relationship agrees well with finding in the previous study [85] in which the pullout forces of unmodified PP fibres show a linear increase to the first peak followed by a sudden drop and then a steadily increase to the second peak.

The pullout force of the silane groups grafted PP fibres increased linearly to the maximum pullout load of 224 N at 5.8 mm with a small flat at around 49 N. When the applied load reached the peak, the load decreased significantly to 135 N at 14 mm. The silane groups grafted PP fibre showed a totally different pullout performance with the unmodified PP fibre.

Meanwhile, the pullout load of the hydrophilic groups grafted PP fibre increased to around 56 N at 0.4 mm, followed by an obvious and long stage with the displacement from 0.5 mm to 3.2 mm. This long flat indicated that the bond between hydrophilic groups grafted PP fibre and UHPC matrix was strong enough to make fibre being elongated before debonding. After this stage, the load increased to a peak of 149 N at 4.6 mm, which is much lower than that of silane groups grafted PP fibre. After the peak load, the load increased once again from the displacement of 6 mm. At the displacement of 14 mm, the load increased to 146 N, which is even higher than that of silane groups grafted PP fibre (135 N).

It is interesting to note that both types of the modified PP fibres responded differently from that of the unmodified PP fibres. The first peak pullout load of modified PP fibres occurred at a larger deformation which was about 2-2.5 times the displacement at the peak force of

unmodified fibres. Besides, in the load-displacement curve, there was a stage at the displacement of 0.5 mm to 1.2mm for the silane groups grafted PP fibres, while there was a longer flat for the hydrophilic groups grafted PP fibres. When the load increased to around 50 N, it could cause a slip of modified molecule between fibres and concrete, thus leading to the flats on the both of silane groups and hydrophilic groups grafted PP fibre. The silane groups and hydrophilic groups grafted PP fibres have different capacity of slip, thus showing a different length of flats. This molecule slip phenomenon was also observed and reported in the literature [86, 87]. Since the unmodified PP fibres did not have any modified molecule between fibres and concrete, there was not any flat on the load-displacement curves. The flat stage of modified PP fibres indicated there were additional chemical bonding between fibres and concrete more than just the physical surface friction and interlock.

Table 3-2 summarises the mean values and standard deviations of the pullout loads at different stages. The energy absorption was estimated as the area of the enclosed load-displacement curves. As can be seen, the energy absorption of the silane groups and hydrophilic groups grafted PP fibres were 2.024 J and 1.646 J, respectively, which increased by 121% and 80% as compared to the unmodified fibres.

Table 3-2. Results of pullout tests

Fibres	Peak load (N)		Load at a displacement of 14 mm (N)		Energy absorption until displacement of 14 mm (10^{-3} J)	
	Mean	Standard deviation	Mean	Standard deviation	Mean	Standard deviation
Silane groups grafted PP fibre	224	18.4	135	15.8	2024	190
Hydrophilic groups grafted PP fibre	149	17.3	146	15.2	1646	120
Unmodified PP fibre	90	8.4	92	7.6	915	76

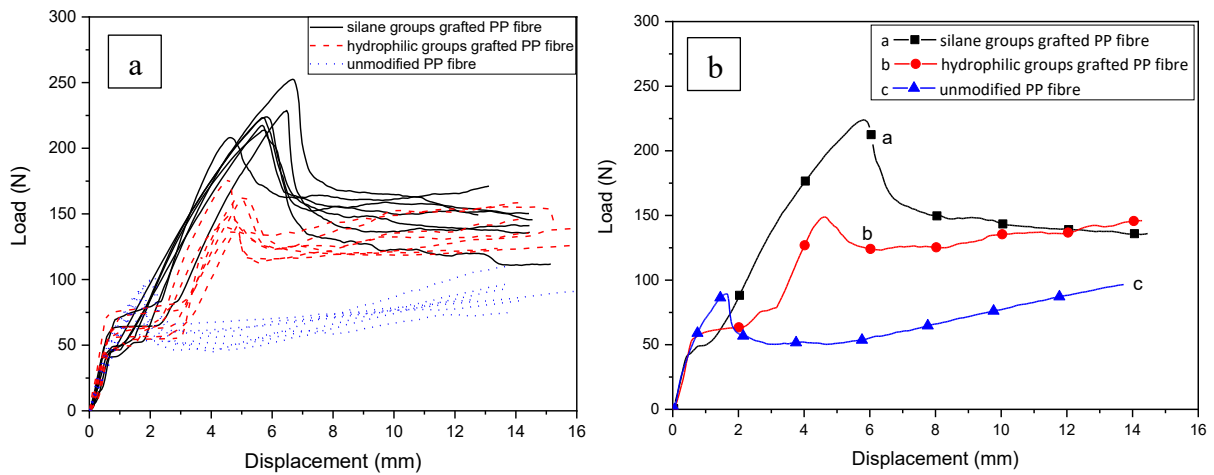


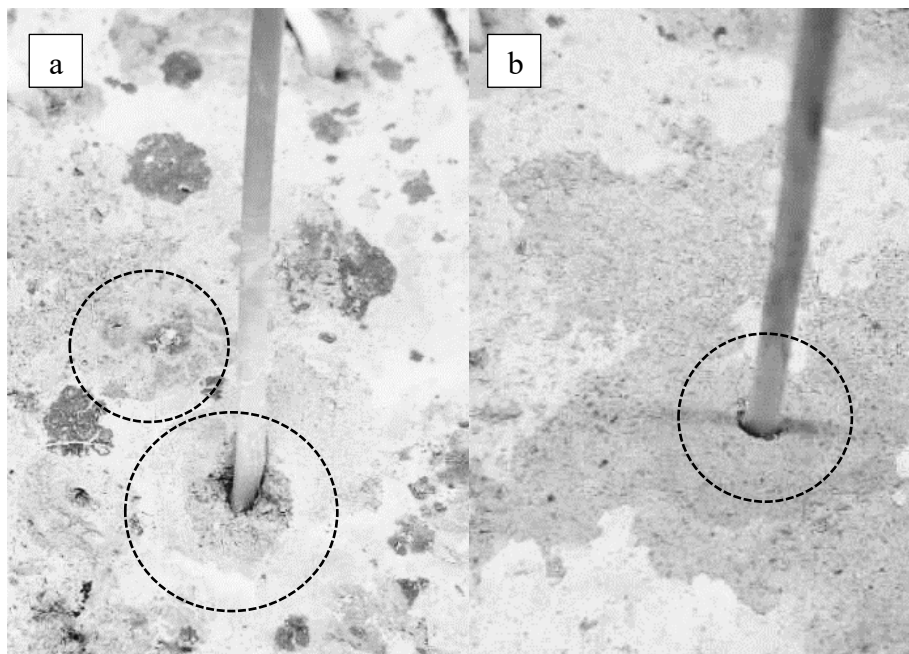
Figure 3-7. All tested samples (a) and typical load-displacement curves of PP fibres in the pullout tests (b)

Figure 3-8 shows the images after pullout tests. It should be noted that each test was stopped when the displacement was about 14 mm, therefore the fibres were not completely pulled out from the concrete. Figure 3-8(a) shows that a small segment of concrete around the fibre was pushed out, showing strong bonding of concrete with the silane groups grafted PP fibre. When silane groups grafted PP fibre fully debonded, there was a loud sound due to concrete fracture in interface with fibre. This is also demonstrated by the high pullout load of 224 N, which was nearly three times of unmodified PP fibre. High pullout load caused damage of concrete around the modified PP fibre, which led to a significant decrease of the pullout load after the peak load as shown in Figure 3-7. Therefore, the modification of surface grafting silane groups produced a very high bonding strength with concrete. This can be attributed to the fact that the silane groups took part in the hydration reaction of concrete and thus improved the bonding with concrete. The high efficiency of using silane groups to graft PP fibres was also reported in the literature [62, 88].

As can be seen from Figure 3-8(b), the hydrophilic groups grafted PP fibres exhibited clear debonding with concrete without any destruction of concrete. When the pullout load reached the bonding strength (149 N), which led to the debonding between fibre and concrete. With the slip out of fibre from concrete, the force between fibre and concrete increased due to surface interlock and surface friction between fibre and concrete, leading to the second increase of the pullout load after the peak load [89]. Therefore, the hydrophilic groups grafted PP fibres also showed a higher bonding strength.

As shown in Figure 3-8(c), the pullout of unmodified PP fibre did not cause concrete damage. This is because the unmodified PP fibre had poor bonding with concrete, Therefore, even when the fibre was pulled out, the concrete destruction was negligible. After the peak pullout load, the contribution of frictional force and interlock between fibre and concrete was still prominent, which led to loading at a displacement of 14 mm was even higher than the peak load, this phenomenon of increase of the applied load was also reported in the literature [84, 89], as shown in Figure 3-7.

As shown in Figure 3-8(d), when the bonding between fibre and concrete was stronger than the tensile strength between small particles (or segment), there were small concrete particles attached on the surface of the fibre. And the size of concrete particles is dependent on the bond strength between fibre and concrete. When the fibre was being pulled out, this debris caused a small gap between fibre and concrete. Therefore, the gap associates with an excellent bonding strength between fibre and concrete. Besides, if the bond strength between fibre and concrete is stronger than the tensile strength of a surface layer of concrete, a small segment spalling out would be expected as shown in Figure 3-8(a).



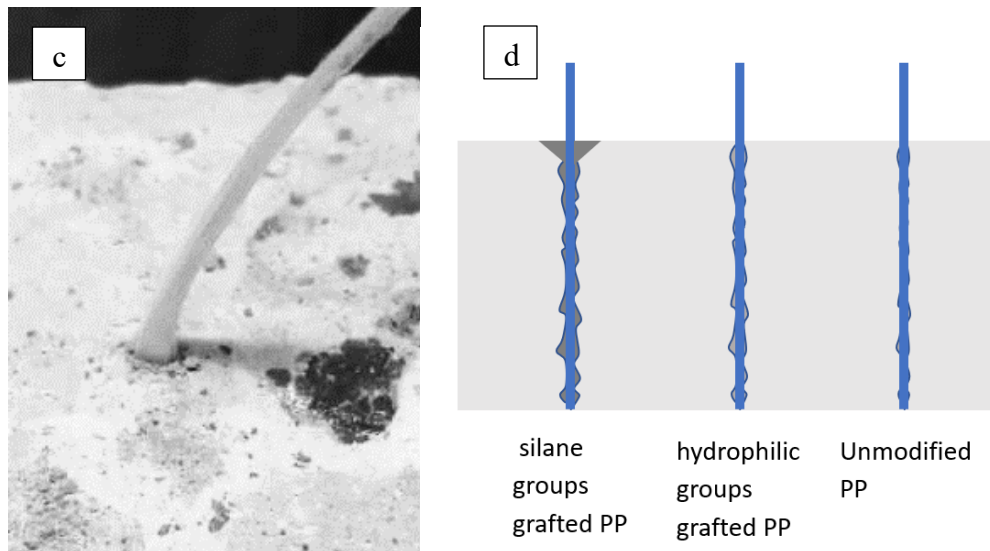


Figure 3-8. Fibre-concrete pullout image when fibre was pulled out: (a) silane groups grafted PP fibre, (b) hydrophilic groups grafted PP fibre, (c) unmodified PP fibre and (d) diagrammatic sketch

3.3.3. Flexural performance of fibre-reinforced UHPC

In this dissertation, three concrete beams each made of one of the three types of fibre-reinforced UHPC were tested. Figure 3-9 shows the flexural performance of fibre-reinforced UHPC. As can be seen from the figure, after the specimens cracked, the applied load of fibre-reinforced UHPC show a sudden reduction with deformation to about 0.5 mm. After that, the applied load of the specimens with unmodified fibres and hydrophilic groups grafted fibres further decrease with deformation, but at a slower rate. The applied load of the specimen with silane groups grafted fibres, however, increases to a second peak with deformation until about 1.5 mm, then gradually decreases with deformation before complete failure. Some fluctuations in the descending part of the curve indicate that the interlock and friction between fibres surface and concrete were strong and associated with stress redistribution in the specimens. This observation agrees well with the phenomenon reported in previous studies [90, 91].

The hydrophilic groups grafted PP fibre-reinforced UHPC had the highest peak load of 45.4 kN among the three fibre-reinforced UHPCs. And the silane groups grafted PP fibre-reinforced UHPC had the comparable highest peak load (44 kN) due to the deflection-hardening phenomenon. Meanwhile, the previous study by Yin et al. [92-94] reported that unmodified PP fibres only had a minor influence on the flexural strength of concrete. On the other hand, PP fibres mainly improved the toughness and post-cracking performance of concrete rather than the flexural strength. Due to the excellent bond performance of the modified PP fibres, they

also exhibited great reinforcing effect in UHPC compared to the unmodified PP fibres. As shown in Table 3-2, the silane groups grafted PP fibre-reinforced UHPC exhibited an outstanding toughness. The energy absorption of silane groups grafted PP fibre-reinforced UHPC was 75.8 J, which increased by 97% as compared to those with unmodified fibres (38.4 J). From Figure 3-9 the deflection-hardening performance can be found for the silane groups grafted PP fibre-reinforced UHPC. The deflection-hardening refers to load still increasing after the first cracking and first peak load. Since the silane groups grafted PP fibres had very high bonding strength with concrete when concrete cracked the fibre bridged on the cracks and exhibited its strong action on bearing the applied load. The hydrophilic groups grafted PP fibre-reinforced UHPC also showed much better post-cracking performance than that of unmodified PP fibre-reinforced UHPC. However, similar to the unmodified PP fibre-reinforced UHPC, the hydrophilic groups grafted PP fibre-reinforced UHPC showed deflection-softening performance, rather than deflection-hardening performance.

To further compare the behaviour of fibre-reinforced UHPC with different fibres, i.e. modified PP fibre and typical steel fibre. The flexural performance of silane groups grafted PP fibre-reinforced UHPC and steel fibre-reinforced UHPC was investigated by using the same specimen size and test setup. Figure 3-10 compared the flexural performance of 27 kg/m³ (3% in volume fraction) silane groups grafted PP fibre-reinforced UHPC with 78 kg/m³ (1% in volume fraction) steel fibre-reinforced UHPC and plain UHPC. As can be seen in Figure 3-10 and Table 3-3, the silane groups grafted PP fibre had comparable reinforcing effects with steel fibres and far better than that of plain UHPC. The energy absorption of silane groups grafted PP fibre-reinforced UHPC was 75.8 J, which was just 5% smaller than that of steel fibre-reinforced UHPC (79.5 J). It should note that the densities of PP fibres and steel fibres were 0.9 g/cm³ and 7.8 g/cm³, respectively, which means the volume fractions of 27 kg/m³ PP fibres and 78 kg/m³ steel fibres were 3% and 1%, respectively.

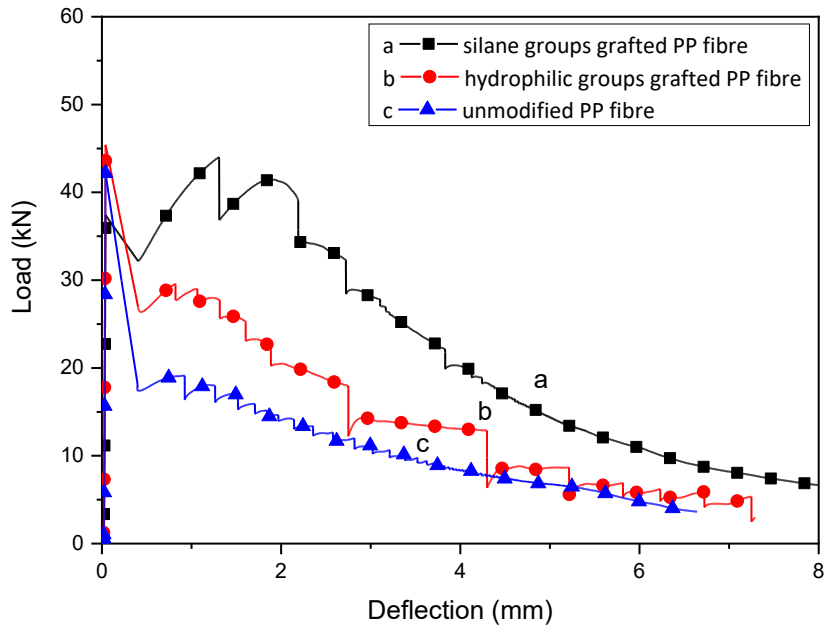


Figure 3-1. The load-deflection curves of modified and unmodified PP fibre-reinforced UHPC

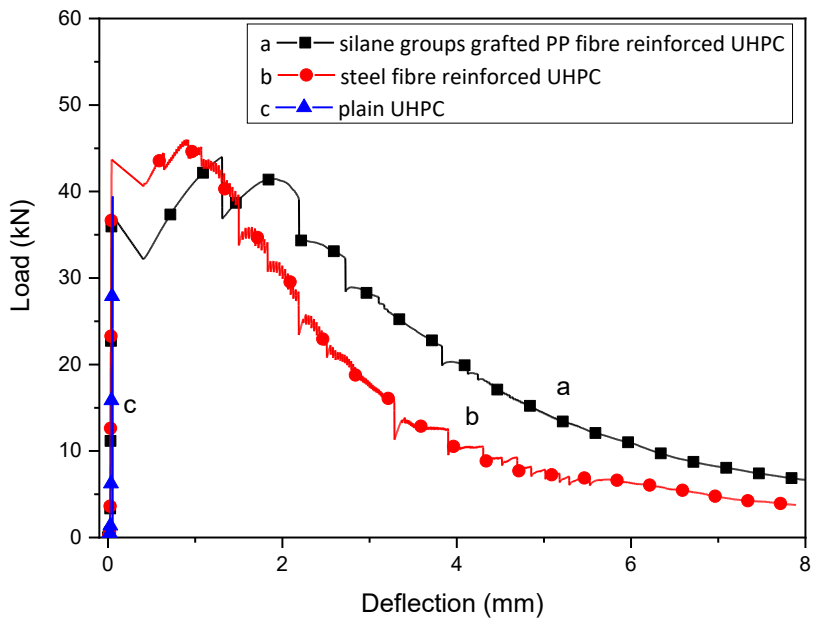


Figure 3-2. The load-deflection curves curve of plain and fibre-reinforced UHPC

Table 3-3 Results of flexural test on fibre-reinforced UHPC

Note	Fibre ratio (kg/m ³)	Peak Stress (MPa)		Residual strength at the deflection of L/150, f_{150}^D (MPa)		Toughness until deflection of 2 mm (J)	
		Mean	Standard deviation	Mean	Standard deviation	Mean	Standard deviation
Plain UHPC	0	11.8	1.2	-	-	-	0
Unmodified PP fibre-reinforced UHPC	27 (3% in volume fraction)	12.7	1.4	4.2	0.3	38.4	5.2
Silane groups grafted PP fibre- reinforced UHPC	27 (3% in volume fraction)	13.2	1.1	12.4.0	0.5	75.8	11.1
Hydrophilic groups grafted PP fibre- reinforced UHPC	27 (3% in volume fraction)	13.5	1.3	6.2	0.4	55.4	8.4
Steel fibre- reinforced UHPC	78 (1% in volume fraction)	13.1	1.0	9.4	0.2	79.5	10.5

3.4. Conclusion

PP fibres are becoming more popular in construction because they improve the concrete performance due to its inherent advantages such as affordable cost, durability and ease handling. In order to further improve the reinforcing effects of PP fibres, many studies have been conducted on the modification of PP fibres. In the various modification methods, surface grafting hydrophilic groups and surface grafting silane groups are considered to be two of the most efficient methods which can be applied at the industrial scale. These two modification methods rely on totally different mechanisms to improve bonding with concrete. This chapter examined the performance of modification of surface grafting hydrophilic groups and modification of surface grafting silane groups and examined their different reinforcing mechanisms. The following conclusions can be drawn:

- The FTIR results proved that the silane groups and hydrophilic groups were successfully grafted on the PP fibres. The water contact angle of silane groups and hydrophilic groups grafted PP fibre was respectively 81° and 69° , which was much lower than that of unmodified PP fibre (90°).
- The modification of surface grafting silane groups produced a very high bonding strength with concrete, due to the fact that the silane groups took part in the hydration reaction of concrete. The peak pullout load was up to 224 N, which was nearly three times of unmodified PP fibres. The hydrophilic groups grafted PP fibre also showed high bonding strength with the peak pullout load of 149 N, which was equal to 1.6 times of that of unmodified PP fibres. The energy absorption of silane groups and hydrophilic groups grafted PP fibres was 2.024 J and 1.646J, which increased by 121% and 80% as compared to unmodified fibres, respectively.
- The silane groups grafted PP fibre-reinforced UHPC showed the outstanding flexural strength, toughness and deflection-hardening performance. Similar to the unmodified PP fibre-reinforced UHPC, the hydrophilic groups grafted PP fibre-reinforced UHPC showed deflection-softening performance, rather than deflection-hardening performance. The flexural performance of 27 kg/m^3 silane groups grafted PP fibre-reinforced UHPC was comparable with 78 kg/m^3 steel fibre-reinforced UHPC.

Chapter 4. Mechanical properties of hybrid fibre-reinforced concrete under dynamic compression and split tension

Abstract³

Various types of fibres have been used to enhance the ductility of concrete material under tensile and compressive loading. In order to effectively enhance the performance of concrete, hybrid fibres have been successfully used to improve the mechanical properties of concrete due to the contribution of multiple sizes and functions of fibres. However, the performance of hybrid FRC has been rarely studied under dynamic loadings. Meanwhile, a new type of hybrid fibres with a combination of 1% low Young's modulus macro PP fibres and 0.1% high Young's modulus micro basalt fibres have been recently proposed and showed better performance under static loading than the sole type of fibre-reinforced concrete. This dissertation further investigates the dynamic compressive and splitting tensile properties of this new basalt-macro PP hybrid fibre-reinforced concrete with different fibre volume dosages. High-velocity impact tests were conducted using the split Hopkinson pressure bar. The experimental results showed that basalt-macro PP hybrid FRC exhibited better impact resistance compared with plain concrete in both dynamic compression and splitting tension. FRC exhibited less number of crack initiation and propagation, ductile failure pattern and small crack opening displacement. The sensitivity of concrete to strain rate was found more significant when 1% hybrid FRC was subjected to dynamic compression or 2% hybrid FRC was under dynamic split tensile tests. Based on testing results empirical formulae were derived to describe the dynamic increase factor (DIF) versus strain rate for both dynamic compressive and tensile strength of hybrid FRC.

4.1 Introduction

Concrete remains as one of the most popular construction materials in the world due to low cost and wide availability of raw materials. Typical concrete has high compressive strength but

³ This chapter was extracted from the paper submitted to Concrete Cement Composites, which is under review. The subsections were modified to follow the flow of the thesis. The full bibliographic citation of the paper is as follows:

Feng Shi, Thong M. Pham, Hong Hao. Mechanical Properties of Hybrid Fibre-Reinforced Concrete under Dynamic Compression and Split Tension. (under review)

low tensile strength (about one-tenth of its compressive strength). Besides, it is vulnerable to small plastic deformation due to its brittle characteristics. The brittleness of concrete can be eliminated by reinforcing with fibres. The use of fibres can obviously improve the mechanical properties of concrete. The main purpose of the addition of fibres in concrete is to reduce the tensile stress concentration in concrete and control the propagation of cracks by acting as a stress-transfer bridge. As a result, FRC becomes a ductile material with much higher energy absorption capacity. Over the last decade, FRC has been widely used in footpath [95], shotcrete [96], and precast bridge decks [97].

Relative Young's modulus of fibres to concrete influences whether fibres can bear sufficient stress relatively compared to concrete and in turn affect the ductility of FRC. Thus, fibres can be classified as high Young's modulus type and low Young's modulus type with respect to the modulus of concrete. Afroughsabet and Ozbakkaloglu [19] investigated the mechanical properties of FRC with steel fibres and PP fibres. The results showed that 0.25% steel fibres (205 GPa in Young's modulus) performed slightly better than 0.3% PP fibres (7 GPa in Young's modulus) in terms of the compressive strength and splitting tensile strength. Similar results were also reported by Jiang, et al. [98] that basalt fibre (102 GPa in Young's modulus) outperformed PP fibres in the compressive, tensile and flexural strengths given the same volume fraction. Yang, et al. [99] compared the influence of steel fibres and macro PP fibres to the flexural behaviour of FRP (fibre-reinforced polymer) reinforced beams. The experimental results indicated macro PP fibres were more effective in controlling crack development than steel fibres in FRP bar-reinforced concrete beams and the ductility indexes of macro PP fibre-reinforced FRP beams were approximately 14% higher than that reinforced by steel fibres. Through reviews of the sole type of fibre-reinforced concrete, it can be concluded that fibres with high Young's modulus can improve tensile and flexural strength more effectively while fibres with low Young's modulus can provide better post-peak behaviour and ductility. However, a single type of fibres cannot perform well in both the peak strength and post-peak behaviour. Therefore, hybrid fibres with different Young's moduli providing multiple reinforcements in different stages have become more and more popular [100]. Further optimization of hybrid fibre system also should consider a combination of micro and macro fibres. Recently, Shi, Pham, Hao and Hao [94] investigated the performance of micro basalt fibre, macro PP fibre and basalt-macro PP hybrid fibre-reinforced concrete and concluded that the hybrid fibre-reinforced concrete could take advantage of high reinforcement efficiency of basalt fibres in the compressive and flexural strengths and macro PP fibres in the

post-cracking response, therefore led to better performance of concrete reinforced with only a single type of fibres.

It is worth mentioning that structures are vulnerable to some natural hazards or accidents during their service life such as earthquake [101, 102], impacts under high velocity [103, 104] or blast loads [105, 106], etc. Material properties of concrete change under dynamic and quasi-static loads due to the strain rate effect, that both the compressive and tensile strengths increase with strain rate [107, 108]. However, most of the studies on FRC material properties focused on the performance of concrete under the quasi-static condition. Only a few researchers investigated the dynamic material properties of fibre-reinforced concrete. The split Hopkinson pressure bar (SHPB) apparatus is usually adopted to study the mechanical properties of concrete material under high strain rate [109]. Zhang, et al. [110] studied the dynamic compressive behaviour of concrete with different compressive strengths (C25, C35 and C45) reinforced by short basalt fibres (0%, 0.05%, 0.1%, 0.15%, 0.2%, 0.25%) by a 74 mm-diameter SHPB equipment. It was found that the dynamic compressive strength of both plain concrete and basalt FRC increased approximately linear with the logarithm of strain rate and the strain rate sensitivity of basalt FRC was slightly lower than plain concrete. Through comparing the influence of the concrete compressive strength grade, it can be concluded that with the increase of concrete grade from C25 to C45, the optimal fibre volume fraction increased from 0.1% to 0.15%. However, the addition of fibres did not always increase the strain rate sensitivity. Fu, et al. [111] studied the influences of micro basalt and micro PP fibres on the dynamic compressive strength of concrete under strain rates of 20-140 s⁻¹. The authors found that the dynamic compressive strength of 0.1% hybrid micro basalt-PFRC was greater than that of single type FRC given the same volume fraction and plain concrete. Besides, hybridization of micro basalt and micro PP fibres significantly improved the strain rate effect of concrete (from 1.2 to 1.9 in the slope of the DIF vs strain rate curve). There have been very limited studies of the mechanical properties of hybrid fibres, particularly the dynamic mechanical properties. The influences of macro PP fibres and hybrid fibres containing macro PP fibres on the dynamic compressive strength are still unknown although macro PP fibres have been widely used in different concrete infrastructure.

On the other hand, although adding fibres improves the dynamic compressive strength of fibre-reinforced concrete, the main purpose of addition of fibres was to improve the tensile behaviour, post-cracking strength and energy absorption of concrete [112, 113]. Thus, understanding the influence of fibres on the dynamic tensile strength of concrete was more crucial. Hao and Hao

[114] conducted dynamic splitting tensile tests on spiral-shaped steel fibres in volume fraction ranging from 0.5% to 2%. The authors reported that fibres improved the tensile strength of concrete under both static and dynamic loadings and the strain rate sensitivity increased with the fibre content. Besides, due to the fibre-bridging effect, crack opening of FRC was much smaller than plain concrete. However, research on the dynamic tensile properties of fibre-reinforced concrete is still very limited. The influences of macro PP fibres and hybrid fibres containing macro PP fibres on the dynamic tensile strength are still unknown and need be investigated.

In this dissertation, the compressive and splitting tensile strengths of macro PP-micro basalt hybrid fibre-reinforced concrete under quasi-static and dynamic loadings were investigated by servo-hydraulic test machine and Ø100 mm SHPB equipment, respectively. The influences of strain rate on the dynamic compressive strength were analyzed by the stress-strain curves and while that on the dynamic splitting tensile strength was analyzed by crack mouth opening displacement (CMOD). The strain-rate effect on the compressive and splitting tensile strengths of the plain concrete and FRC is discussed. Empirical formulas of DIF with respect to strain rate for the compressive and tensile strength were derived for predicting the dynamic strengths of FRC. Progressive failure and failure modes of plain concrete and FRC under dynamic compression and split tension were examined to explain the strain rate effect on the dynamic material strengths and the contributions of fibres in resisting the impact loads.

4.2. Materials and experimental methods

4.2.1 Concrete mix and fibre properties

This study was performed on high strength concrete with the target compressive strength of 60 MPa. Details of the mixture properties are shown in Table 4-1. The properties of raw materials are the same as chapter 2. In this dissertation, P10B01 (defined in Table 4-1) concrete and plain concrete were compared to examine the influence of hybrid fibre on compressive strength under static and dynamic loadings. macro PP fibres showed a minor influence on the compressive strength of FRC while they exhibited more significant influences on the tensile and flexural behaviours. Therefore, only one type of FRC (P10B01) was investigated under compression tests while two types of FRC (P10B01 and P20B01) were examined under tensile tests.

Table 4-1. C60 concrete mix design (kg/m³)

Mix	Portland cement	Sand	Coarse aggregates	Water	Basalt Volume fraction	Macro PP volume fraction
PC	521	500	1151	229	0	0
P10B01	521	500	1151	229	0.1%	1%
P20B01	521	500	1151	229	0.1%	2%

4.2.2. Sample preparation

All aggregates were maintained in a saturated-surface-dry state before mixing for minimising strength fluctuation in different batches due to change of water-cement ratio. A 70L pan mixer was used with coarse aggregates, sand, cement, fibres placed in order. Water was lately added until fibres were distributed evenly in the mix. After further three minutes mixing, fresh concrete was poured into moulds on a vibration table and vibrated until there was barely entrapped air bubbles ring to the surface. The specimens were placed in a 23 °C water storage tank for 28 days after being demoulded.

The size of the cylinder specimen for static loading tests was $\phi 150 \times 300$ mm. According to the previous study [115], the thickness of specimens for dynamic tests should be equal to half of the diameter. Therefore, the size of specimens for compression tests under dynamic loadings was $\phi 74 \times 37$ mm cylinders. In order to achieve even distribution of fibres, concrete was cast into a large mould first with size of $1000 \times 240 \times 120$ mm and then $\phi 74 \times 37$ mm specimens were drilled and then ground. The size of specimens for splitting tensile tests was $\phi 100 \times 50$ mm cylinders for better wave signal capture. These $\phi 100 \times 50$ mm cylinders were drilled out from a large concrete sample of $800 \times 300 \times 200$ mm. In the present study, 15 specimens were prepared for the static compressive and splitting tests and 100 specimens for the dynamic compressive and splitting tensile tests.

4.2.3. Test methods and equipment details

4.2.3.1 Quasi-static compressive tests

The quasi-static compressive tests were conducted on the specimens with dimensions of $\phi 150 \times 300$ mm in accordance with ASTM C39 [30]. The large size of specimens was chosen for better fibre distribution. Prior to the tests, the cylinder top was capped with Sulphur mortar to

get even flat contact with the loading plate surface. The axial loading was applied at 0.18 MPa/s by a hydraulic test machine to achieve a quasi-static strain rate at approximately $2 \times 10^{-5} \text{ s}^{-1}$.

4.2.3.2. Quasi-static split-tensile tests

The quasi-static split tensile tests were conducted on the specimens with dimensions of $\phi 100 \times 50 \text{ mm}$ to maintain a consistent size as specimens used in the dynamic split tensile tests. The method to use the same size specimens to derive more reliable DIF (ratio of dynamic strength to static strength) has been commonly adopted in the previous studies [116]. The setup for quasi-static splitting tensile tests is shown in Figure 4-1. The tests were carried out with the applied load at a speed of 0.5 mm/minute according to ASTM C496 [117] and the corresponding strain rate was approximately $8 \times 10^{-5} \text{ s}^{-1}$. Two linear variable differential transducers (LVDTs) were placed at the both sides of the specimens to record the lateral deformation. Crack mouth opening displacement (CMOD) was derived from the two LVDTs. To achieve uniform stress distribution in the specimens, plywood with a thickness of 3 mm was used in the gaps between specimens and loading plates. Besides, to accurately capture the CMOD, strain gauges were attached to the centre of specimens at the same horizontal position of LVDTs.

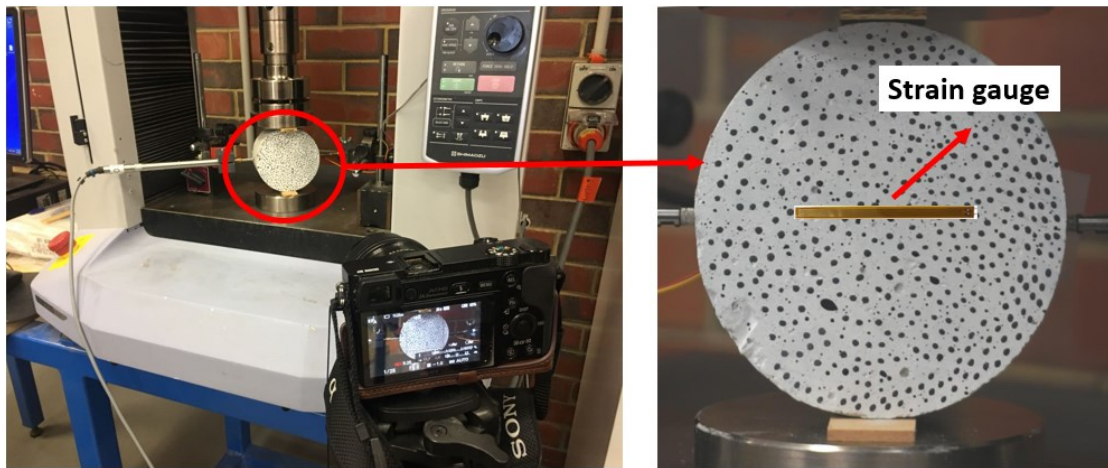


Figure 4-1. Testing setup for quasi-static splitting tensile tests

4.2.3.3. Dynamic compressive and splitting tensile strength tests and SHPB equipment

The dynamic compressive and splitting tensile tests were performed by using $\phi 100$ SHPB test equipment at Curtin University as shown in Figure 4-2. Five samples were tested under each strain rate for the dynamic compressive and splitting tensile tests. The SHPB consists of a

striker bar (0.3 m in length), an incident bar (5.5 m in length), a transmitted bar (3 m in length) and an absorption bar (1 m in length). All four bars are made of stainless steel with a density of 7800 kg/m^3 , Young's modulus of 240 GPa, and Poisson's ratio of 0.3. To get half-sine shaped incident wave a rubber wave shaper with the size of $\phi 20 \times 2 \text{ mm}$ was placed between the striker bar and incident bar. During the tests, the specimens supported by a foam column was placed between the incident bar and the transmitted bar tightly with petroleum jelly applied at the contact interface to minimize the frictional effect. Strain rate in the specimens was controlled by changing the launch pressure in the pressure chamber and the strain was captured by two semiconductor strain gauges with a high gauge factor of 80. To capture the fracture development of specimen, a high-speed camera was used in this test with the sampling rate of 30,000 - 40,000 frames per second.

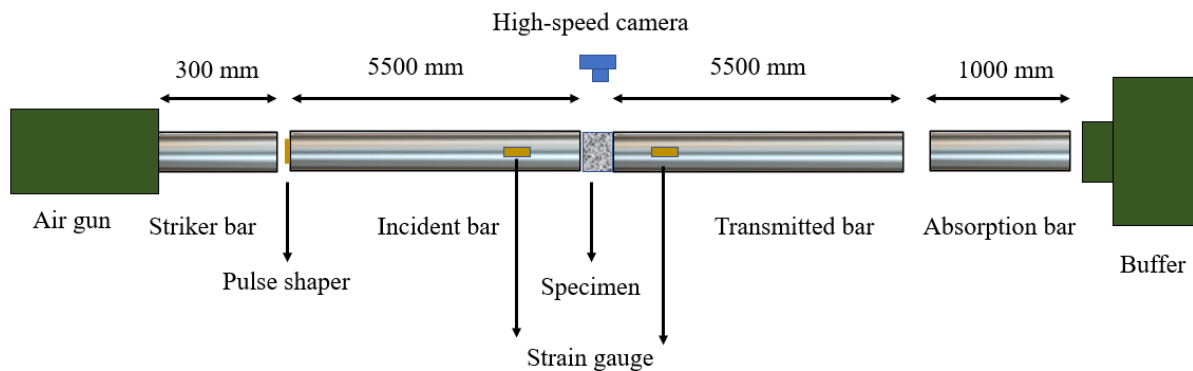


Figure 4-2. Setup of SHPB equipment

4.2.3.4. Digital image correlation (DIC) set-up and analysis

Due to large and quick deformation during the dynamic splitting tensile tests, LVDTs or other traditional methods cannot be used to measure the CMOD of the samples. Therefore, only the non-contact method, the DIC technique was used. By tracking changes of each pixel block, DIC can measure displacements, strain, and CMOD of the sample surface. The accuracy of the DIC technique has been verified carefully with the measurement from strain gauges and presented in the previous studies [118, 119]. To make the DIC work effectively, adjacent pixel points need to have sufficient colour contrast. Thus, the surface of the samples was sprayed with white colour as the background and drawn speckle by black colour as shown in Figure 4-1. Besides, two high lumen LED lights were used to provide sufficient lights on the specimens under dynamic loading. In this dissertation, the DIC technique is mainly used to record the time histories of the CMOD. The frame rate of high-speed camera was set at 30,000 and 40,000 frames per second in the dynamic compression and splitting tension tests, respectively.

4.3 Results and discussions

4.3.1. Quasi-static compressive and splitting tensile tests

4.3.1.1. Quasi-static Compressive strength of plain concrete and hybrid FRC

Figure 4-3 shows the typical stress-strain curve of plain concrete and P10B01 FRC in the quasi-static compressive tests. Plain concrete showed brittle characteristic while P10B01 FRC exhibited ductile characteristics associated with bulging failure as observed in the previous study by Shi et al. [7]. The average compressive strength of P10B01 FRC increased by 11% compared with plain concrete (60.7 MPa versus 54.5 MPa), the average critical strain corresponding to the peak stress of P10B01 FRC also increased to 0.30%, which was about 36% higher than plain concrete of 0.22%. Although the residual strength of P10B01 concrete was only 6 MPa at the strain of 0.8%, fibres could still bridge cracked parts and keep the relative integrity of FRC specimen as shown in Figure 4-4. Besides, it can be seen that the addition of fibres had almost no influence on the Young's modulus of concrete (34.2 GPa).

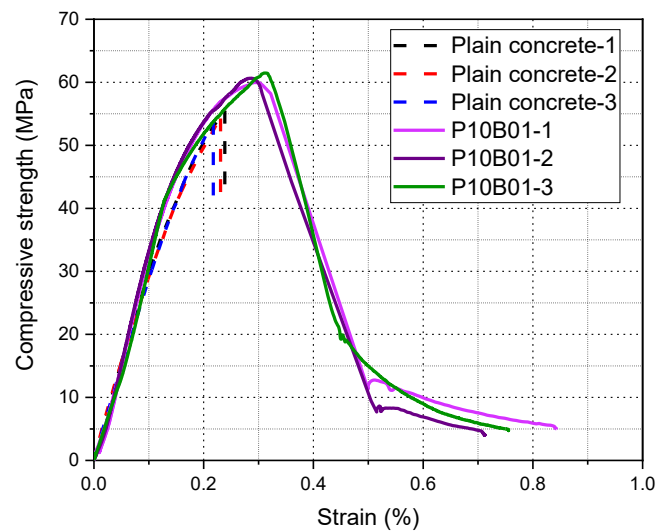


Figure 4-3. Comparison of quasi-static stress-strain relation of plain concrete and hybrid FRC

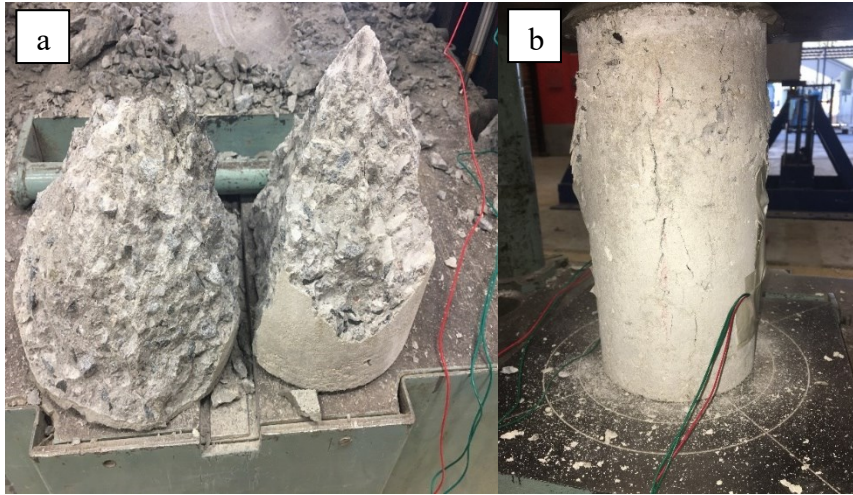


Figure 4-4. Failure patterns of (a) plain concrete and (b) P10B01 FRC

4.3.1.2. Quasi-static splitting tensile strength of plain concrete and hybrid FRC

The quasi-static splitting tensile strength of plain and hybrid FRC was calculated by the following formula:

$$\sigma = \frac{2P}{\pi LD} \quad (4-1)$$

where σ is the quasi-static splitting tensile strength in MPa, P is the maximum compressive load in N, L and D are the thickness and diameter of samples in mm, respectively.

In Table 4-2, the tensile strength of plain concrete under quasi-static loads was the lowest (3.95 MPa) compared with hybrid FRC. There was a significant improvement in the tensile strength of P10B01 (29%) which was higher than that of P20B01 (6%) compared to the plain concrete. Figure 4-5 shows the typical quasi-static splitting tensile load versus CMOD of plain concrete and hybrid FRC. It could be found that deformability of hybrid FRC was much larger than plain concrete, indicating ductile failure. On the other hand, plain concrete was completely broken at 0.003 mm of CMOD, showing extremely brittle failure. After the specimen cracked, the applied load of hybrid FRC suddenly dropped to 10.5 kN for P10B01 and 3.4 kN for P20B01 at about 2 mm of CMOD, respectively before increasing to the second peak. When the CMOD was greater than 4 mm, the applied load of P10B01 began to decrease slowly from 3.9 kN to 3.6 kN at 10 mm while the applied load of P20B01 increased from 9.5 kN to its third peak (18.6 kN) at 9.1 mm.

Adding hybrid fibres into concrete resulted in improvement of the splitting strength because the distributed fibres could reduce crack-tip stress concentration. Due to high Young's modulus and a large number of fibres, basalt fibre is effective in improving the tensile splitting strength. This observation agrees well with the results reported in the previous studies [94, 120]. On the other hand, due to the low Young's modulus and less number of fibres, macro PP fibres had marginal influence on the splitting tensile strength of concrete. However, once the volume fraction of PP fibres exceeds the threshold (between 1% - 2% in this dissertation), the quasi-static tensile strength decreases due to pores formed by fibre agglomeration [121]. For instance, increasing the volume fraction of macro PP fibre from 1% to 2% led to a reduction in the peak tensile strength (about 20%). Shi et al. [7] reported an improvement in the flexural strength of hybrid FRC as the volume fraction of macro PP increased from 0.3% to 0.7% and 1%, which is a low fibre volume fraction below the threshold. It is worth mentioning that the main contribution of macro PP fibres was to provide post-cracking strength. The performance of these specimens showed significant improvement of the post-peak behaviour with a higher volume fraction of macro PP fibres as expected.

Table 4-2. Quasi-static tensile splitting strength and energy absorption of plain concrete and hybrid FRC

Mix	Tensile strength (MPa)			Avg. Tensile strength (MPa)	Improvement (%)	Energy absorption until 10 mm (J)
PC	4.12	3.66	3.95	3.91	N/A	0.7
P10B01	4.61	5.13	5.40	5.05	29%	63
P20B01	4.10	4.21	4.19	4.15	6%	131

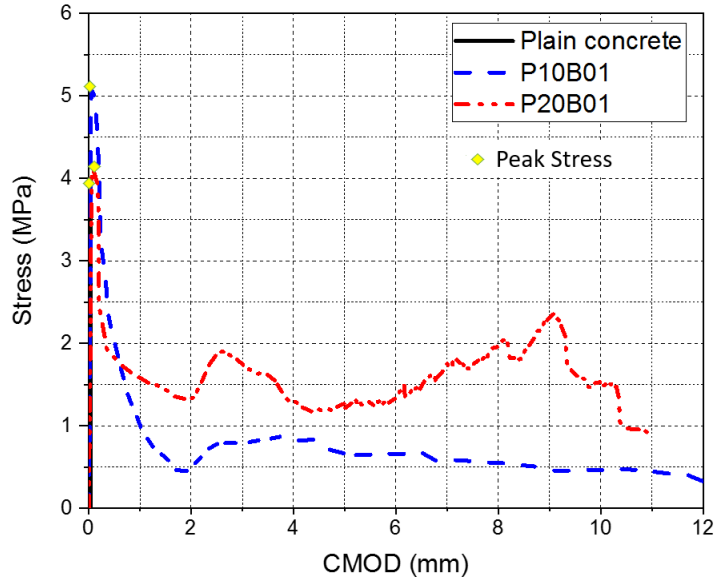


Figure 4-5. Typical quasi-static splitting tensile stress vs CMOD of plain concrete and hybrid FRC

The typical failure modes of plain concrete and hybrid FRC are presented in Figure 4-6. There was only one main crack in the middle of the specimens causing the failure. The specimens were split into two nearly semicircle as soon as the applied load reaching the maximum value. The plain concrete specimens broke into halves while the FRC specimens were damaged with significant cracking, but their ‘two halves’ were not fully separated and remained intact by the incorporated fibres even when the COMD was more than 10 mm, showing a strong bond between fibres and concrete matrix. During the tests, the crack developed with most of the fibres near the crack gradually being pullout from hybrid FRC specimens. Besides, rupture of fibres was also found in the upper part of the specimens while in the bottom part, fibres were still bridging concrete matrix. Compared with Specimen P10B01, Specimen P20B01 showed less damage and even concrete chips were still connected with concrete matrix by fibres, which indicated macro PP fibres played an important role in holding segments in cracked concrete and more macro PP fibres used, the more integrity cracked specimens were.

4.3.2. Dynamic compressive strength of plain and hybrid FRC

4.3.2.1 Validation the SHPB equipment

Prior to testing, the working condition of SHPB was checked by conducting a validation test without a specimen. The incident bar against the transmitted bar impact test was used to check the level of these two bars.

Figure 4-7 shows the amplified incident signal and transmitted signal of the validation tests. The incident signal was almost identical to the transmitted signal, which indicated that the ends of both bars were flat and parallel. After the incident bar struck the transmitted bar, there was no stress wave rebound back to the incident bar, which proved that the contact surfaces of the incident and transmission bars matched well.

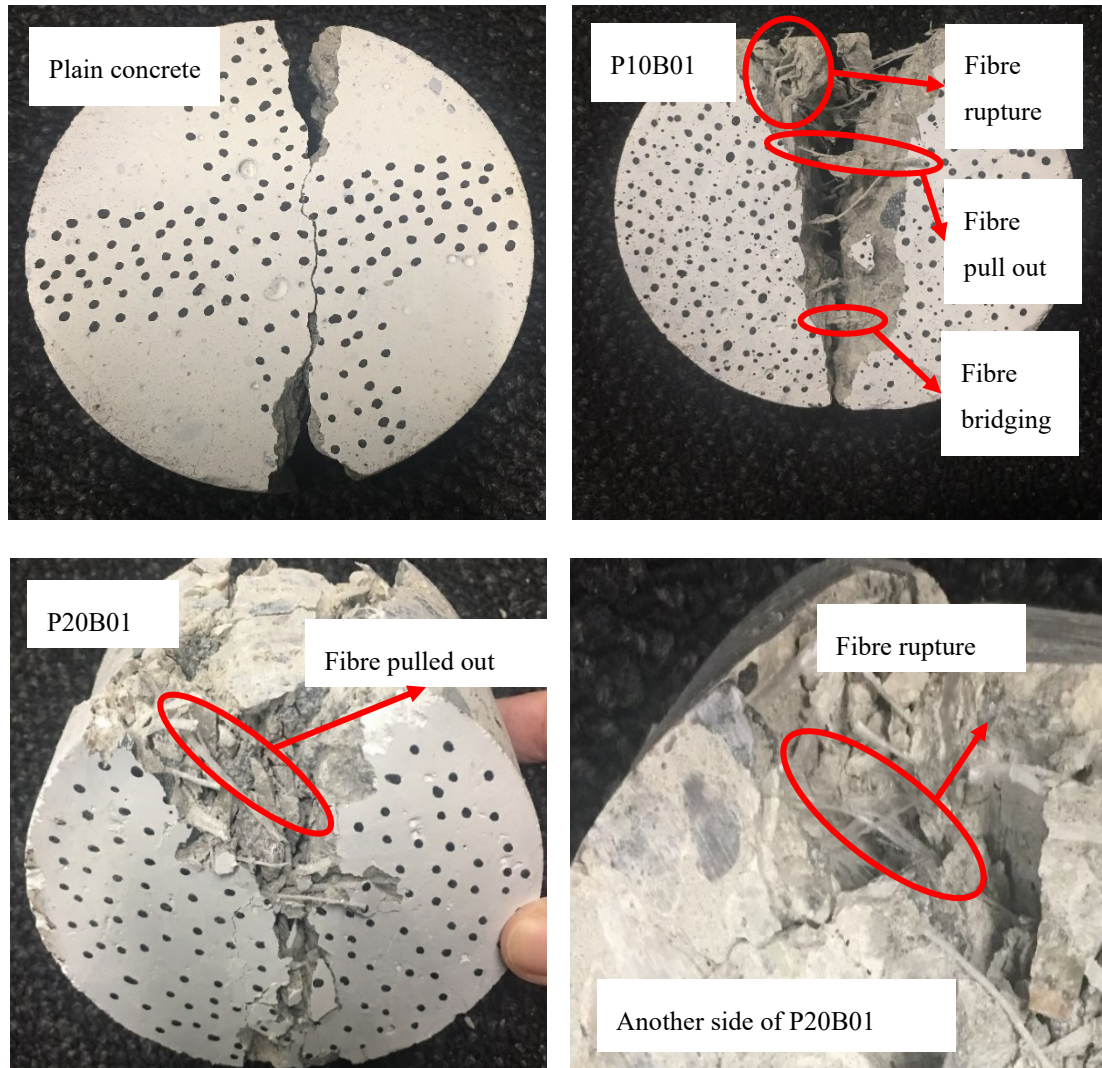


Figure 4-6. Typical failure modes of the specimens under quasi-static splitting tensile loading

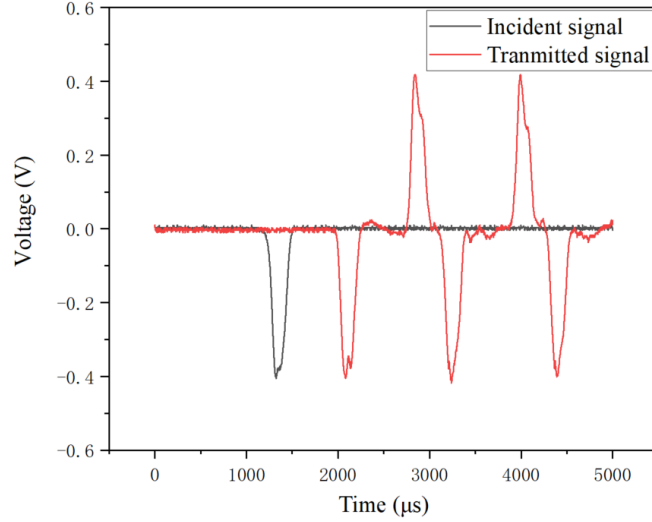


Figure 4-7. Validation of SHPB without a sample

4.3.2.2. Data processing and stress equilibrium check

The voltage signal data was acquired at 2.4 μs time interval by a quarter-bridge circuit connected to strain gauges attached on the incident bar and transmitted bar. The following formula was used to calculate the original strain from the voltage signal data:

$$\varepsilon = \frac{4V_0}{AMP \times V_{ex} \times GF} \quad (4-2)$$

where ε is the strain of the bar, V_0 is the output voltage data, V_{ex} is the input excitation voltage in the quarter-bridge circuit, AMP is magnification times in the amplifier, and GF is the gauge factor.

Besides, the data processing is based on the assumption of one-dimensional stress wave propagation in the bars. Accordingly, the stress is in the linear elastic state and the long bars have homogeneous, uniform and isotropic cross-section [122]. Based on the validity of the mentioned assumption, dynamic stress is proportional to the ratio of cross-sectional area (bars vs specimens). And the thickness of specimens has a direct influence on the strain rate of the dynamic compressive loading. The following three formulas can be used to determine the dynamic stress $\sigma(t)$, strain rate ($\dot{\varepsilon}$) and strain (ε) for the dynamic compression tests.

$$\sigma(t) = \frac{AE}{A_s} \times \varepsilon_t(t) \quad (4-3)$$

$$\dot{\varepsilon}(t) = \frac{2C_0}{L} \varepsilon_r(t) \quad (4-4)$$

$$\varepsilon(t) = \int_0^T \dot{\varepsilon}(t) dt \quad (4-5)$$

where A_E and A_S are the cross-sectional area of bar and specimen, respectively, C_o and L are the velocity of the longitudinal wave in the bar and the thickness of specimen, respectively.

For the stress equilibrium check, the sum of the incident stress wave (σ_i) and reflected stress wave (σ_r) should be equal to the transmitted stress wave (σ_t) as expressed in Equation 4-3. A typical stress equilibrium checks are shown in Figure 4-8. After removing the time lag of waves, it could be found that the transmitted stress matched well with the sum of the incident wave and reflected wave during the whole range of stress waves. The stress at two concrete-bar contact areas was nearly the same and the stress equilibrium was achieved for the reliability of results.

$$\sigma_t = \sigma_i + \sigma_r \quad (4-6)$$

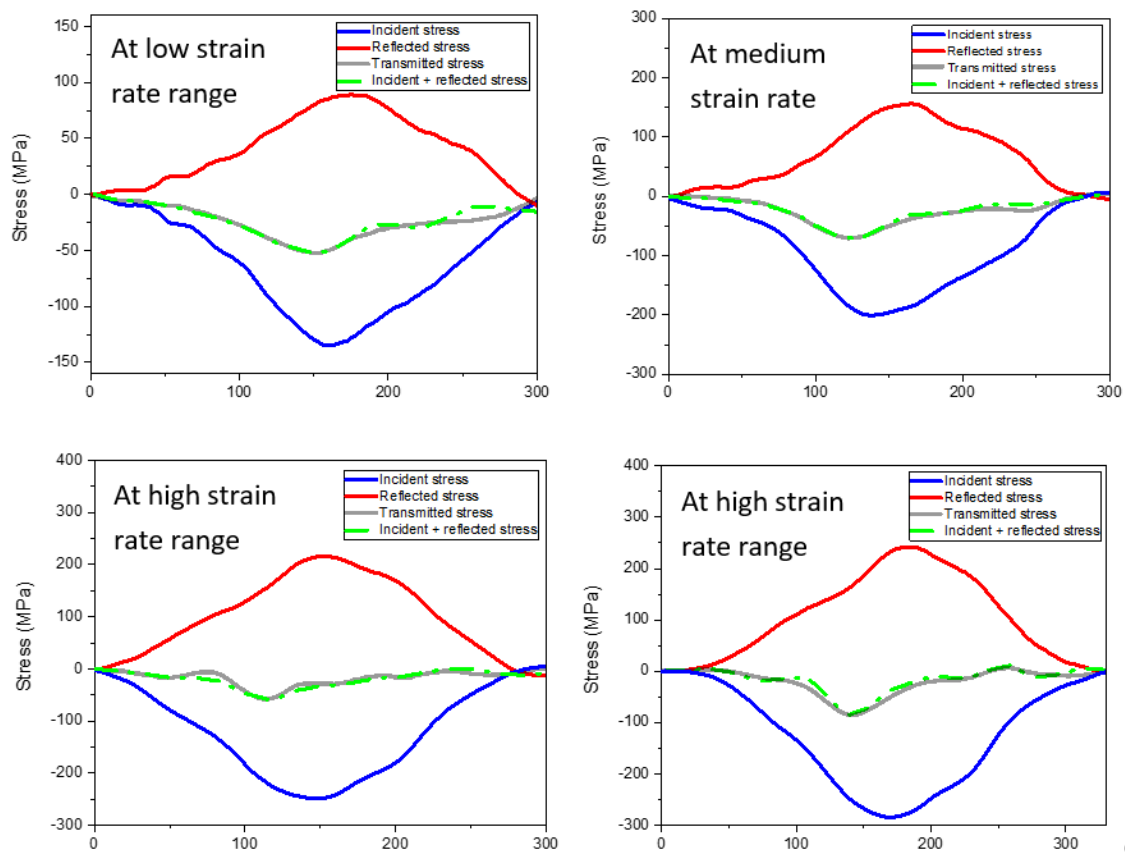


Figure 4-8. Typical dynamic stress-time relationship in the equilibrium condition

4.3.2.3 Dynamic stress-strain curves of plain concrete and hybrid FRC

The typical dynamic compressive stress-strain curves of plain and hybrid FRC associated with strain rate between 57 s^{-1} and 165 s^{-1} are shown in Figure 4-9. The dynamic compressive strength of P10B01 concrete was obviously higher than that of plain concrete. Besides, with an increase of strain rate, the slope of the stress-strain curve and axial strain corresponding to peak stress also increased. This phenomenon agreed well with results reported in the previous studies [123, 124]. At a similar strain rate, the increase in the compressive strength, axial strain at peak stress, and the ultimate strain were attributed to the addition of fibres. For example, the compressive strength, axial strain at peak stress, and ultimate strain of P10B01 concrete were 8%, 30%, and 46% higher than those of plain concrete at the strain rate of about 94 s^{-1} , respectively.

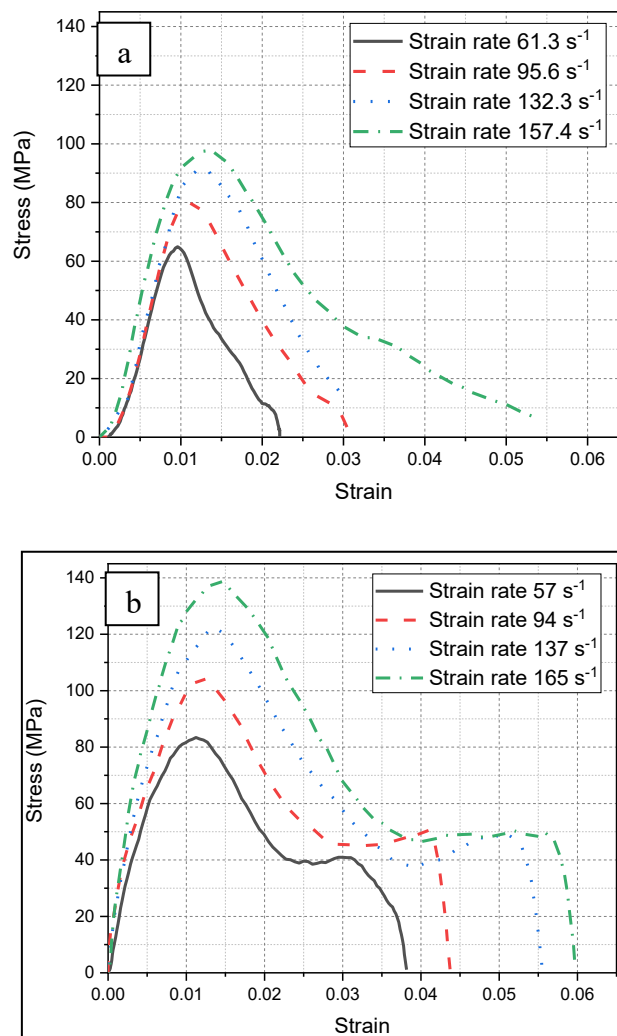


Figure 4-9. Stress-strain curve of (a) plain concrete and (b) P10B01 FRC under various strain rates

Figure 4-10 illustrates the influence of strain rate on the dynamic compressive strength of plain and P10B01 FRC and the corresponding data are listed in Table 4-3. All the specimens showed an increase in the compressive strength with strain rate and P10B01 FRC was slightly more sensitive to strain rate, which was also observed in the previous study [114]. The compressive dynamic increase factor (DIF_c) was used to quantify the influence of strain rate on the dynamic compressive strength. DIF_c is the ratio between the dynamic and static compressive strengths. The empirical relationships between dynamic compressive strength and strain rate were obtained by linear fitting the test data and are given as

$$DIF = 1.78 \ln(\dot{\epsilon}) - 1.93 \quad \text{For Plain concrete } (61 \leq \dot{\epsilon} \leq 157) \quad (4-7)$$

$$DIF = 2.16 \ln(\dot{\epsilon}) - 2.55 \quad \text{For Hybrid FRC } (57 \leq \dot{\epsilon} \leq 165) \quad (4-8)$$

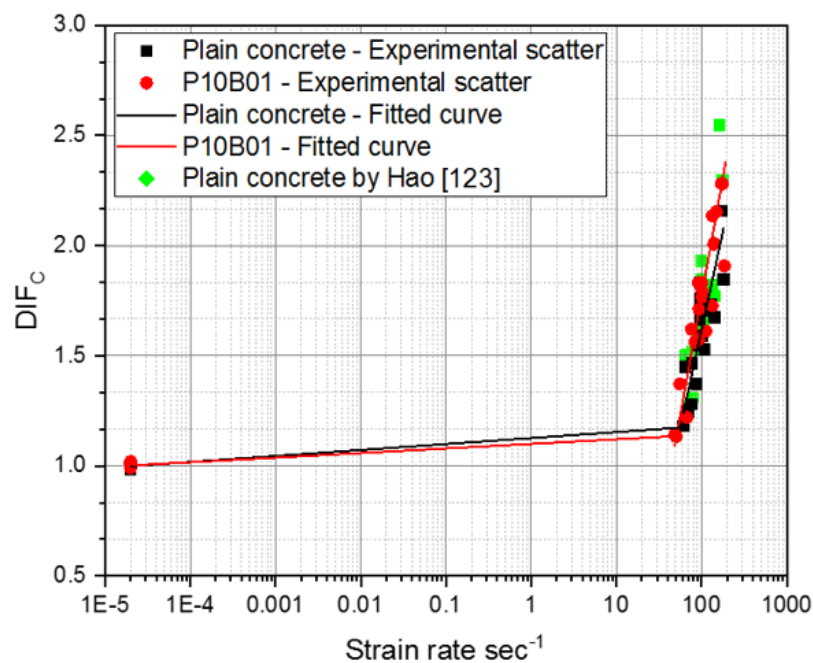


Figure 4-10. Relationship between the compressive DIF and strain rate of plain concrete and P10B01 concrete

4.3.2.4 Crack development processes of plain and hybrid FRC specimens

Figure 4-11 illustrates the failure process of the specimens with or without fibres at the strain rate about 50 s^{-1} . Initiation of cracks was observed from both ends of the specimens and propagated toward the middle part. This observation demonstrated that stress in specimen approximately achieved the equilibrium condition. At $T = 75 \mu\text{s}$ and $125 \mu\text{s}$, the number of cracks on the specimens was basically the same in the two groups. This observation agrees well

with the compression tests under quasi-static loads when the plain concrete and P10B01 FRC showed similar peak response. Afterwards, the hybrid FRC specimen performed better than the plain concrete. As expected, the plain concrete specimen showed total failure after $T = 375 \mu\text{s}$ while the hybrid FRC specimen remained intact and the number of cracks no longer increase even to the end of the tests. There was a smaller number of cracks in FRC at the end of the test because fibres in concrete enhanced its energy absorption capacity and bridged cracks. This phenomenon can be attributed to the fact that crack initiation required more energy than crack development [125]. Given similar impact energy, FRC absorbs more energy than that of plain concrete as the fibre debonding and fracture consumed additional energy, therefore less energy is available for crack initiation and thus fewer number of cracks and smaller crack width.

Table 4-3. Summary of dynamic compression test results of plain and P10B01 FRC

Plain concrete			P10B01 FRC		
Strain rate (s ⁻¹)	Dynamic compressive strength (MPa)	DIF	Strain rate (s ⁻¹)	Dynamic compressive strength (MPa)	DIF
61.3	64.8	1.2	50.5	68.9	1.1
69.2	68.2	1.2	48.7	69.4	1.1
77.2	70.2	1.3	67.0	74.2	1.2
86.8	75.2	1.4	55.5	83.4	1.4
64.1	79.4	1.5	84.0	95.0	1.6
77.2	80.4	1.5	92.9	95.7	1.6
109.6	83.7	1.5	112.8	98.0	1.6
87.7	84.7	1.6	93.5	104.1	1.7
100.6	87.2	1.6	133.4	105.0	1.7
96.2	91.0	1.7	100.9	107.5	1.8
142.6	91.8	1.7	101.1	109.2	1.8
126.7	93.5	1.7	91.8	111.4	1.8
130.8	94.9	1.7	100.1	111.4	1.8
95.8	96.4	1.8	139.4	122.0	2.0
96.4	100.3	1.8	141.5	122.2	2.0
181.4	101.2	1.9	134.0	129.8	2.1

168.6	118.3	2.2	149.9	131.0	2.2
170.4	118.3	2.2	176.0	138.6	2.3
157.4	170.4	3.1	170.7	138.7	2.3

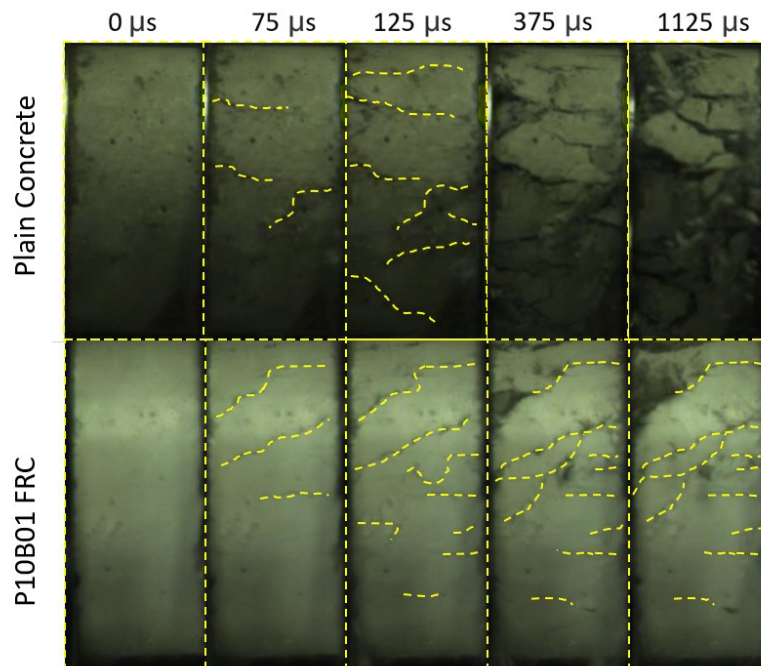


Figure 4-11. Progressive failure of plain concrete and P10B01 FRC under strain rate about 50 s^{-1}

Figure 4-12 shows the final failure of plain concrete and P10B01 FRC under various strain rates. For plain concrete, it broke into medium fragments at the strain rate of 48 s^{-1} . With strain rate rising to 65 s^{-1} , more small fragments were observed and the plain concrete sample was fully shattered into small fragments at the strain rate of 95 s^{-1} , which indicates the typical brittle failure pattern. This observation is also observed in the previous studies on plain concrete [122]. Meanwhile, P10B01 FRC demonstrated better impact resistance especially at the strain rate of 48 s^{-1} , where the specimen remained almost intact. At strain rate of 65 s^{-1} , there were two large fragments with micro cracks and numerous small fragments. With further increase of strain rate to 95 s^{-1} , hybrid FRC fully cracked like plain concrete with many numbers of small fragments. The improved performance for P10B01 FRC can be attributed to crack arresting ability of fibres and P10B01 FRC showed high ductility under strain rate of 50 s^{-1} .

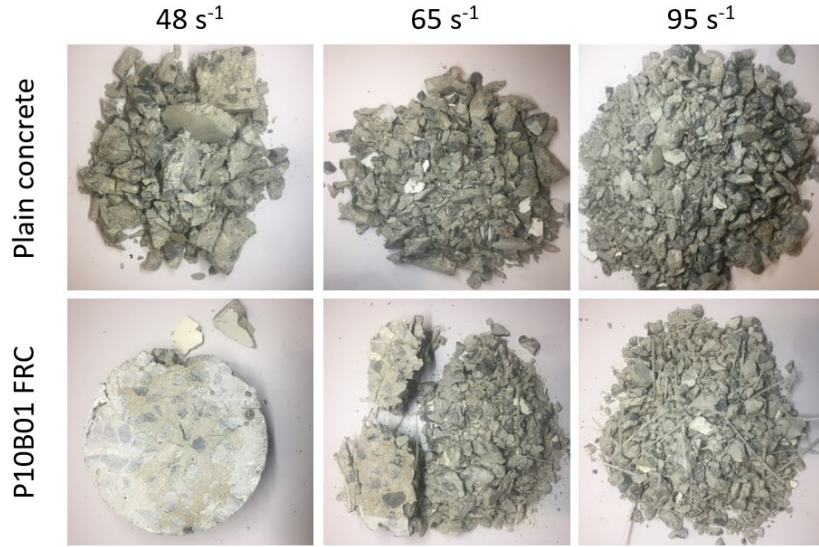


Figure 4-12. The final failure of concrete and P10B01 FRC specimens under compression impact at various strain rates

4.3.3. Dynamic splitting tensile strength of plain and hybrid FRC

4.3.3.1. Processing of the SHPB test data and stress equilibrium

Based on the validity of the mentioned assumption, dynamic stress (f_t) of cylindrical specimens in dynamic splitting tensile tests is proportional to the amplitude of strain of the transmitted bar $\varepsilon(t)$. The following formulas can be used to estimate the peak dynamic stress (f_t), loading rate ($\dot{\sigma}$) and strain rate ($\dot{\varepsilon}$) [126]:

$$f_t = \frac{2R_B^2 \times E_B}{L \times D} \times \varepsilon(t) \quad (4-9)$$

$$\dot{\sigma} = \frac{f_t}{t} \quad (4-10)$$

$$\dot{\varepsilon} = \frac{\dot{\sigma}}{E_C} \quad (4-11)$$

where R_B and E_B are the radius and modulus of elasticity of pressure bar, respectively, L and D are respectively the height and radius of the sample, t is the time lag between the begin and the peak of the transmitted stress wave, $\dot{\sigma}$ is the loading rate and E_C is Young's modulus of the sample.

To check the stress equilibrium in dynamic splitting tensile tests, the stress-time curves of transmitted wave and sum of incident and reflected waves are shown in Figure 4-13. As shown, the stress equilibrium is almost reached and the test data is therefore considered valid.

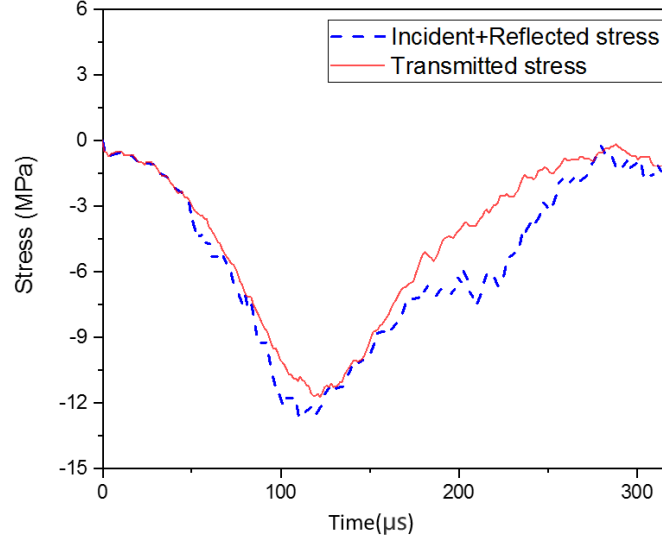


Figure 4-13. Typical stress equilibrium check for dynamic indirect tensile tests

4.3.3.2. Effect of strain rate on DIF_t and tensile strength characteristics of plain concrete and hybrid FRC

The dynamic increase factor (DIF_t) is usually used to quantify the increase of the dynamic splitting tensile strength in concrete by calculating the ratio of dynamic strength (f_{td}) at high strain rate to quasi-static strength (f_{ts}), as shown in the following equation:

$$DIF_t = \frac{f_{td}}{f_{ts}} \quad (4-12)$$

Figure 4-14 shows the influence of strain rate on the DIF_t of plain and hybrid FRC while the tested data are summarised in Table 4-4. All types of concrete showed an increase of the dynamic indirect tensile strength at higher strain rates. It is noted that the testing results from the previous study [114] are also plotted for comparison. The DIF_t reported by Hao [114] is higher than those in this dissertation probably because of different material tested in Hao [22] with the tensile strength of 2.04 MPa vs 3.91 MPa in this dissertation. The empirical relationships between the splitting tensile strength and strain rate were obtained by linear fitting the test data and are given as

$$DIF = 1.46 \ln(\dot{\epsilon}) + 1.46 \quad \text{For Plain concrete } (4.4 \leq \dot{\epsilon} \leq 28.4) \quad (4-13)$$

$$DIF = 1.27 \ln(\dot{\epsilon}) + 0.62 \quad \text{For P10B01 } (5.6 \leq \dot{\epsilon} \leq 33.4) \quad (4-14)$$

$$DIF = 3.11 \ln(\dot{\epsilon}) - 0.94 \quad \text{For P20B01 } (6.4 \leq \dot{\epsilon} \leq 27.2) \quad (4-15)$$

From the equation, it can be seen that the dynamic splitting tensile strength of plain concrete had approximately similar strain rate sensitivity to that of P10B01 FRC, which indicated that FRC with about 1% fibres had a marginal influence on the slope of DIF_t . This observation agrees well with the phenomenon reported in the previous study [114], where FRC with 1% steel fibre showed a minor influence on the slope of DIF_t . Besides, for the same strain rate, although dynamic strength of P10B01 FRC was higher than plain concrete, corresponding DIF_t became slightly lower than that of plain concrete, which indicated the FRC is less strain rate sensitive. It is interesting to note that after increasing the volume fraction of macro PP fibre to 2%, hybrid FRC became more sensitive to strain rate than plain concrete and P10B01 FRC. In addition to the contribution of fibres to the tensile resistance of FRC, the enhanced pull-out resistance under high loading rate was also attributed to this phenomenon. It has been reported that an increase in the loading rate would enhance the maximum pull-out load and the energy absorption of fibres [85, 127]. Banthia, et al. [128] indicated that under impact, FRC was found to become stronger and tougher, and higher fibre volume dosage could pronounce this improvement. Besides, the high volume fraction of fibres introduced more air content to the specimen, which also led the increase of sensitivity of strain rate [129]. Therefore, the increase of strain rate sensitivity of P20B01 FRC under dynamic splitting loading could be explained by the comprehensive combination of dynamic fibre pull-out response and higher air content.

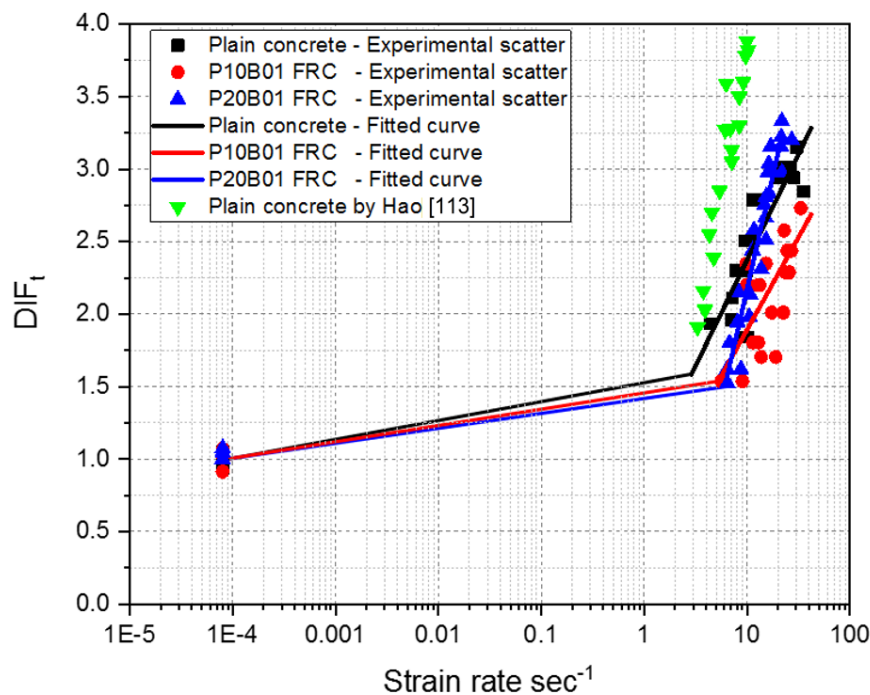


Figure 4-14. DIF_t versus strain rate relationship of plain concrete and hybrid FRC

Table 4-4. Summary of dynamic splitting tension test results of plain, P10B01 FRC and P20B01 FRC

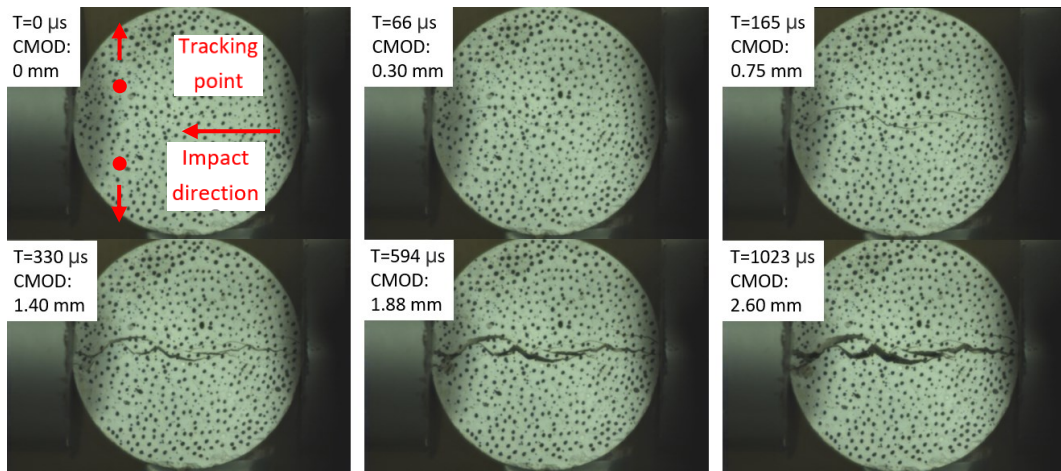
Plain concrete			P10B01 FRC			P20B01 FRC		
Strain rate (s ⁻¹)	Dynamic splitting tensile strength (MPa)	DIF _t	Strain rate (s ⁻¹)	Dynamic splitting tensile strength (MPa)	DIF _t	Strain rate (s ⁻¹)	Dynamic splitting tensile strength (MPa)	DIF _t
4.4	7.6	1.9	5.6	7.8	1.5	6.4	6.7	1.6
7.0	7.7	2.0	9.0	7.8	1.5	6.5	6.3	1.5
7.2	8.3	2.1	9.8	11.9	2.3	8.1	8.1	1.9
7.8	9.0	2.3	9.9	11.1	2.2	8.7	6.7	1.6
9.3	7.2	1.8	10.2	11.1	2.2	10.5	8.2	2.0
9.5	9.8	2.5	11.4	9.1	1.8	11.3	10.1	2.4
10.0	9.0	2.3	12.8	11.1	2.2	11.7	10.7	2.6
10.1	7.2	1.8	12.9	9.1	1.8	14.8	11.4	2.8
11.3	10.9	2.8	13.3	11.1	2.2	15.1	11.1	2.7
11.5	9.8	2.5	13.7	8.6	1.7	15.3	11.7	2.8
12.6	10.9	2.8	15.3	11.9	2.3	16.0	12.4	3.0
20.1	11.7	3.0	17.4	10.2	2.0	16.3	12.6	3.0
20.6	11.5	2.9	19.0	8.6	1.7	16.5	11.7	2.8
21.9	11.8	3.0	22.6	10.2	2.0	17.0	13.1	3.2
24.4	11.7	3.0	23.0	13.0	2.6	17.4	12.4	3.0
25.0	11.6	3.0	23.7	11.6	2.3	21.2	13.1	3.2
26.2	11.8	3.0	24.6	12.3	2.4	21.5	13.4	3.2
28.4	11.5	2.9	25.7	11.6	2.3	27.2	13.3	3.2

4.3.3.3. Crack development of plain and hybrid FRC

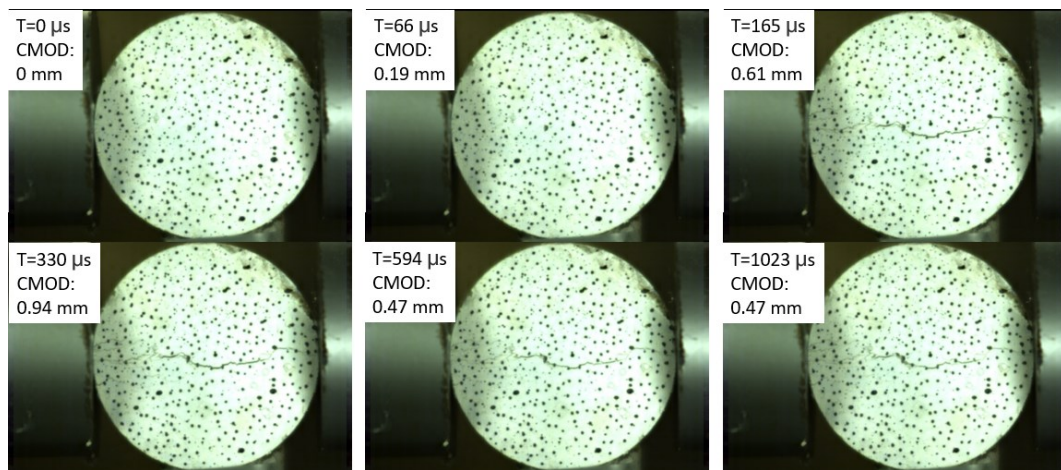
The high-speed camera was used to capture at every time instant at every 33 μs to observe the development of cracks of the specimens. In order to better compare with results from the previous study [126], the stress rate was used in this section instead of strain rate.

In all types of the specimens under stress rate of 180 GPa/s, the initial crack was found at the middle as shown in Figure 4-15. For plain concrete, a crack kept opening its width with time and the crack width was much larger than the hybrid FRC specimens. For Specimens P10B01, the crack width also increased with time until $T = 330 \mu\text{s}$, which was the widest crack (0.94 mm). After that, the crack width reduced to 0.47 mm at $T = 594 \mu\text{s}$ and remained at the same level at $T = 1023 \mu\text{s}$. The similar crack recovery phenomenon was also observed in P20B01 specimen, but the widest crack (0.30 mm) occurred earlier at $T = 165 \mu\text{s}$. When time continued to increase to 330 μs , the crack closed back to the level when $T = 66 \mu\text{s}$ and the crack width maintained the same value with time.

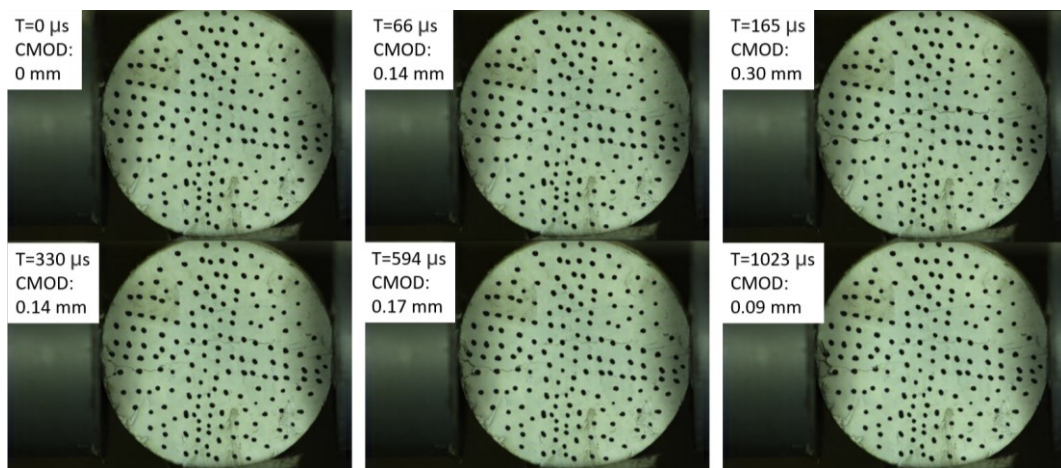
As can be seen, under relatively low dynamic loading, hybrid FRC showed significant crack control ability compared with plain concrete. Due to low Young's modulus of macro PP fibre, fibres would be significantly elongated at cracks before breaking. During impact, macro PP fibres would spring back to some extent because of their elastic property. Similar crack opening and closing during the impact tests were also reported in [36] with the spiral steel fibre-reinforced concrete. It was because of the strong bonding of spiral fibre with concrete matrix and its large deformation ability, spiral fibres were still capable of pulling back the cracked specimen. Young's modulus of macro PP fibres is higher than resilience modulus of spiral fibres, hybrid FRC thus also had even stronger crack width recovery ability than spiral steel fibres with high Young's modulus [126]. However, the similar phenomenon of crack recovery during dynamic splitting tension test was not found in other types of steel FRC [130] because of the variation of Young's modulus, bonding strength and deformation capability of the fibres used to reinforce concrete. Steel fibres have very high moduli and may break or debond when a crack opens as compared to that of macro PP fibres. Therefore, the crack recovery ability only found in low Young's modulus fibres, i.e. macro PP fibres and spiral steel fibres. This phenomenon requires more comprehensive investigation to unveil the crack recovery mechanism.



Plain concrete (180 GPa/s)



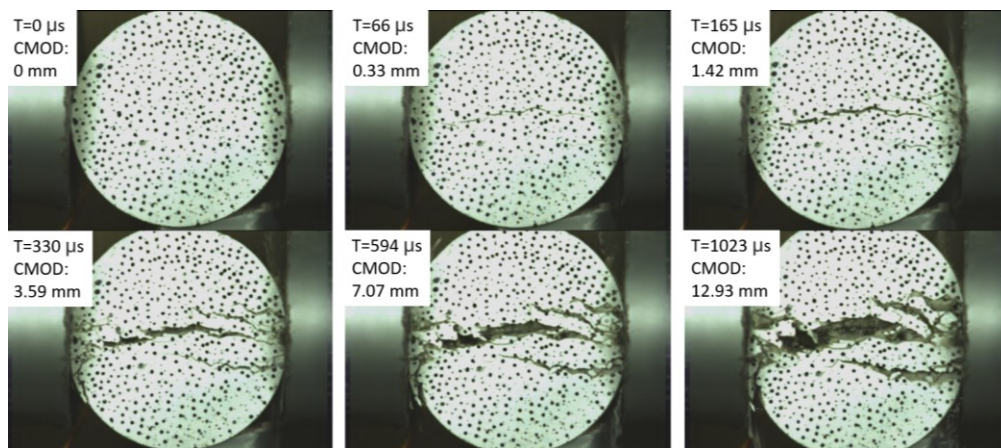
P10B01 (180 GPa/s)



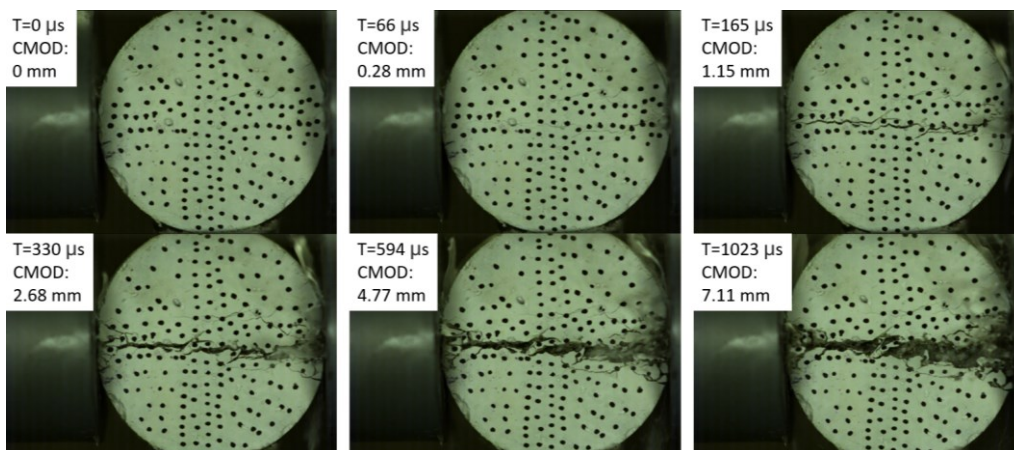
P20B01 (180 GPa/s)

Figure 4-15. Crack development of plain and hybrid FRC specimens under the stress rate of 180 GPa/s

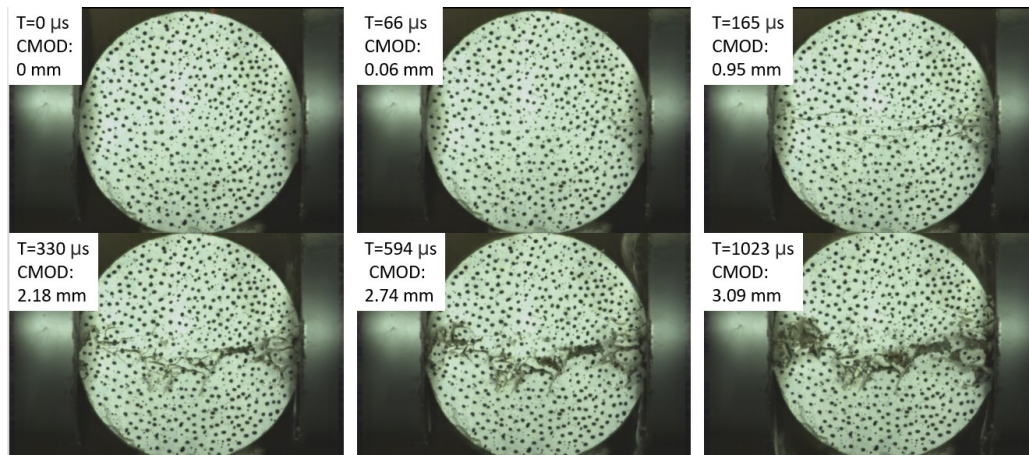
Figure 4-16 shows the failure processes of plain and hybrid FRC under higher stress rate of 310 GPa/s. The CMOD of plain concrete increased gradually to 12.93 mm at 1023 μ s. During the same period, the CMOD of specimen P10B01 was smaller (7.11 mm) than plain concrete, which indicated that hybrid fibre could slow and mitigate the crack widening. When the content of macro PP fibre increased to 2%, this ability could be further enhanced, e.g. the CMOD of specimen P20B01 was 3.09 mm at 1023 μ s. Besides, through comparing the CMOD of the three groups of specimens at $T = 165 \mu$ s, it could be found that the COMD of specimens P10B01 and P20B01 was 81% and 67% of that of concrete, respectively. However, when $T = 1023 \mu$ s, the COMD of P10B01 and P20B01 decreased to 55% and 24% compared with plain concrete, respectively. This observation demonstrated that roles of fibre in concrete collapse resistance after dynamic impact was more significant at relatively large cracks.



Plain concrete (310 GPa/s)



P10B01 (310 GPa/s)



P20B01 (310 GPa/s)

Figure 4-16. Crack development of plain and hybrid FRC specimens under the stress rate of 310 GPa/s

4.3.3.4. Development of CMOD of plain and hybrid FRC

In the dynamic splitting tensile tests, due to small contact area between the incident bar and specimens, a large portion of stress wave will rebound back to the incident bar and reverse its direction at the far end [126]. As a result, the incident stress wave will keep rebound and strike the damaged specimens for several times in a very short period. Although only the first voltage signal of the transmitted wave was used to analyze the dynamic splitting tensile strength. The post-cracking behaviour of samples could not be derived from strain gauges attached to the incident and transmitted bars. Fortunately, by using the DIC technique associated with the high-speed camera, the CMOD of the specimens in the post-cracking stage can be analysed and discussed in this section.

Figure 4-17 shows a comparison of the time history of the CMOD of plain and hybrid FRC under stress rate of 180 GPa/s. It can be found that the CMOD of plain concrete at 5 milliseconds was 7.82 mm which was much larger than P10B01 (0.63 mm) and P20B01 (0.07 mm). After being impacted by the incident bar, plain concrete was fully split into two parts and the upper parts kept moving away. Meanwhile, fibres in concrete could effectively control the development of crack width and maintain it at a low value with time, especially for Specimens P20B01. It is interesting to note that the upper and lower parts of cracked specimens even could be pulled back at 320 μ s and 180 μ s for Specimens P10B01 and P20B01, respectively. And the more macro PP fibres used, the earlier the two split parts of specimens were pulled back. This is attributed to the reason that macro PP fibres have lower Young's modulus and elastic modulus compared to concrete [93], which enables macro PP fibres partly spring back and pull

back the CMOD before breaking. During the time gap of each incident bar strike, macro PP fibres recovered their elastic elongation deformation, thus reduced the CMOD. It is noted that this phenomenon was not observed for FRC reinforced with steel fibres with high modulus except spiral steel fibres as mentioned previously.

Figure 4-18 compares the time histories of the CMOD of plain and hybrid FRC specimens under higher stress rate at 310 GPa/s. It can be found that the CMOD of plain concrete at 2 ms was 24.74 mm which was nearly 2.4 times of Specimen P10B01 (10.4 mm) and nearly 10 times of Specimen P20B01 (2.5 mm). The CMOD of plain concrete showed a quick and linear growth while that of Specimen P10B01 experienced a relatively slow increase. These two specimens completely failed into two halves. Meanwhile, the phenomenon of the CMOD recovery still could be observed in Specimen P20B01, e.g. the CMOD widened and then closed a couple of times. Compared with impact under the lower stress rate of 180 GPa/s, the ability of CMOD recovery from macro PP fibre was not observed in Specimen P10B01 and became less significant in Specimen P20B01 by impact under stress rate at 310 GPa/s. A similar observation about the recovery of CMOD was also reported by Khan, Hao and Hao [126] at the stress rate of 230 GPa/s. In this previous study, the CMOD recovery was from the elasticity of springs of spiral steel fibres rather than steel material itself. Therefore, larger fibre deformation was required for spiral steel fibres to exhibit the recovery phenomenon.

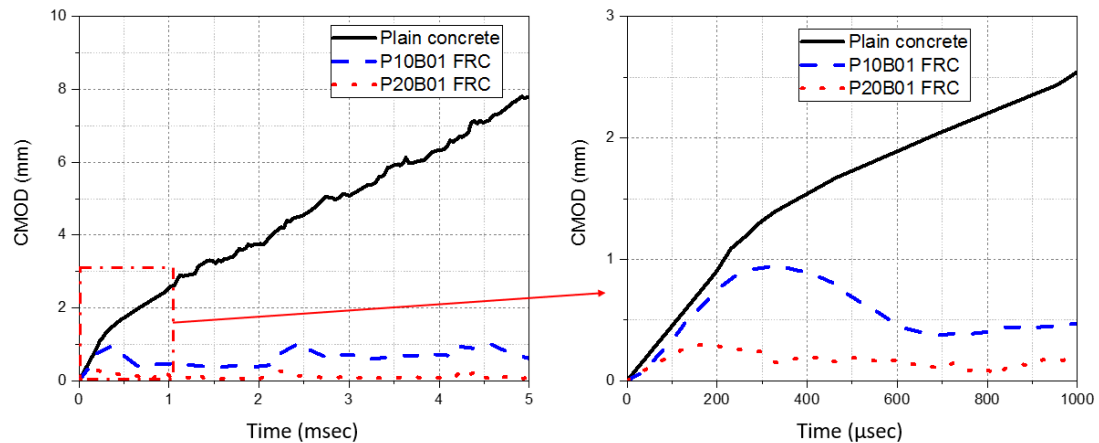


Figure 4-18. Time histories of the CMOD of plain and hybrid FRC specimens under stress rate of 180 GPa/s

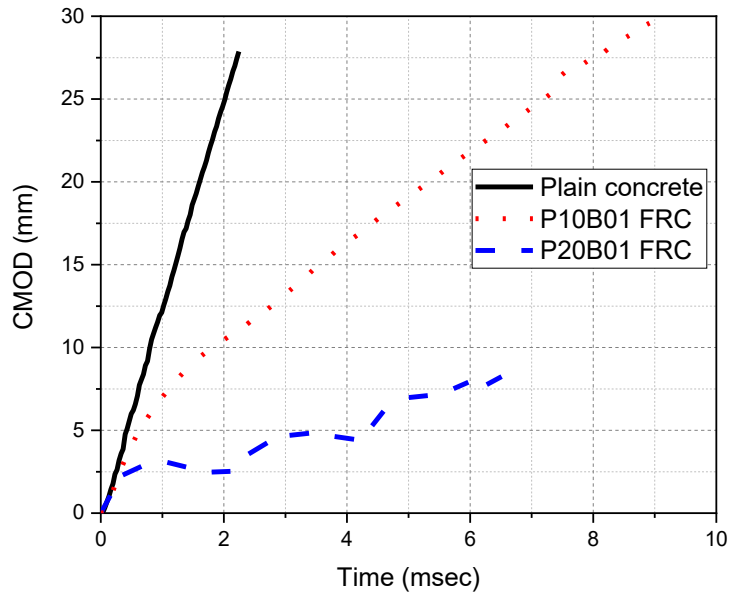


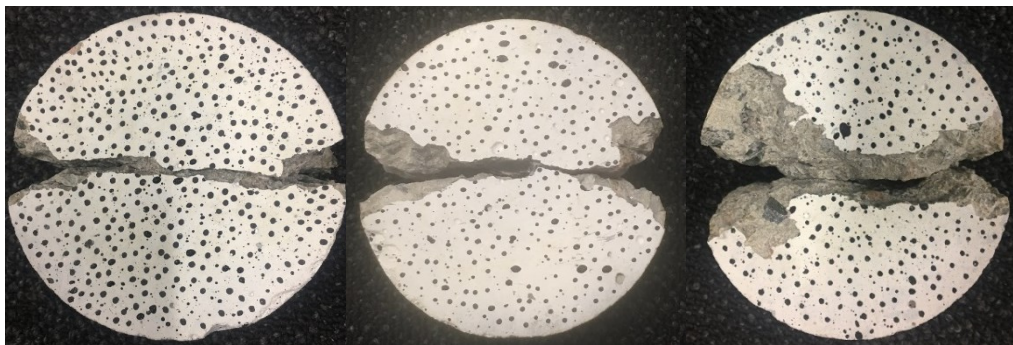
Figure 4-18. Time histories of CMOD of plain and hybrid FRC under stress rate of 310 GPa/s

4.3.3.5. Final failure patterns of plain and hybrid FRC specimens

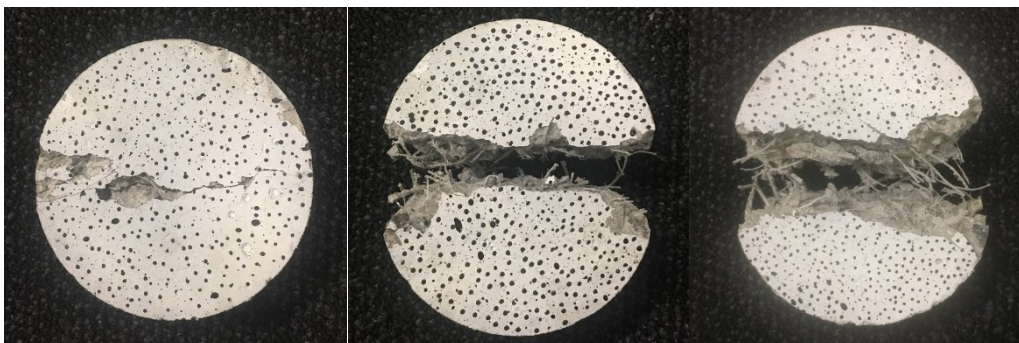
Figure 4-19 shows the typical failure patterns of plain concrete and hybrid FRC under three different stress rates of 180 GPa/s, 205 GPa/s, and 720 GPa/s. The stress rate and fibre dosage were the main factors governing the failure pattern. For plain concrete, due to no reinforcement, the specimens split apart directly as under quasi-static loadings. But with the increase of stress rate, damage degree of concrete specimens including triangle shape gap at two sides and the width of central cracking became larger. As uniform stress waves only went through specimens by specimen-bar contact area, which limited initiation and propagation of the centre crack in the dynamic splitting tensile tests. For Specimens P10B01, under stress rate of 180 GPa/s, there was only a minor crack in the centre of the specimen with some small fragments spalling from the surface. The specimen kept its integrity rather than splitting into two halves. After stress rate reaching 205 GPa/s or 720 GPa/s, the specimens still split into two parts as fibres were not strong enough to hold them together. The difference was that more fibre rupture was observed at the stress rate of 205 GPa/s than that at stress rate of 720 GPa/s. Fibres experienced elongation, fibre/matrix debonding, fibre rupture and fibre pullout from concrete under stress rate of 205 GPa/s, while at the stress rate of 720 GPa/s, fibre elongation, fibre/matrix debonding and fibre rupture was partly interrupted by matrix being fully crushed into small chips (or fine debris). As a result, some separated fibres in the middle part of the specimen were observed rather than being pulled out or ruptured because concrete matrix bonded to fibres was destroyed

by strong stress rate impact. This phenomenon was also reported in a previous study by Yoo and Kim [131] where the authors found that significant deterioration of concrete after fibre pullout under impact loads for FRC.

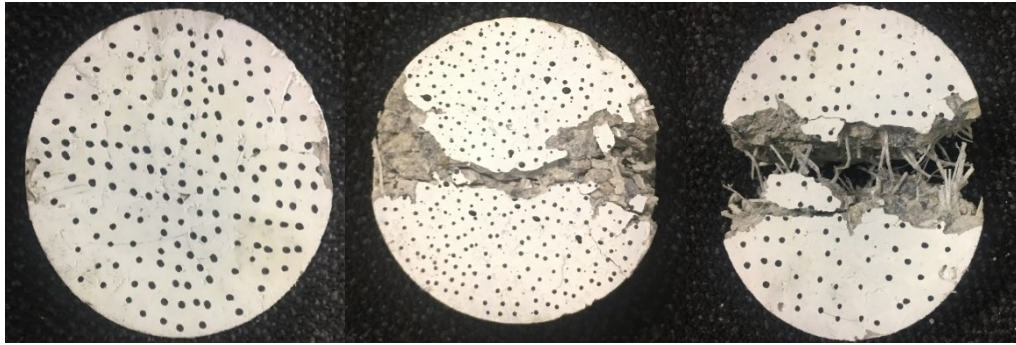
When the volume of macro PP fibres increased to 2%, Specimens P20B01 also remained almost intact and experienced less damage than Specimens P10B01 under the stress rate of 180 GPa/s. Only a very tiny hairline crack was observed in the middle part of specimen P20B01. When stress rate was 205 GPa/s, the split halves were tightly held together by fibres and no fibre rupture was observed. At this level of stress rate, only two sides of the samples close to the loading points suffered severe damage, the crack width of the specimen central part was less than 2 mm. This demonstrates the excellent capability of P20B01 in maintaining the structural integrity after experiencing dynamic splitting loadings. However, due to concrete matrix in the centre was completely damaged by the extensive loading at the stress rate of 720 GPa/s, the final failure pattern of Specimen P20B01 was similar to that of Specimen P10B01, except that there were some segments connected to the split parts of Specimen P20B01. In general, the hybrid fibres have shown great ability in resisting tensile stresses and maintaining the integrity and higher fibre volume fraction was more effective in resisting dynamic tensile cracks and stresses.



Plain concrete (180 GPa/s) Plain concrete (205 GPa/s) Plain concrete (720 GPa/s)



P10B01 (180 GPa/s) P10B01 (205 GPa/s) P10B01 (720 GPa/s)



P20B01 (180 GPa/s) P20B01 (205 GPa/s) P20B01 (720 GPa/s)

Figure 4-19. Failure patterns of plain and hybrid FRC specimens under different stress rates

4.4. Conclusion

This chapter investigated the dynamic compressive and splitting tensile properties of basalt-macro PP hybrid FRC by conducting SHPB tests. Hybrid FRC exhibited significant sensitivity to loading rate with the strain rate up to 170 s^{-1} in the dynamic compressive tests and to 40 s^{-1} in the dynamic splitting tensile tests. The main findings can be summarized as follows:

- In the quasi-static tests, the addition of 1% macro PP + 0.1% basalt fibres could slightly improve the compressive strength (11%) and splitting tensile strength (12%). The improvement of the quasi-static splitting tensile strength was not observed for high volume fraction of macro PP fibres (2%) due to excessive voids induced by adding fibres. Adding fibres could change the brittle failure of concrete to the ductile response.
- Through comparing different failure modes, the impact resistance of hybrid FRC under the compressive tests was improved especially at the strain rate of 50 s^{-1} , where FRC specimens could remain relatively intact whereas plain specimens fully shattered into fragments.
- The crack mouth opening displacement (CMOD) of hybrid FRC was significantly reduced (75.8% for P10B01 and 90.3 % for P20B01) at 2 milliseconds compared with plain concrete at same time instant under stress rate of 310 GPa/s. At lower dynamic stress rate (180 GPa/s), both Specimens P10B01 and P20B01 could remain intact with the CMOD of 0.6 mm and 0.08 mm at the middle of the specimens, respectively.
- Dynamic increase factor was derived from the test results and empirical formulae were proposed to describe DIF versus strain rate relations for both the dynamic compressive and indirect tensile tests. As compared to plain concrete, the strain rate sensitivity of P10B01 was slightly higher in the dynamic compressive tests and similar in the

dynamic splitting tensile tests. However, the high volume fraction of hybrid FRC P20B01 showed much more strain rate sensitivity in the dynamic splitting tensile tests.

In general, hybrid FRC has shown great performance in both static and dynamic loads. Various sizes and functions of hybrids FRC show good performance both at the peak and post-peak stages. Even though the integrity of concrete improves with increasing fibre volume fraction, the optimal fibre content for peak stress in the static split test is about 1% macro PP and 0.1% basalt fibres.

Chapter 5. Experimental study on the performance of ground slabs and beams reinforced with macro polypropylene fibre, steel Fibre and steel mesh

Abstract⁴

This chapter investigates the structural performance of concrete slabs and beams reinforced with different reinforcements. Ground slabs reinforced with steel meshes (A142), steel fibres (30 kg/m³) or macro PP fibres (6 kg/m³) were subjected to central concentrated loading until failure. The fracture behaviour of the slabs on the ground and the performance enhancement with the inclusion of steel and macro PP fibres are discussed through load-strain and load-deflection responses, slab deflection profile and crack patterns. There was a significant increase in the flexural strength of fibre or steel mesh reinforced slab on the ground. The flexural behaviour of fibre-reinforced concrete beams was also investigated to compare the effectiveness of using various fibres in beams and slabs. The flexural strength of fibre-reinforced beams was utilized to predict the load-carrying capacity of concrete ground slabs. Prediction based on beam tests and physical properties of steel mesh slightly overestimates the flexural strength of the ground slab by 12%, while the corresponding predictions of macro PP fibre-reinforced slab and steel fibre-reinforced slab were 45% and 24% higher than the experimental results. Compared to the plain concrete slab, the use of macro PP fibres, steel fibres and steel meshes can improve the flexural cracking strength by 28%, 47% and 79% respectively. Macro PP fibres compared favourably with steel fibres in terms of the post-cracking performance and energy absorption in ground slab applications.

5.1. Introduction

Concrete ground slabs have been widely used in industrial slabs, footpaths, highways and decorative floorboards. Concrete industrial slabs are required to bear heavy loads from operational movements of vehicles and stored materials [132]. An innovative solution for repair, rehabilitation and reconstruction of pavement called Precast Concrete Pavement Systems has

⁴ This chapter was extracted from the paper submitted to Structural Concrete, which is under review. The subsections were modified to follow the flow of the thesis. The full bibliographic citation of the paper is as follows:

Feng Shi, Thong M. Pham, Rabin Tuladhar, Zongcai Deng, Shi Yin, Hong Hao. Experimental Study on the Performance of Ground Slabs and Beams Reinforced with Macro Polypropylene Fibre, Steel Fibre and Steel Mesh. (under review)

been developed in recent years. It has many advantages, including long life expectancy with low maintenance cost and placement in a short time avoiding traffic congestion [133]. Decorative concrete floorboards are becoming popular in modern buildings [134]. They have similar surface patterns, skid resisting and fire safety like natural granite thin slabs.

No matter whether they are residential, industrial or commercial buildings, the performance of the ground slabs is affected by various conditions, including the compressive and tensile strengths of concrete and properties of soil underneath [6]. In order to obtain crack-free slab surfaces, it is important to provide slabs with sufficient load capacity and effective control of cracking and crack widths. Therefore, reinforcement bars or welded meshes are normally used to reinforce concrete slabs.

However, the use of steel bars and meshes is not only time- and labour- consuming, but also sometimes not suitable for ultra-thin slabs or mechanised production. Steel bars and meshes also cannot control surface cracking well because they need to be placed a distance from the surface. In recent years FRC ground slabs have obtained considerable momentum. Steel fibres and macro PP fibres are increasingly used to replace steel meshes in concrete slabs [112, 135]. Steel fibres can not only effectively improve the compressive and tensile strengths of concrete, but also prevent concrete cracking and improve toughness and post-cracking performance of concrete [51]. Since steel fibres are vulnerable to rusting and may cause cuts and bruises to the construction workers and users, macro PP fibres are increasingly becoming popular to reinforce concrete slabs. Macro PP fibres can efficiently control cracking and improve the toughness and post-cracking performance of concrete [93]. Moreover, macro PP fibres are easy to disperse in concrete, safe to handle and are corrosion resistant [136].

The majority of previous studies on the performance of fibre-reinforced concrete has focused on the flexural tests on concrete beams, which are used in the design analysis of ground slabs [26, 137-139]. However, the behaviour of flexural tests on beams may not truly represent the response of ground slabs. Only a few studies on fibre-reinforced concrete ground slabs have been reported so far [6]. Meanwhile, it is insufficient to use the results of the flexural tests to predict the performance of concrete ground slabs. This lack of results and understanding highlights the need for more studies on fibre-reinforced concrete ground slabs.

Jan Øverli [140] conducted an experimental and numerical investigation of a ground slab subjected to concentrated loading at the centre, the edges and the corners. The main goal was to study the formation of cracks on the top surface which is often of concern in this type of

structure. The slab had a square geometry with dimensions $3500 \times 3500 \times 120$ mm. The nonlinear behaviour of the slab was captured by performing nonlinear finite element analyses. The results indicated that drying shrinkage could cause severe cracking in slabs on the ground. Amir [6, 141] studied the mechanical and physical performance of steel and macro PP fibre-reinforced concrete ground slabs at an industrial scale. The loadings were carried out at different locations (centre, edges and corners) of a $6 \times 6 \times 0.15$ m fibre-reinforced concrete slab. The results showed that the applied loads at the punching shear failure of macro PP fibre-reinforced concrete slabs were comparable to those reported for the steel fibre-reinforced concrete slabs under similar conditions. Roesler et al. [142, 143] completed concentric loading tests on plain, steel fibre and macro PP fibre-reinforced concrete ground slabs. The slab dimensions were 2.2×2.2 m with a nominal thickness of 127 mm. The shape of the load-deflection curves indicated that the PP and the steel fibre-reinforced concrete slabs behaved similarly at different stages of cracking. Although PP fibres only slightly improved the tensile cracking load compared with the plain concrete slab, the flexural cracking load of the PP fibre slab (with the fibre ratio of 0.32% and 0.48% by volume) increased by 25% and 32% with respect to the reference specimen under the centre loading, respectively. It should be noted that the previous studies only compared the performance of plain concrete and FRC slabs while there is no direct and comprehensive comparison between plain concrete ground slab and those with steel meshes.

This dissertation carries out an experimental investigation on the structural performance of concrete ground slabs with various types of reinforcements. The performance of plain ground slab and slabs reinforced with steel meshes, steel fibres and macro PP fibres subjected to concentrated loading was examined. The fracture behaviour and the contribution of fibres to the performance of concrete slabs on the ground were discussed. In addition, the flexural behaviour of concrete beams with the same concrete mixes used for the slabs were tested and compared to the ground slabs to demonstrate the different effects of using fibres in beams and slabs. The test results demonstrated that the performance of FRC ground slabs was different from that of FRC beams, therefore the design analysis based on the beams might not give good results of ground slabs.

5.2. Methodology and procedures

5.2.1 Fibre, steel mesh and concrete mix

In this dissertation, PP fibres, steel fibres and steel meshes were used to reinforce the concrete slabs as shown in Figure 5-1. The properties of fibres and steel meshes are shown in Table 5-1. For A142 steel meshes, a diameter of 6 mm and the distance between the main wire and cross wire of 150 mm was used in this dissertation. In order to maintain an appropriate concrete cover, 30 mm wood bar chairs were used under the steel to raise it slightly off the bottom. Based on industry practice, standard mix designs for 40 MPa concrete was used in this dissertation (as shown in Table 5-2). This design is commonly used to construct concrete pavements. Fibres were added into the concrete batch plant and mixed with the concrete. The fibre-reinforced concrete was delivered by a standard concrete truck. The average slump was 100 mm based on AS 1012.3.1-2014 [144]. Four slabs with the dimension of $1800 \times 1800 \times 120$ mm were cast and vibrated by a vibration rod. As per AS 1012.8.1:2014 [145], concrete slabs, beams and cubes were removed from moulds after 24 hours. All the specimens were then cured in a standard moisture room for 28 days. The processes are shown in Figure 5-2.

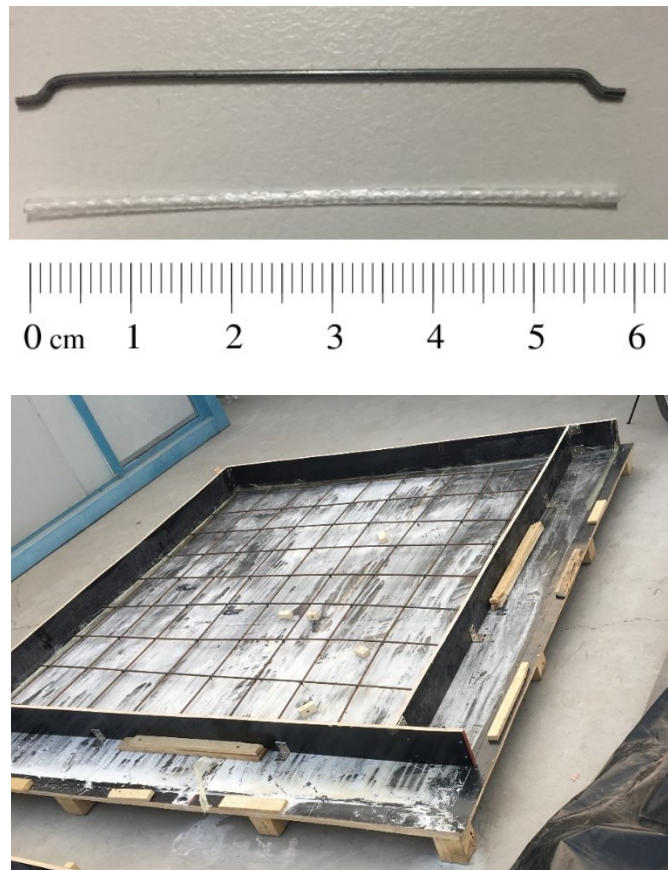


Figure 5-1. Macro PP fibres, steel fibres and steel meshes used in this dissertation

Table 5-1. Properties of fibres and steel mesh

Properties	Macro PP fibre	Steel fibre	Steel mesh
Diameter (mm)	0.6	0.3	6
Length (mm)	50	50	-
Length-to-diameter ratio	83	167	-
Tensile strength (MPa)	650	1500	300 (yield stress)-
Elastic modulus (GPa)	10	210	195
Surface and shape	Indented surface	Hooked-end	Deformed bar
Dosage (volume percentage)	6 kg/m ³ (0.7%)	30 kg/m ³ (0.4%)	One layer at bottom

Table 5-2. Concrete mix proportion

40 MPa Concrete	Material (kg/m ³)
Cement	186
Fly ash	134
0.075-0.3 mm Fine sand	350
0.6-4.75 mm Fine aggregates	610
6.7-9.5 mm Coarse aggregates	260
9.5-19 mm Coarse aggregates	690
Superplasticizer	2.8
Air-entraining admixture	70.4
Water	116





Figure 5-2. Concrete slab casting

5.2.2 Slab testing configuration

5.2.2.1 Subgrade conditions of testing facility

This dissertation aims to investigate the flexural performance of fibre-reinforced concrete ground slabs. As mentioned in the previous studies by Alani and Beckett [6], if the ground conditions are too stiff, it is hard to attain adequate bending of the slab. Therefore, the soil was filled into a soil containment box of $2.1 \times 2.1 \times 0.4$ m (as shown in Figure 5-3) as the subgrade. The modulus of subgrade reaction (κ) of near-to-surface properties of the subgrade is normally used in the thickness design of a slab. The κ of soil was about 0.05 N/mm^3 . The soil was compacted into a low-plasticity condition.



Figure 5-3. The compacted and low-plasticity soil in the soil containment box

5.2.3.2 Slab test setup

A loading was applied at the centre of 1800×1800 mm slabs with a nominal thickness of 120 mm placed on the soil in the soil box. The tests were performed by using a 1000 kN hydraulic actuator. Under the hydraulic actuator, there was a load cell recording the applied load. The load was applied to the slab through a steel plate ($100 \times 100 \times 10$ mm) and a rubber plate ($100 \times 100 \times 5$ mm) to counteract any uneven surface on the slabs, as shown in Figure 5-4. The load was applied with displacement control and the loading rate was 0.3 mm/min. In total, 20 linear variable differential transformers (LVDTs) and 8 strain gauges were placed at the top and bottom of each slab, as shown in Figure 5-5.

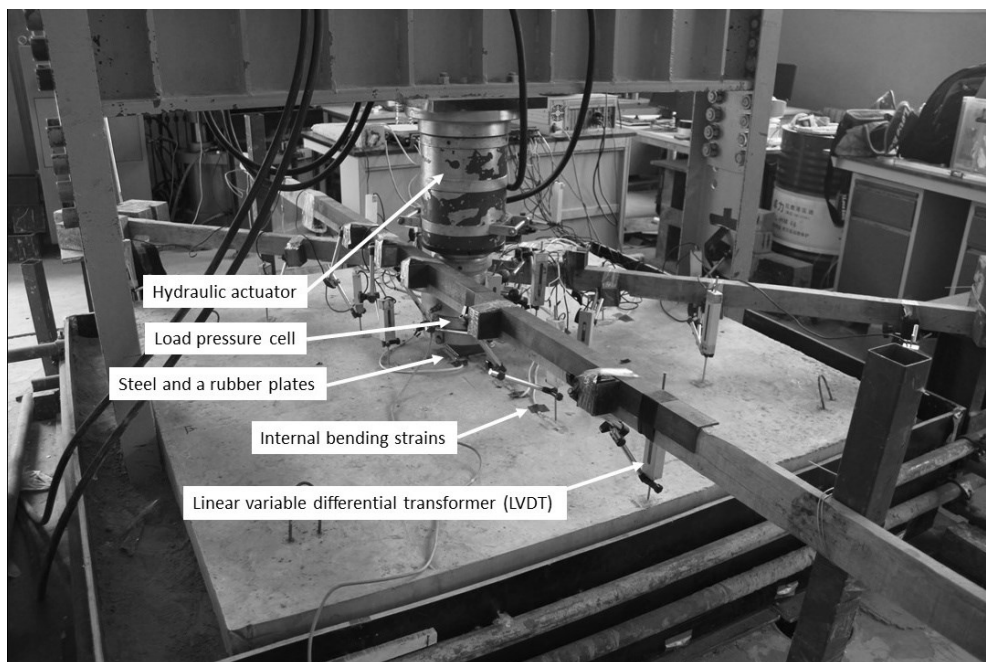


Figure 5-4. The layout of the ground slab and test rigs

5.2.3.3 Instrumentation and data acquisition system

The deflections of slabs, internal bending strain, and the applied load were measured during the testing until failure. Deflections of the slabs in different locations were monitored using totally 20 LVDTs at various locations across the slab surface as shown in Figure 5-5.

The tensile/compressive strain of the concrete slabs was recorded by 8 strain gauges (SGs) and their locations are shown in Figure 5-5. The compressive strain (SG 5 and 7 in cross directions) and tensile strain (SG 6 and 8 in cross directions) were measured by the strain gauges installed at the top and bottom of the slab next to the load plate, respectively. SGs 1 to 4 were used to

monitor strain on the top of the slab once the initial flexural cracking occurred on the top surface of the slab. These strain gauges were used to discuss/derive the point of crack initiation.

The comprehensive flexural performance of the slabs is discussed with respect to several parameters, including the visual crack observations, abrupt reductions of the applied load, and significant changes in the load-strain data. The tensile cracking load is defined when strain gauges begin displaying nonlinear behaviour [143]. The flexural cracking load is defined at the turning point in the load-deflection curve, considerable change in internal strain distribution and visual cracking on the slabs [142]. The ultimate load-carrying capacity is defined as the collapse load, which was either a punching shear failure or a circumferential crack on top of the slab near the load plate.

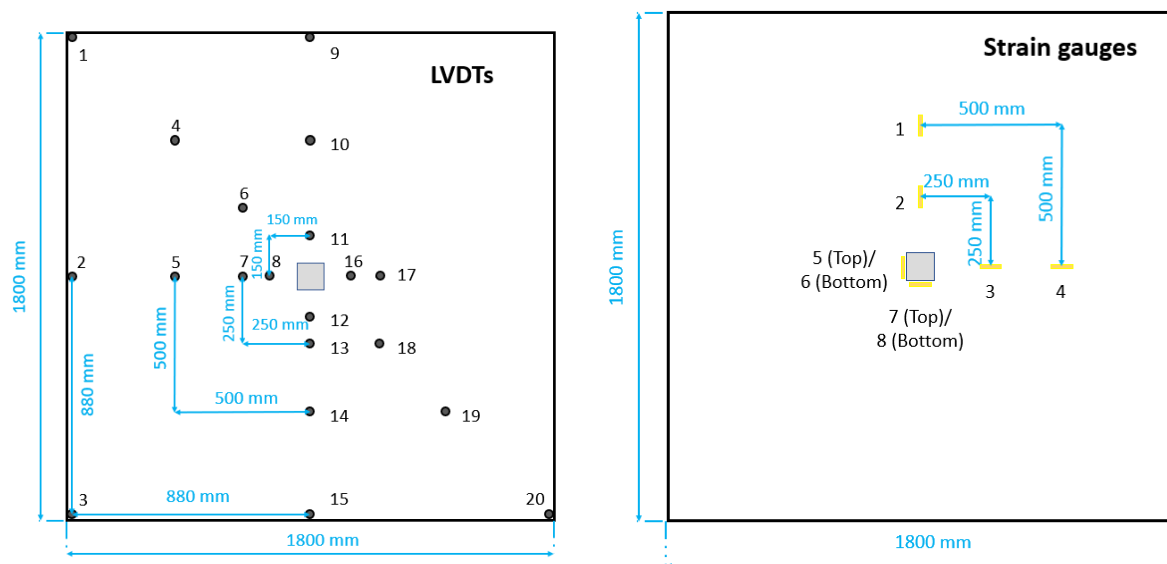


Figure 5-5. Locations of the LVDTs and strain gauges on each slab

5.2.3 Fibre-reinforced concrete material tests

5.2.3.1 Compression tests

Compression tests were performed on cube concrete specimens according to GB/T 50081-2002B [146]. Fibre-reinforced concrete cubes of $100 \times 100 \times 100$ mm were tested after curing in water for 28 days. The cube specimens were tested until failure by using the universal testing machine. The compressive strength of concrete with each type of fibre was the average value of four identical specimens.

5.2.3.2 Residual flexural strength with CMOD

The behaviour of FRC beams after the peak load was examined according to BS EN 14651-2005+A1-2007 [147]. The size of flexural beams was $150 \times 150 \times 600$ mm with a notch of 2 mm width and 25 mm length at the mid-span of each beam. The specimens were tested using three-point loading setup with a span of 500 mm. The crack mouth opening displacement (CMOD) was averaged from readings of two clip gauges installed at each side of the notch, as shown in Figure 5-6. The tests were set to displacement-controlled in which the CMOD increased at a constant rate of 0.05 mm/min. Three identical samples for each fibre type and two plain concrete beams as the control specimens were tested.

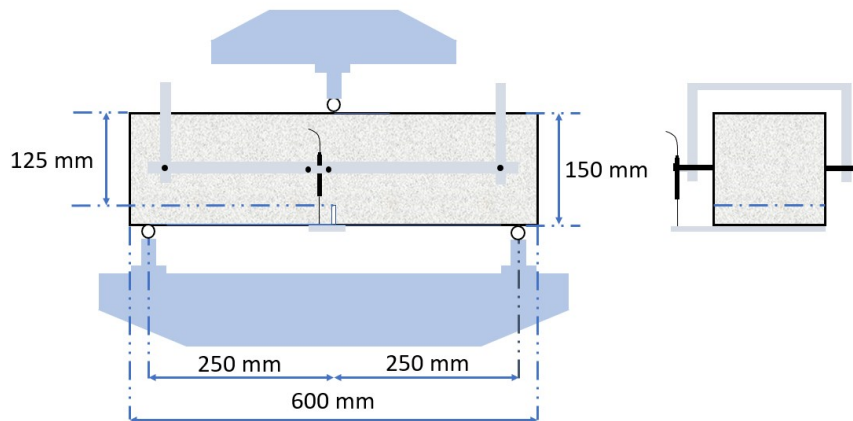


Figure 5-6. Experimental set up for determining load-CMOD relationships

5.2.3.3 Flexural performance of beams with four-point loading

The flexural performance of fibre-reinforced concrete beams was studied using flexural tests with four-point loading on the unnotched beams, according to ASTM C1609 [147]. The tested

beams had a square cross-section of 150×150 mm, a total length of 600 mm, and an effective span of 450 mm. The net deflection was measured using two LVDTs installed at the mid-span section of the concrete beams, as shown in Figure 5-7. The tests were displacement controlled to achieve a constant rate of net deflection at 0.1 mm/min. Three identical samples for each fibre type were tested. Two plain concrete beams were tested as the control specimens.

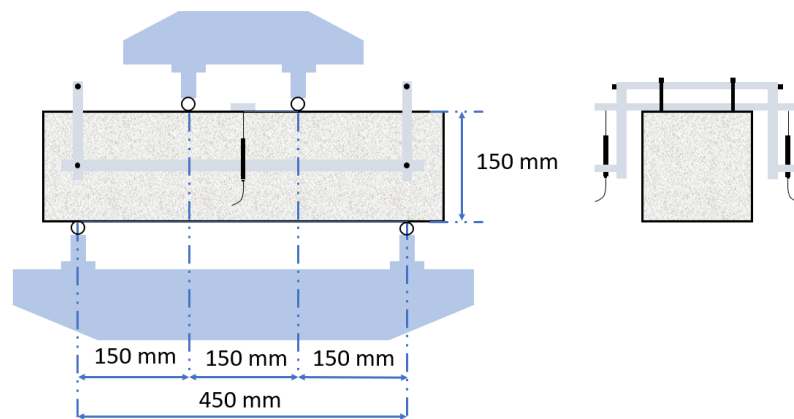


Figure 5-7. Experimental set up for determining load-deflection relationships

5.3. Results and discussion

The effects of macro PP and steel fibres on the flexural performance of concrete beams and ground slabs are not necessarily similar. Therefore, the flexural performance of notched beams, unnotched beams, and ground slabs are examined to evaluate the effectiveness of these two types of fibres on concrete beams vs ground slabs. Also, a comparison between FRC ground slabs vs the one reinforced with steel meshes is made in this section.

5.3.1 Compressive strength

Figure 5-8 shows the compressive strength of the fibre-reinforced concrete cubes. As can be seen, the addition of macro PP and steel fibres increased the compressive strength from 43.8 MPa to 45.7 MPa and 47.5 MPa, respectively. Both types of fibres could reduce crack-tip stress concentration by fibre acting as stress-transfer bridges. Since the steel fibres have higher elastic modulus (210 GPa) than concrete (22-38 GPa) and macro PP fibres (7 GPa) [148], steel fibres could carry more load in concrete than macro PP fibres at the same loading level. The experimental results agree well with findings from the previous studies [149].

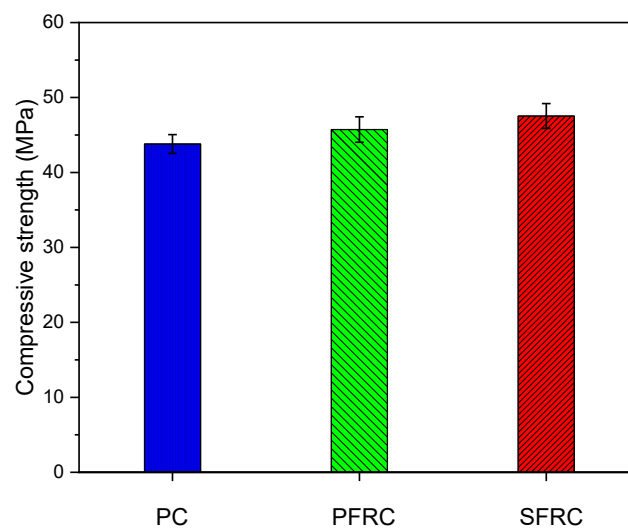


Figure 5-8. Compressive strength of the plain concrete and fibre-reinforced concrete

5.3.2 Post-cracking behaviour of fibre-reinforced concrete

Since the notched beam specimens are subjected to mid-point loading in the CMOD tests, a crack initiated at the notch-tip and propagated along the notch plane and hence, deformation was always localised at the notch-plane while the rest of the beam did not undergo significant inelastic deformation. This behaviour minimises the energy dissipated over the entire volume of the specimen and, therefore, all the energy absorbed can be directly attributed to fracture along the notch plane. Consequently, the energy dissipated in these tests can be directly correlated to material response (i.e. fibre reinforcements) [150].

Figure 5-9 and Table 5-3 show the post-cracking behaviour of fibre-reinforced concrete, which can be characterised by the residual flexural strength of the notched concrete beams. The steel fibre and macro PP fibre-reinforced concrete showed a slightly higher flexural strength than

that of plain concrete. With an increase of the CMOD, the applied loads of all the concrete beams reached the peak (around 16.5 kN), followed by a sudden drop at the CMOD around 0.5 mm. The load of plain concrete decreased to nearly 0 kN at the CMOD₁, while the applied loads of macro PP fibre and steel fibre-reinforced concrete decreased to about 7.3 kN and 12.7 kN on average at the CMOD₁, respectively. The SFRC further decreased to 11.4 kN at the CMOD₃, while the PFRC increased to 8.7 kN at the CMOD₃. The energy absorption can be estimated as the areas of the Load-CMOD diagrams. The average energy absorptions of macro PP fibre and steel fibre-reinforced concrete were 33.0 J and 48.5 J, respectively, while the plain concrete was only 4.0 J, which demonstrated a significant improvement (8-12 times) in the energy absorption of FRC as compared to plain concrete. The energy absorption of SFRC was about 50% higher than that of PFRC.

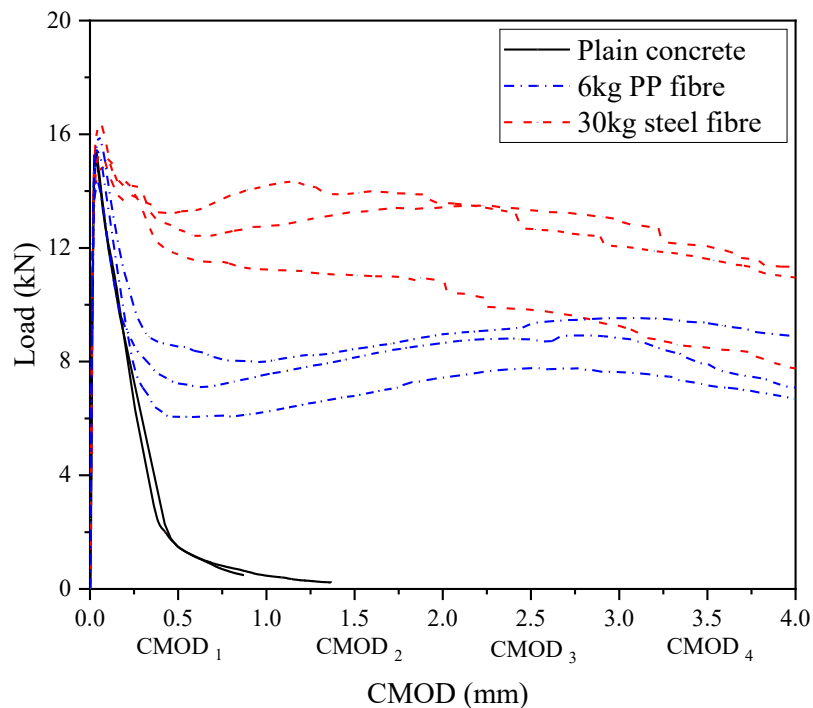


Figure 5-1. Load-CMOD diagrams of fibre-reinforced concrete

Table 5-3. Results of residual flexural strength of concrete

Sample		Flexural strength (MPa)	Residual flexural strength (MPa) at				Energy absorption (J)
			CMOD ₁ 0.5 mm	CMOD ₂ 1.5 mm	CMOD ₃ 2.5 mm	CMOD ₄ 3.5 mm	
Plain concrete	1	4.91	0.15	0	0	0	4.20
	2	4.89	0	0	0	0	3.83
30 kg/m ³ Steel fibre	1	4.89	4.54	4.36	3.86	3.51	52.18
	2	4.85	3.60	3.46	2.96	2.48	41.79
	3	5.24	4.09	4.30	4.16	3.63	51.66
6 kg/m ³ macro PP fibre	1	4.61	2.42	2.77	2.82	2.27	33.23
	2	4.98	2.00	2.38	2.44	2.14	29.32
	3	5.12	2.56	2.87	3.05	2.85	36.46

5.3.3 Flexural performance of fibre-reinforced concrete

The flexural performance was also studied by using four-point loading tests on the unnotched beams, which characterises the flexural performance of the whole fibre-reinforced concrete beams. According to ASTM C1609, the first peak strength, residual strength, toughness and equivalent flexural strength ratio are calculated. Toughness was calculated by the total area under the load-deflection curve up to deflection of 1/150 (3 mm) of the span length. The equivalent flexural strength ratio was calculated according to the following equation:

$$R_{e,3} = \frac{150 \times T_{150}^D}{f_1 \times b \times d^2} \quad (5-1)$$

where $R_{e,3}$ is the equivalent flexural strength ratio, T_{150}^D is the toughness in J, f_1 is the first peak strength in MPa, and b and d are the width and depth of specimens in mm, respectively, which are both 150 mm.

As shown in Figure 5-10, the SFRC beam had the highest first peak strength among all the concrete beams. The first peak strength was then followed by the second peak strength which was similar or even higher than the first peak strength, showing deflection-hardening performance. The PFRC beam had a slightly lower first peak strength than that of steel fibre-reinforced beam, but the first peak strength was followed by a sudden drop, showing deflection-softening behaviour. It is interesting to note that macro PP fibre-reinforced beam showed

comparable toughness with steel fibre-reinforced beam when the deflection increased to approximately 2-3 mm, as listed in Table 5-4. This phenomenon has shown that at large deformation, the performance of PFRC is as good as that of SFRC. Similar observations were also made in previous studies [37, 151].

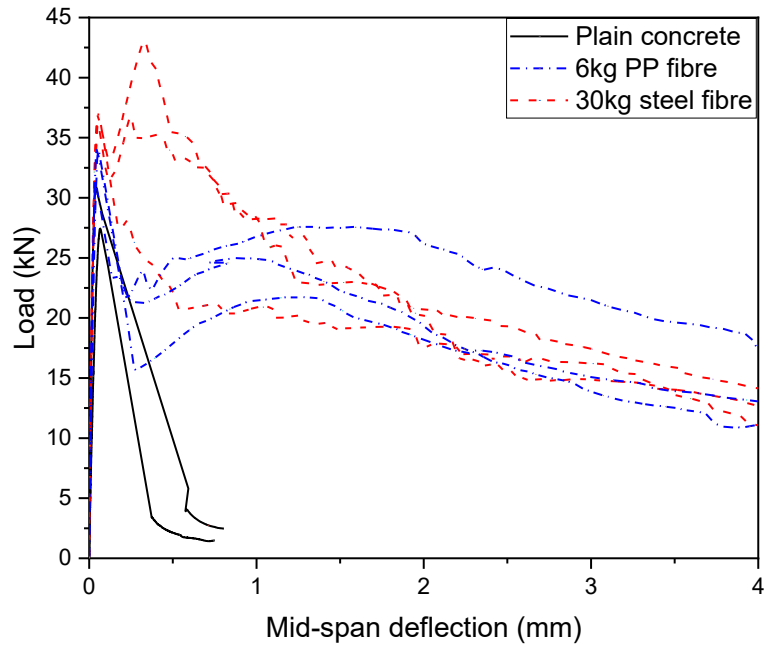


Figure 5-10. Load-deflection diagrams of plain and fibre-reinforced concrete beams

Table 5-4. Results of the flexural strength of concrete beam

Sample		First peak strength (MPa)	At the deflection of 3 mm		
			Residual strength (MPa)	Toughness (J)	Equivalent flexural strength ratio ($R_{e,3}$)
Plain concrete	1	3.66	0	6.724	8.2%
	2	4.13	0	10.670	11.5%
30 kg/m ³ Steel fibre	1	4.97	2.16	60.267	53.9%
	2	4.92	1.98	73.310	66.2%
	3	4.82	2.32	75.728	69.8%
6 kg/m ³ macro PP fibre	1	4.17	1.85	62.145	66.1%
	2	4.55	2.01	57.631	56.3%
	3	4.52	2.86	76.263	74.9%

5.3.4 Responses of ground slabs

5.3.4.1 Applied load-strain responses

In order to examine the crack initiation and propagation, the strain gauges were attached close to the loading point. Two strain gauges (SG 5 and 7) were positioned on the top concrete surface for the compressive strain while the tensile strain gauges (SG 6 and 8) were attached to the bottom surface of the slab. In this dissertation, cracks on the surface of slabs did not cross over SGs 1-4, so only the strains recorded at gauges (SG 5 to 8) will be discussed.

As shown in Figure 5-11, the tensile strain gauges at the bottom of plain concrete slab detected that the initial micro cracks produced at the load of 25 kN, where the strain began to display nonlinear behaviour. When the applied load increased to 45 kN, there was another turning point, indicating that the micro cracks were expanding to macro cracks and cracked slab could not bear the higher load with the increase of strain. For the PFRC slab, the macro cracks were observed at the applied load of 50 kN, and the applied load continued to increase with the tensile strain, indicating that fibres bridged the cracks and bore the applied load. It is interesting to note that only the load-strain curve of the plain concrete showed an obvious micro cracking point when initial micro cracks occurred, followed by the turning point when macro cracks formed. It is because without reinforcements, stress concentrated on the loading point could not be transferred by reinforcements. Therefore, micro cracks formed at a very low loading level. The fibre or steel mesh reinforcements can effectively mitigate the concentrated stress, thus no obvious turning point is shown when micro-cracks initiated and only macro cracks can be detected by the strain gauges.

The macro cracks of macro PP fibre-reinforced slab were observed at the applied load of 50 kN, which was slightly higher than that of plain concrete. The macro PP fibres had a lower elastic modulus (7 GPa) than that of concrete (20-30 GPa), thus the actions of macro PP fibres became prominent only after concrete experienced relatively large strain and deformation. Then fibres began to reinforce after concrete cracking and the applied load of PFRC slab continued to increase with the increase of strain after the macro cracking point, while the applied load of plain slab remained approximately flat. This observation of ground slab response was consistent with the results of flexural tests of concrete beams in Figure 5-9 and Figure 5-10, where PFRC beam had slightly higher flexural strength and first peak load than plain concrete beam. On the other hand, the elastic modulus of steel fibres was 210 GPa, which was much higher than those of macro PP fibres and plain concrete, thus steel fibres began to

significantly reinforce concrete at an early deformation stage. As a result, steel fibres reinforced concrete slab could bear a higher load (around 75 kN) before showing macro cracks. The applied load continued to increase with the increase of strain until macro cracking point due to the crack bridging effects of steel fibres.

The applied load of SMRC slab reached 100 kN before the tensile strain significantly increased. The results showed that using steel mesh was the most effective reinforcing method on bearing the applied load. However, once the load reached 100 kN, the concrete cover under the steel mesh totally cracked. The applied load did not increase while the strain rose significantly, which was very different from the other three ground slabs as shown in Figure 5-11.

All the slabs showed a similar increasing trend in load-compressive strain responses before strain reached about 500 microstrains as shown in Figure 5-11, indicating that fibre and mesh reinforcements had slight effects on the concrete compressive behaviour. When the compressive strain further increased to -3000, the rise (slope) of the applied load of the SMRC slab was highest followed by that of steel fibre-reinforced ground slab, indicating that the steel mesh and steel fibre-reinforced concrete slabs had higher stiffness than other slabs. The PFRC slab and plain concrete slab had a lower load increase and even load reduction, showing their lower stiffness. This observation is reasonable due to the low modulus of macro PP fibres as mentioned previously.

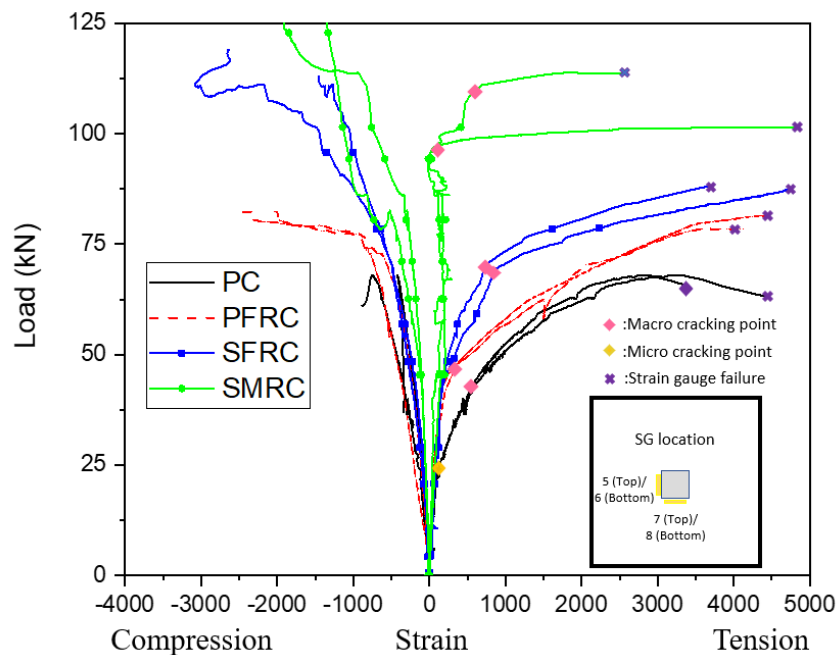


Figure 5-2. Applied Load-strain responses of concrete slabs (SGs 5 to 8)

5.3.4.2 Applied load-deflection responses

The applied load-deflection responses of the concrete slabs on the ground are shown in Figure 5-12. The central deflection was averaged from the four LVDTs closely attached to the specimens around the loading plate. The SMRC slab had the highest flexural cracking load (122 kN), while the steel fibre and macro PP fibre-reinforced concrete slabs had the flexural cracking load of 100 kN and 87 kN, respectively. For the specimens with fibre or steel mesh reinforcements, stress transferred to the fibres or steel meshes as concrete cracked, thus the slabs still kept resisting load and resulted in a high load-carrying capacity. The plain concrete slab had the lowest flexural cracking load of 68 kN, followed by a sudden reduction in the applied load to 40 kN. When the central deflection was over 6 mm, the plain concrete slab still resisted load. At this stage, the load was in fact mainly bore by the ground and the slab had lost its load-carrying capacity. At 23.3 mm, cracked plain concrete slab experienced punching shear failure at 95.9kN. It was different from the beam tests in Figure 5-9 and Figure 5-10, where fibre-reinforced concrete beams had slightly higher flexural strength and first peak strength than plain concrete, the cracking load of the PFRC ground slab was significantly higher than that of the plain concrete ground slab. It also could be found that SFRC beams performed better than PFRC beams in both the residual flexural strength and flexural strength. However, when these two types of fibres were used to reinforce ground slab, they had comparable reinforcing effects that the energy absorption of SFRC slab was 2872.4 J and that of PFRC slab was 2947.8 J. The applied load of PFRC ground slab was even higher than that of SFRC ground slab at deflection between 12.8 to 20 mm. At deflection of 20 mm, the applied load of PFRC and SFRC ground slabs was similar, about 120 kN.

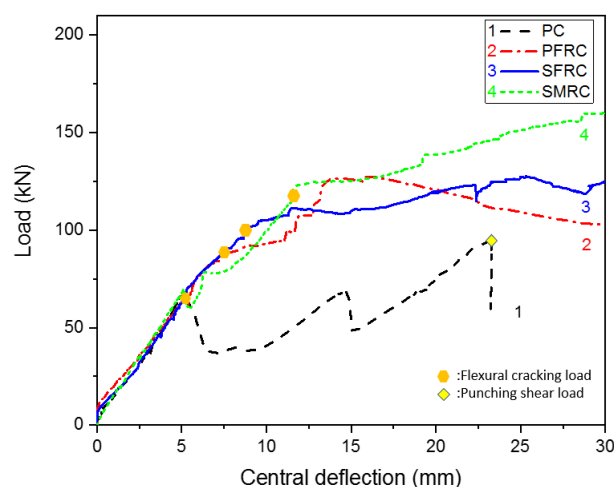
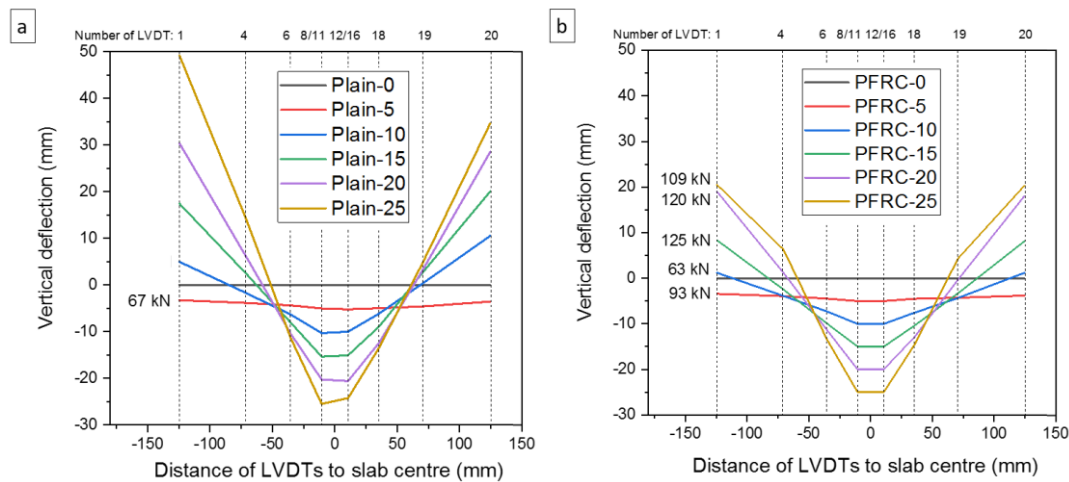


Figure 5-12. Load-deflection responses of concrete slabs

5.3.4.3 Slab deflection profile and cracking levels

The surface deflection profiles at different levels of the ground slab central deflections are shown in Figure 5-13. Deflection in the diagonal line of the slab was captured by LVDTs. When the central deflection increased from 0 to 5 mm, all the slabs maintained full contact with subgrade soil, which deformed almost uniformly with the slab. Since the plain concrete had already severely cracked at the deflection of 5 mm as shown in Figure 5-12, when the central deflection increased to 10 mm, the edges and corners of the plain concrete slab and PFRC slab began to lose contact with the soil layer since they deflected upward. In Figure 5-13, the steel fibre and steel mesh reinforced slabs still maintained nearly full contact with the soil at the central deflection of 10 mm, at which these slabs just began cracking as shown in Figure 5-12. With the further increase of the central deflection to 20 mm, an increase of non-contact area between the slab and supporting soil was observed in all the slabs due to a higher level of deformations. When the central deflection reached 25 mm, the distance between edge and centre of plain concrete was 75 mm, while this distance of both the macro PP fibre and steel fibre-reinforced slabs was about 45 mm, which was slightly higher than that of the steel mesh reinforced slab (40 mm). In conclusion, similar to steel mesh reinforcement, the macro PP fibre and steel fibre reinforcement significantly decreased deformation of the slabs subjecting to a central load.



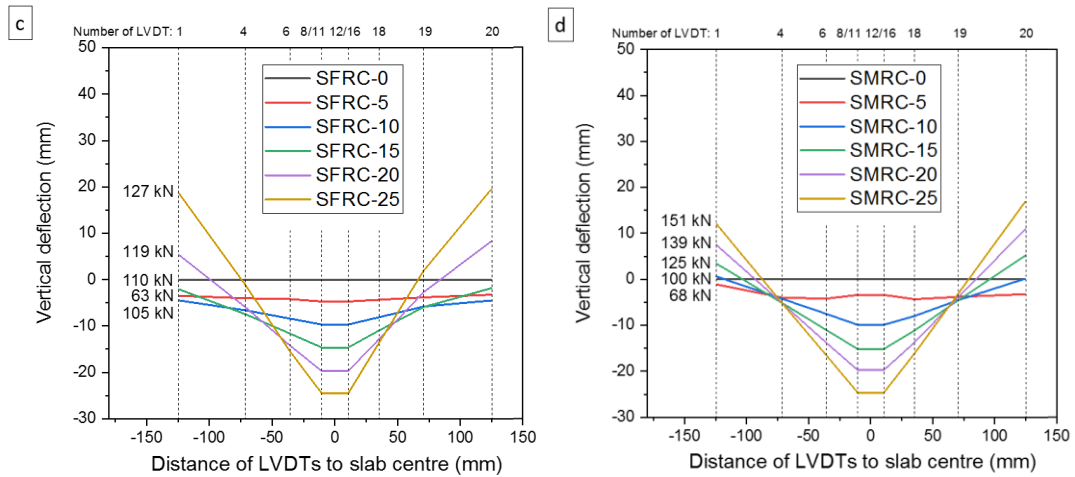


Figure 5-13. Surface deflection profile at the levels of central deflection of 0, 5, 10, 15, 20 and 25 mm: (a) Plain concrete slab, (b) macro PP fibre-reinforced slab, (c) Steel fibre-reinforced slab, (d) steel mesh reinforced slab

Figure 5-14 shows the crack patterns of all the slabs after testing. As can be seen, the plain concrete slab and fibre-reinforced concrete slabs failed with the initiation of four major cracks which started from the slab centre and developed along the median lines, while the steel mesh reinforced slab failed with five major cracks. The failure mode of the PFRC slab is similar to those in the previous study [143].



Figure 5-14. Crack patterns in the slabs: (a) plain concrete; (b) PFRC; (c) SFRC; (d) SMRC

Figure 5-15 shows the zoomed-in views of the patterns of cracks underneath the applied central load. During the tests, the plain concrete showed brittle instantaneous failure, followed by the sudden growth of cracks across the entire slab. Continuously applying load on plain concrete resulted in a shear failure in the centre of the slab. The maximum distance between the periphery of cracks and the centre point was 13 cm. The fibre and steel mesh reinforced slabs also showed circumferential cracks on top of the slab around the load plate. Meanwhile, the maximum distance between the periphery of cracks and the centre point of macro PP fibre and steel fibre-reinforced slabs were 13 cm and 27 cm, respectively, while the slab reinforced by steel meshes showed the largest distance of 40 cm. The diameter of circumferential cracks of the PFRC slab was slightly greater than that of the plain concrete slab while that for SFRC slab was in between those of PFRC and SMRC slab. It can be found that with the reinforcement in concrete, the diameter of cracks become larger than plain concrete and only plain concrete slab experienced clear punching shear failure.

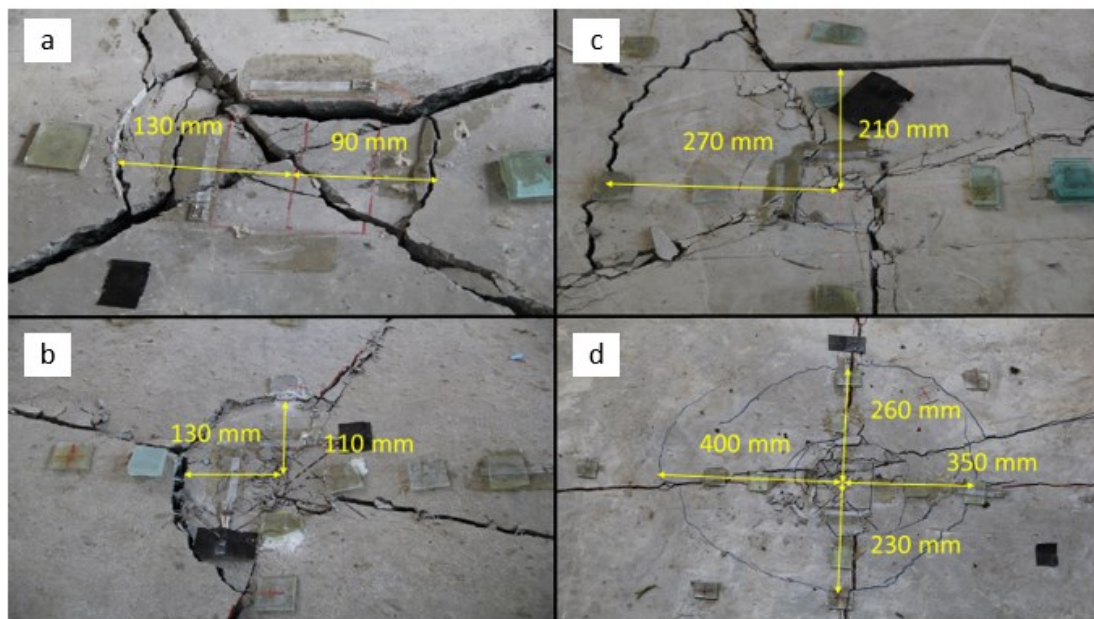


Figure 5-15. Distance between the periphery of cracks and the centre point on the top surface of concrete slab: (a) plain concrete, (b) PFRC, (c) SFRC, and (d) SMRC

5.3.5 Flexural and punching shear strength of ground slab

The flexural performance of FRC beams can be used to calculate the ultimate load-capacity of FRC ground slabs according to Technical Report 34 [152] based on the yield line theory.

For an internal load, using conventional yield line theory with true point load and ignoring the contribution of the subgrade reaction, the collapse load per unit length, P_u could be calculated by the following equation:

$$P_u = 2\pi \times (M_p + M_n) \quad (5-2)$$

where P_u is the collapse load capacity in kNm/m, M_p is the ultimate positive resistance moment per unit length of slab in kNm/m, M_n the ultimate negative resistance moment per unit length of slab in kNm/m.

The equivalent flexural strength ratio (in equation 5-1), $R_{e,3}$, as a characterization of the ductility of fibre-reinforced concrete is used to calculate the residual positive bending moment capacity per unit length, $M_{p,fibre}$ as follows:

$$M_{p,fibre} = \frac{f_{ctk,fl}}{\gamma_c} \times (R_{e,3}) \times \left(\frac{h^2}{6}\right) \quad (5-3)$$

where $f_{ctk,fl}$ is the characteristic flexural strength of concrete in MPa, γ_c is the partial safety factor for concrete and h is the slab thickness in mm.

The negative bending moment capacity per unit length, M_n is assumed that cracking stress is not influenced by the increase of ductility due to fibre. The following equation is used to calculate M_n as follows:

$$M_n = \frac{f_{ctk,fl}}{\gamma_c} \times \left(\frac{h^2}{6}\right) \quad (5-4)$$

For steel mesh reinforcement, the negative bending moment capacity per unit length is the same as Equation 4 and the positive bending moment capacity per unit length is calculated by the following equation:

$$M_{p,SM} = \frac{0.95 A_s \times f_y \times d}{\gamma_s} \quad (5-5)$$

where A_s is the area of steel mesh in mm^2 , f_y is the characteristic strength of steel in MPa, d is the effective depth in mm and γ_s is the partial safety factor for steel.

Table 5-5 shows the test results of beams and slabs and calculated results based on TR34 [152]. It can be seen that the improvements in the flexural strengths of plain and FRC from four-point beam flexural tests were small (1.13 and 1.26 times for PFRC and SFRC larger than plain concrete) as compared to those obtained in the tests of ground slabs in this study. The corresponding values are 1.28 and 1.47 times for PFRC and SFRC.. Comparing the

normalized flexural cracking load of slabs (fibres, mesh/plain) with calculated normalized collapse load (fibres, mesh/plain), it could be seen that the method from TR34 could be used to estimate the collapse load of ground slabs with steel mesh or SFRC. However, the calculated collapse loads based on TR34 were higher than the actual test results of slabs on the ground. Flexural cracking load/collapse load ratio of plain concrete and SMRC are the same, at 1.12, while that of PFRC and SFRC is higher at 1.45 and 1.24, respectively. This indicated that this method would overly predict the cracking load of slab on the ground reinforced by fibres, especially macro PP fibres, because this method was derived from $R_{e,3}$ (equivalent flexural strength ratio) from the post-cracking performance of FRC beams to predict the cracking load of slabs on the ground. It means the contribution of post-cracking performance of FRC to ground slab is not accurately estimated. For different types of fibres, as long as they had similar equivalent flexural strength ratio, the calculated results from TR34 method would be similar. Therefore, this design procedure cannot accurately predict the performance of FRC slab reinforced with different fibres which have dissimilar post-peak performance.

Table 5-5. Summary of test results and calculated cracking load and shear load

Note	Plain concrete	6 kg/m ³ macro PP fibre	30 kg/m ³ Steel fibre	Steel mesh
Notched beam flexural strength (MPa)	4.90	4.90	5.00	-
Normalized against plain concrete	1.00	1.00	1.02	-
Four-point bending peak strength (MPa)	3.90	4.41	4.90	-
Normalized against plain concrete	1.00	1.13	1.26	-
Calculated collapse load (kN) for 1.8x1.8 m slabs	76.0	126.0	124.2	136.3
Experimental flexural cracking load of slab (kN) for 1.8x1.8 m slabs	68.00	87.00	100.00	122.00
Error between the calculated collapse load and experimental flexural cracking load	10.53%	30.95%	19.48%	10.49%
Normalized against plain concrete	1.00	1.28	1.47	1.79
Calculated/testing flexural cracking	1.12	1.45	1.24	1.12
Calculated shear strength on critical perimeter	96.16	96.16	123.55	200.29
Normalized against plain concrete	1.00	1.00	1.28	1.62

Punching shear capacity of slabs is also an important property during the slab design. In this dissertation, the estimated punching shear load as per TR34 was used to compare with the test results. According to TR34, the shear stress at the face of the contact area should be lower than a value V_{max} as follows:

$$V_{max} = 0.5 \times k_2 \times f_{cd} \quad (5-6)$$

where f_{cd} is the design concrete compressive strength (cylinder) in MPa.

Therefore, the maximum punching load capacity, $P_{p,max}$ can be calculated as follows:

$$P_{p,max} = V_{max} \times u_0 \times h_{ed} \quad (5-7)$$

where u_0 is the length of the perimeter at the face of the loaded area, h_{ed} is the effective depth, taken as $0.75 h$ for plain concrete and FRC.

As shown in Figure 5-12, the applied load of slabs was all lower than the predicted punching shear capacity of 201 kN, implying the tested slabs met the requirement of punching load capacity, but failed due to flexural bending as observed above. Punching shear is a result of a concentrated load on a relatively small area around the loaded area and control area on the top and bottom of the slab, respectively. Therefore, the shear stress is checked on the critical shear perimeter at a distance $2h$ (thickness of slab) from the loaded area.

For plain slab, the minimum shear strength should be taken as:

$$V_{Rd,c} = 0.035 \times k_1^{\frac{3}{2}} \times f_{ck}^{\frac{1}{2}} \quad (5-8)$$

$$k_1 = 1 + (200/h_{ed})^{0.5} \leq 2 \quad (5-9)$$

where k_1 equals to 2.49. Therefore, k_1 is taken as 2.

Thus, the plain slab load capacity, P_p , can be calculated as follows:

$$P_p = V_{Rd,c,plain} \times u_1 \times h_{ed} \quad (5-10)$$

where u_1 is the length of the perimeter at a distance $2h_{ed}$ from the loaded area.

For SFRC slab, the increased shear capacity from steel fibres V_f over that of plain concrete based on TR34 guidance can be calculated as:

$$V_f = 0.12 \times f_{ctk,fl} \times R_{e,3} \quad (5-11)$$

Combined with the minimum shear strength $V_{Rd,c}$, the SFRC slab shear capacity is given by:

$$P_{SF} = (V_{Rd,c,plain} + V_f) \times u_1 \times h_{ed} \quad (5-12)$$

For SMRC slab, the average shear stress can be calculated by:

$$V_{Rd,c} = \frac{0.18}{\gamma_c} \times k_1 \times (100 \times \rho_1 \times f_{ck})^{\frac{1}{3}} \geq 0.035 \times k_1^{\frac{3}{2}} \times f_{ck}^{\frac{1}{2}} \quad (5-13)$$

where $\rho_1 = (\rho_x \times \rho_y)^{\frac{1}{2}}$, ρ_x and ρ_y are the reinforcement ratios by area in the x- and y-direction, respectively.

For PFRC slab, there is no guidance available currently to calculate shear capacity. Obviously, using the same formula from TR34 is not suitable due to macro PP fibre cannot provide the similar reinforcing effect on shear strength like steel fibres. Therefore, it should be assumed that shear capacity is that of plain concrete as suggested by TR34.

In brief, the estimated shear strength on the critical perimeter was listed in Table 5. It can be seen that the shear strength of plain slab from the test (95.9 kN) matched well with the calculated shear strength (96.2 kN) while other slabs did not show a pure punching shear failure.

5.4. Conclusion

This chapter performed experimental tests of concrete ground slabs with different reinforcing types, including plain, steel meshes, steel fibres and macro PP fibres. Four different slabs on the ground were subjected to concentrated loading at the centre of the slab. The influences of different fibre reinforcements on the performance of concrete ground slabs were discussed. The following conclusions can be drawn.

- The experimental results have shown that the structural performance of PFRC ground slab was much better than the plain concrete slab and comparable to the SFRC ground slab. However, the macro PP fibre reinforcement did not effectively mitigate the flexural crack as steel fibre reinforcement of ground slabs.
- Addition of 30 kg/m³ steel fibres and 6 kg/m³ macro PP fibres increased the flexural cracking load by 47% and 28% compared to the plain concrete slab, respectively, while the slab with A142 steel meshes had the highest load capacity, i.e., 79% higher than the plain concrete slab. The use of 6 kg/m³ macro PP fibres compared favourably with 30

kg/m³ steel fibres in terms of post-cracking performance and energy absorption of ground slabs.

- The use of macro PP fibre had little influence on the distance between the periphery of cracks and centre point on the top surface while steel fibres and steel meshes could increase that distance by 220% and 280%, respectively. In terms of deformation resistance, steel fibre and macro PP fibre reinforcement could significantly improve the ability of deformation resistance of slabs under central load compared with the plain concrete slab. Using steel meshes was the most effective to control slab deformation.
- Adding 30 kg/m³ steel fibres and 6 kg/m³ macro PP fibres could improve the flexural strength of concrete beam by 13% and 26%, and ground slab by 28% and 47%.
- The collapse loads predicted based on beam flexural test and steel mesh properties were larger than the experimental flexural strength of the tested ground slabs. Overestimations of the flexural strength for plain concrete and SMRC ground slab are approximately 10%, while those for PFRC and SFRC are 45% and 24%, respectively.
- The predictive method from TR34 overestimates the flexural cracking loads of fibre-reinforced ground slabs.

Chapter 6. Conclusions and future work

6.1 Main findings

In recent years, macro PP fibres have been widely used to replace traditional steel reinforcements. However, low Young's modulus and weak bonding to concrete limit the applications of macro PP fibres as a reinforcing material. In this dissertation, for improving the mechanical performance of macro PFRC, combining macro PP fibres with high modulus basalt fibres to overcome the problem of low Young's modulus and surface grafting organic groups to overcome the weak bonding problem are proposed and examined. Both the static and dynamic properties of macro PFRC were investigated and quantified through intensive laboratory tests. To compare the reinforcing effect of macro PP fibres with other popular reinforcing materials, the structural performance of reinforced ground slabs was experimentally studied. The following conclusions were drawn from the results of this dissertation.

- For hybrid FRC, the inclusion of macro PP fibres and basalt fibres reduced the workability of fresh concrete. Hybrid fibres showed a larger reduction extent than macro PP fibres when the fibre volume fraction increases. Both basalt and macro PP fibres could increase the compressive strength of concrete, and basalt fibres were more effective than macro PP fibres. Approximately 10% improvement on the compressive strength was found in hybrid fibre-reinforced concrete. The addition of 0.1% basalt fibres into traditional macro PP fibre-reinforced concrete could increase the flexural strength. There was approximately 20% improvement to the peak stress of hybrid PP (1%) and basalt (0.1%) FRC regarding the reference specimens. The use of 0.1% basalt fibres improved the initial post-cracking strength of macro PP fibre-reinforced concrete. The obvious enhancement of post-peak strength, ductility and energy absorption capability in high content macro PP fibre-reinforced concrete were observed, hybrid fibres reinforcement further improved the post-failure performances of the FRC.
- For grafted PP fibres, the FTIR results proved that the silane groups and hydrophilic groups were successfully grafted on the PP fibres through the two mentioned methods. The modification of surface grafting silane groups produced a very high bonding strength with concrete, due to the fact that the silane groups took part in the hydration reaction of concrete. The peak pullout load was up to 224 N, which was nearly three times of that of the unmodified PP fibres. The hydrophilic groups grafted PP fibre also

showed high bonding strength with the peak pullout load of 149 N, which was equal to 1.6 times of that of the unmodified PP fibres. The energy absorptions of specimens reinforced with silane groups and hydrophilic groups grafted PP fibres were 2.024 J and 1.646J, which increased by 121% and 80% as compared to the unmodified fibre reinforced specimen, respectively. Among these two organic groups, the silane groups grafted PP fibre-reinforced UHPC showed the outstanding flexural strength, toughness and deflection-hardening performance. Similar to the unmodified PP fibre-reinforced UHPC, the hydrophilic groups grafted PP fibre-reinforced UHPC showed deflection-softening performance, rather than deflection-hardening performance. The flexural performance of 27 kg/m³ silane groups grafted PP fibre-reinforced UHPC was comparable with 78 kg/m³ steel fibre-reinforced UHPC.

- For the dynamic compressive and splitting tensile tests, the properties of basalt-macro PP hybrid FRC were investigated by conducting SHPB tests. Hybrid FRC exhibited significant sensitivity to loading rate with the strain rate up to 170 s⁻¹ in the dynamic compressive tests and to 40 s⁻¹ in the dynamic splitting tensile tests. In the quasi-static splitting tensile tests, the addition of 1% macro PP + 0.1% basalt fibres could slightly improve the static splitting tensile strength (12%). The improvement of the quasi-static splitting tensile strength was not observed when the specimens were reinforced with high volume fraction of macro PP fibres (2%) due to excessive voids induced by adding fibres. Adding fibres could change the brittle failure of concrete to the ductile response. Through comparing different failure modes, the impact resistance of hybrid FRC under the compressive tests was improved especially at the strain rate of 50 s⁻¹, where FRC specimens could remain relatively intact whereas plain concrete specimens were fully shattered into fragments. The crack mouth opening displacement (CMOD) of hybrid FRC was significantly reduced (75.8% for P10B01 and 90.3% for P20B01) at 2 milliseconds compared with plain concrete at same time instant under stress rate of 310 GPa/s. At lower dynamic stress rate (180 GPa/s), both Specimens P10B01 and P20B01 remained intact with the CMOD of 0.6 mm and 0.08 mm at the middle of the specimens, respectively. Besides, the dynamic increase factor was derived from the test results and empirical formulae were proposed to describe DIF versus strain rate relations for both the dynamic compressive and indirect tensile tests. As compared to plain concrete, the strain rate sensitivity of P10B01 was slightly higher in dynamic compression and similar in dynamic splitting tension. However, the high volume fraction of hybrid FRC P20B01 showed much higher strain rate sensitivity in the dynamic splitting tensile tests.

- For structural tests, the experimental results have shown that the structural performance of PFRC ground slab was much better than the plain concrete slab and comparable to the SFRC ground slab. However, the PP fibre reinforcement did not effectively mitigate the flexural crack as compared to steel fibre reinforcement of ground slabs. The addition of 30 kg/m³ steel fibres or 6 kg/m³ PP fibres respectively increased the flexural cracking load by 47% and 28% compared to the plain concrete slab while the slab with A142 steel meshes had the highest load capacity, i.e., 79% higher than the plain concrete slab. The use of 6 kg/m³ PP fibres compared favourably with 30 kg/m³ steel fibres in terms of the post-cracking performance and energy absorption of ground slabs. The use of PP fibres had a marginal influence on the distance between the periphery of cracks and centre point on top surface while steel fibres and steel meshes could increase that distance by 220% and 280%, respectively. In terms of deformation resistance, steel fibre and PP fibre reinforcement could significantly improve the ability of deformation resistance of slabs under central load compared with the plain concrete slab. Using steel meshes was the most effective to control slab deformation. Besides, adding 30 kg/m³ steel fibres or 6 kg/m³ PP fibres could improve the flexural strength of concrete beams by 13% and 26%, and ground slabs by 28% and 47%. The collapse loads predicted based on beam flexural tests and steel mesh properties were larger than the experimental flexural strength of the tested ground slabs. Overestimations of the flexural strength for plain concrete and SMRC ground slabs are approximately 10%, while those for PFRC and SFRC are 45% and 24%, respectively. Through analytical calculation, the predictive method from TR34 overestimates the flexural cracking loads of fibre-reinforced ground slabs.

6.2 Recommendations for future work

In Chapter 2, the influence of macro PP volume fraction on the compressive and flexural strength of concrete has been experimentally investigated. However, the influence of different combinations of basalt fibre volume fraction and the macro PFRC was not investigated in this dissertation, which is deemed necessary for further investigations.

In Chapter 3, grafted PP fibres showed good bonding with UHPC. It is necessary to evaluate the performance of the new PP fibre in other types of concrete such as normal strength concrete with coarse aggregates, engineering ceramic composites and the dynamic bonding strength.

In Chapter 4, the performance of hybrid FRC has been investigated under dynamic compression and splitting tension. The static and dynamic constitutive relations of the material under stress states such as biaxial compression, triaxial compression and direct tension need also be studied.

In Chapter 5, the performance of grounded slabs reinforced with macro PP and steel fibres, steel mesh has been investigated. The performance of other types of structures, e.g., beams and columns made of macro PFRC could be investigated in future work.

Reference

- [1] A. Committee, Building code requirements for structural concrete (ACI 318-08) and commentary, International Organization for Standardization, American Concrete Institute, 2008.
- [2] R.F. Zollo, Fiber-reinforced concrete: an overview after 30 years of development, *Cement Concrete Comp* 19(2) (1997) 107-122.
- [3] D.Y. Yoo, J.J. Park, S.W. Kim, Y.S. Yoon, Early age setting, shrinkage and tensile characteristics of ultra high performance fiber reinforced concrete, *Construction and Building Materials* 41 (2013) 427-438.
- [4] D.Y. Yoo, K.H. Min, J.H. Lee, Y.S. Yoon, Shrinkage and cracking of restrained ultra-high-performance fiber-reinforced concrete slabs at early age, *Construction and Building Materials* 73 (2014) 357-365.
- [5] S.S. Park, Unconfined compressive strength and ductility of fiber-reinforced cemented sand, *Construction and Building Materials* 25(2) (2011) 1134-1138.
- [6] A.M. Alani, D. Beckett, Mechanical properties of a large scale synthetic fibre reinforced concrete ground slab, *Construction and Building Materials* 41 (2013) 335-344.
- [7] J. Kaufmann, K. Frech, P. Schuetz, B. Munch, Rebound and orientation of fibers in wet sprayed concrete applications, *Construction and Building Materials* 49 (2013) 15-22.
- [8] A. Peyvandi, P. Soroushian, S. Jahangirnejad, Enhancement of the structural efficiency and performance of concrete pipes through fiber reinforcement, *Construction and Building Materials* 45 (2013) 36-44.
- [9] R. Tepfers, Cracking of Concrete Cover Along Anchored Deformed Reinforcing Bars, *Magazine of Concrete Research* 31(106) (1979) 3-12.
- [10] Y. Chen, P. Qiao, Crack growth resistance of hybrid fiber-reinforced cement matrix composites, *Journal of Aerospace Engineering* 24(2) (2010) 154-161.
- [11] ACI-Committee, ACI Committee 544. Report on Fiber Reinforced Concrete, Detroit: American Concrete Institute (1996).
- [12] S.U. Balouch, J.P. Forth, J.L. Granju, Surface corrosion of steel fibre reinforced concrete, *Cement and Concrete Research* 40(3) (2010) 410-414.
- [13] Q. Xiaochun, L. Xiaoming, C. Xiaopei, The applicability of alkaline-resistant glass fiber in cement mortar of road pavement: Corrosion mechanism and performance analysis, *International Journal of Pavement Research and Technology* 10(6) (2017) 536-544.
- [14] K.T. Soe, Y.X. Zhang, L.C. Zhang, Material properties of a new hybrid fibre-reinforced engineered cementitious composite, *Construction and Building Materials* 43 (2013) 399-407.
- [15] D.J. Kim, S.H. Park, G.S. Ryu, K.T. Koh, Comparative flexural behavior of Hybrid Ultra High Performance Fiber Reinforced Concrete with different macro fibers, *Construction and Building Materials* 25(11) (2011) 4144-4155.
- [16] H. Tian, Y.X. Zhang, L. Ye, C.H. Yang, Mechanical behaviours of green hybrid fibre-reinforced cementitious composites, *Construction and Building Materials* 95 (2015) 152-163.
- [17] A. Sivakumar, M. Santhanam, Mechanical properties of high strength concrete reinforced with metallic and non-metallic fibres, *Cement and Concrete Composites* 29(8) (2007) 603-608.
- [18] C.X. Qian, P. Stroeven, Development of hybrid polypropylene-steel fibre-reinforced concrete, *Cement and Concrete Research* 30(1) (2000) 63-69.
- [19] V. Afroughsabet, T. Ozbakkaloglu, Mechanical and durability properties of high-strength concrete containing steel and polypropylene fibers, *Construction and Building Materials* 94 (2015) 73-82.

- [20] P. Song, J. Wu, S. Hwang, B. Sheu, Statistical analysis of impact strength and strength reliability of steel–polypropylene hybrid fiber-reinforced concrete, *Construction and Building Materials* 19(1) (2005) 1-9.
- [21] M. Tabatabaeian, A. Khaloo, A. Joshaghani, E. Hajibandeh, Experimental investigation on effects of hybrid fibers on rheological, mechanical, and durability properties of high-strength SCC, *Construction and Building Materials* 147 (2017) 497-509.
- [22] M. Hsie, C. Tu, P. Song, Mechanical properties of polypropylene hybrid fiber-reinforced concrete, *Materials Science and Engineering: A* 494(1-2) (2008) 153-157.
- [23] C.-h. JIANG, H. ZHAO, D. CHEN, W. ZHANG, Comparing and Analyzing Influence of Basalt and Polypropylene Fibers on the Cement Mortar [J], *Bulletin of the Chinese Ceramic Society* 6 (2007).
- [24] R. Swamy, H. Stavrides, Some properties of high workability steel fibre concrete, *Fibre-reinforced cement and concrete*, Rilem Symposium, Sheffield, 1975, pp. 197-208.
- [25] K. Wille, A.E. Naaman, Pullout Behavior of High-Strength Steel Fibers Embedded in Ultra-High-Performance Concrete, *ACI Materials Journal* 109(4) (2012).
- [26] Z.C. Deng, F. Shi, S. Yin, R. Tuladhar, Characterisation of macro polyolefin fibre reinforcement in concrete through round determinate panel test, *Construction and Building Materials* 121 (2016) 229-235.
- [27] BarChip, Product data sheet (Barchip 60). <https://barchip.com/product/>.
- [28] M. Ruijie, J. Yang, Y. Liu, X. Zheng, Influence of length-to-diameter ratio on shrinkage of basalt fiber concrete, *IOP Conference Series: Materials Science and Engineering*, IOP Publishing, 2017, p. 012027.
- [29] ASTM, ASTM C143 Standard Test Method for Slump of Hydraulic-Cement Concrete, *Book of ASTM Standards*. (2015).
- [30] ASTM, ASTM C39 Standard test method for compressive strength of cylindrical concrete specimens, *book of ASTM Standards* (2018).
- [31] ASTM, ASTM C1609 Standard Test Method for Flexural Performance of Fiber-Reinforced Concrete (Using Beam With Third-Point Loading), *Book of ASTM Standards* (2011).
- [32] J.H. Lee, B. Cho, E. Choi, Y.H. Kim, Experimental study of the reinforcement effect of macro-type high strength polypropylene on the flexural capacity of concrete, *Construction and Building Materials* 126 (2016) 967-975.
- [33] P. Iyer, S.Y. Kenno, S. Das, Mechanical Properties of Fiber-Reinforced Concrete Made with Basalt Filament Fibers, *Journal of Materials in Civil Engineering* 27(11) (2015) 04015015.
- [34] C.H. Jiang, K. Fan, F. Wu, D. Chen, Experimental study on the mechanical properties and microstructure of chopped basalt fibre reinforced concrete, *Materials & Design* 58 (2014) 187-193.
- [35] A.J. Babafemi, W.P. Boshoff, Tensile creep of macro-synthetic fibre reinforced concrete (MSFRC) under uni-axial tensile loading, *Cement & Concrete Composites* 55 (2015) 62-69.
- [36] S. Yin, R. Tuladhar, F. Shi, M. Combe, T. Collister, N. Sivakugan, Use of macro plastic fibres in concrete: A review, *Construction and Building Materials* 93 (2015) 180-188.
- [37] N. Buratti, C. Mazzotti, M. Savoia, Post-cracking behaviour of steel and macro-synthetic fibre-reinforced concretes, *Construction and Building Materials* 25(5) (2011) 2713-2722.
- [38] S. Singh, A. Shukla, R. Brown, Pullout behavior of polypropylene fibers from cementitious matrix, *Cement and Concrete Research* 34(10) (2004) 1919-1925.
- [39] A.C. 239, Ultra-high-performance concrete: An emerging technology report, *The American Concrete Institute* (2018).

- [40] M.S.M. Norhasri, M.S. Hamidah, A.M. Fadzil, Inclusion of nano metaclayed as additive in ultra high performance concrete (UHPC), *Construction and Building Materials* 201 (2019) 590-598.
- [41] J.Y. Guo, J.Y. Wang, K. Wu, Effects of self-healing on tensile behavior and air permeability of high strain hardening UHPC, *Construction and Building Materials* 204 (2019) 342-356.
- [42] F.U.A. Shaikh, S. Luhar, H.Ş. Arel, I. Luhar, Performance evaluation of Ultrahigh performance fibre reinforced concrete—A review, *Construction and Building Materials* 232 (2020) 117152.
- [43] K. Ragalwar, W.F. Heard, B.A. Williams, R. Ranade, Significance of the particle size distribution modulus for strain-hardening-ultra-high performance concrete (SH-UHPC) matrix design, *Construction and Building Materials* 234 (2020) 117423.
- [44] Y. Dong, Performance assessment and design of ultra-high performance concrete (UHPC) structures incorporating life-cycle cost and environmental impacts, *Construction and Building Materials* 167 (2018) 414-425.
- [45] H.H. Huang, A.S. Su, X.J. Gao, Y.Z. Yang, Influence of formwork wall effect on fiber orientation of UHPC with two casting methods, *Construction and Building Materials* 215 (2019) 310-320.
- [46] Y. Zhang, Y.P. Zhu, M. Yeseta, D.L. Meng, X.D. Shao, Q. Dang, G.D. Chen, Flexural behaviors and capacity prediction on damaged reinforcement concrete (RC) bridge deck strengthened by ultra-high performance concrete (UHPC) layer, *Construction and Building Materials* 215 (2019) 347-359.
- [47] A.H.A. Raheem, M. Mahdy, A.A. Mashaly, Mechanical and fracture mechanics properties of ultra-high-performance concrete, *Construction and Building Materials* 213 (2019) 561-566.
- [48] N.A. Soliman, A. Tagnit-Hamou, Partial substitution of silica fume with fine glass powder in UHPC: Filling the micro gap, *Construction and Building Materials* 139 (2017) 374-383.
- [49] M. Courtial, M.N. de Noirfontaine, F. Dunstetter, M. Signes-Frehel, P. Mounanga, K. Cherkaoui, A. Khelidj, Effect of polycarboxylate and crushed quartz in UHPC: Microstructural investigation, *Construction and Building Materials* 44 (2013) 699-705.
- [50] S.H.G. Mosavinejad, M.A.M. Langaroudi, J. Barandoust, A. Ghanizadeh, Electrical and microstructural analysis of UHPC containing short PVA fibers, *Construction and Building Materials* 235 (2020) 117448.
- [51] Y.F. Hao, H. Hao, Pull-out behaviour of spiral-shaped steel fibres from normal-strength concrete matrix, *Construction and Building Materials* 139 (2017) 34-44.
- [52] H. Caetano, J.P.C. Rodrigues, P. Pimienta, Flexural strength at high temperatures of a high strength steel and polypropylene fibre concrete, *Construction and Building Materials* 227 (2019) 116721.
- [53] X.H. Wang, S.R. Zhang, C. Wang, K.L. Cao, P.Y. Wei, J.X. Wang, Effect of steel fibers on the compressive and splitting-tensile behaviors of cellular concrete with millimeter-size pores, *Construction and Building Materials* 221 (2019) 60-73.
- [54] Z.M. Wu, C.J. Shi, W. He, L.M. Wu, Effects of steel fiber content and shape on mechanical properties of ultra high performance concrete, *Construction and Building Materials* 103 (2016) 8-14.
- [55] J. Wang, D. Niu, Influence of freeze–thaw cycles and sulfate corrosion resistance on shotcrete with and without steel fiber, *Construction and Building Materials* 122 (2016) 628-636.

- [56] D.-Y. Yoo, S. Kim, G.-J. Park, J.-J. Park, Residual performance of HPFRCC exposed to fire—Effects of matrix strength, synthetic fiber, and fire duration, *Construction and Building Materials* 241 (2020) 118038.
- [57] K.-Q. Yu, J.-T. Yu, J.-G. Dai, Z.-D. Lu, S.P. Shah, Development of ultra-high performance engineered cementitious composites using polyethylene (PE) fibers, *Construction and Building Materials* 158 (2018) 217-227.
- [58] K. Hannawi, H. Bian, W. Prince-Agbodjan, B. Raghavan, Effect of different types of fibers on the microstructure and the mechanical behavior of Ultra-High Performance Fiber-Reinforced Concretes, *Composites Part B-Engineering* 86 (2016) 214-220.
- [59] D. Feldman, F. Denes, Z. Zeng, A. Denes, D. Banu, Polypropylene fiber–matrix bonds in cementitious composites, *Journal of Adhesion Science and Technology* 14(13) (2000) 1705-1721.
- [60] G.Y. Feng, X.Y. Wang, D.T. Zhang, H.J. Cao, K. Qian, X.L. Xiao, A comparative study on mechanical properties of surface modified polypropylene (PP) fabric reinforced concrete composites, *Construction and Building Materials* 157 (2017) 372-381.
- [61] D. Barnat-Hunek, P. Smarzewski, Influence of hydrophobisation on surface free energy of hybrid fiber reinforced ultra-high performance concrete, *Construction and Building Materials* 102 (2016) 367-377.
- [62] Y.W. Fei, J. Ma, S. Sun, L.P. Tong, H.M. Liu, Surface Hydrophilic Modification of Polypropylene Fiber by Hydrolysis of Silane Coupling Agent, *Key Engineering Materials*, Trans Tech Publ, 2018, pp. 80-85.
- [63] Y. Ding, S. Liu, Y. Zhang, A. Thomas, The investigation on the workability of fibre cocktail reinforced self-compacting high performance concrete, *Construction and Building Materials* 22(7) (2008) 1462-1470.
- [64] W. Wang, L. Wang, Q. Shi, H.J. Yu, T. Chen, C.L. Wang, T.X. Sun, Progress of the surface modification of PP fiber used in concrete, *Polymer-Plastics Technology and Engineering* 45(1) (2006) 29-34.
- [65] A. Saffar, P.J. Carreau, M.R. Kamal, A. Ajji, Hydrophilic modification of polypropylene microporous membranes by grafting TiO₂ nanoparticles with acrylic acid groups on the surface, *Polymer* 55(23) (2014) 6069-6075.
- [66] Z.Q. Yang, J.Z. Liu, J.P. Liu, C.F. Li, H.X. Zhou, Silica modified PP fiber for improving crack-resistance of cementitious composites, *Advanced Materials Research*, Trans Tech Publ, 2011, pp. 2058-2064.
- [67] Y. SHi, Product data sheet (MA20).
- [68] Subote, Product data sheet (SBT®-UDC).
- [69] Sika, Product data sheet (KS-JS50).
- [70] Y.Z. Lin, J.C. Yan, Z.F. Wang, F. Fan, C.Y. Zou, Effect of silica fumes on fluidity of UHPC: Experiments, influence mechanism and evaluation methods, *Construction and Building Materials* 210 (2019) 451-460.
- [71] A. Khabaz, Determination of friction coefficient between straight steel fiber and the concrete (SSF. C), *Advances in Materials* 4 (2015) 20-29.
- [72] D. Bikiaris, P. Matzinos, A. Larena, V. Flaris, C. Panayiotou, Use of silane agents and poly (propylene - g - maleic anhydride) copolymer as adhesion promoters in glass fiber/polypropylene composites, *Journal of Applied Polymer Science* 81(3) (2001) 701-709.
- [73] W. Yu, J. Shi, L. Wang, X. Chen, M. Min, L. Wang, Y. Liu, The structure and mechanical property of silane-grafted-polyethylene/SiO₂ nanocomposite fiber rope, *Aquaculture and Fisheries* 2(1) (2017) 34-38.
- [74] T. Paunikallio, M. Suvanto, T.T. Pakkanen, Grafting of 3-(trimethoxysilyl)propyl methacrylate onto polypropylene and use as a coupling agent in viscose fiber/polypropylene composites, *Reactive & Functional Polymers* 68(3) (2008) 797-808.

- [75] H.C. Han, X.L. Gong, Effect of fiber surface modification with different functional groups silane agents on mechanical properties of hems/polypropylene composites, *Applied mechanics and materials*, Trans Tech Publ, 2014, pp. 23-26.
- [76] G. Li, G. Min, L. Fei, X. Ni, W. Lu, One-step synthesis to photoelectric hybrid composite of N-vinylcarbazole–methyl acrylate copolymer and ZnO nanocrystals via nanocrystals-initiated polymerization, *Journal of colloid interface science* 334(1) (2009) 8-12.
- [77] M. Sclavons, M. Laurent, J. Devaux, V. Carlier, Maleic anhydride-grafted polypropylene: FTIR study of a model polymer grafted by ene-reaction, *Polymer* 46(19) (2005) 8062-8067.
- [78] H.S. Kim, B.H. Lee, S.W. Choi, S. Kim, H.J. Kim, The effect of types of maleic anhydride-grafted polypropylene (MAPP) on the interfacial adhesion properties of bio-flour-filled polypropylene composites, *Composites Part a-Applied Science and Manufacturing* 38(6) (2007) 1473-1482.
- [79] L. Wang, J.F. Wei, K.Y. Zhao, B. Wu, Preparation and characterization of high-hydrophilic polyhydroxy functional PP hollow fiber membrane, *Materials Letters* 159 (2015) 189-192.
- [80] S. Süzer, A. Argun, O. Vatansever, O. Aral, XPS and water contact angle measurements on aged and corona - treated PP, *Journal of Applied Polymer Science* 74(7) (1999) 1846-1850.
- [81] J.K. Shim, H.S. Na, Y.M. Lee, H. Huh, Y.C. Nho, Surface modification of polypropylene membranes by γ -ray induced graft copolymerization and their solute permeation characteristics, *Journal of Membrane Science* 190(2) (2001) 215-226.
- [82] K.L. Wang, W.C. Wang, D.Z. Yang, Y. Huo, D.Z. Wang, Surface modification of polypropylene non-woven fabric using atmospheric nitrogen dielectric barrier discharge plasma, *Applied Surface Science* 256(22) (2010) 6859-6864.
- [83] A. Beglarigale, H. Yazici, Pull-out behavior of steel fiber embedded in flowable RPC and ordinary mortar, *Construction and Building Materials* 75 (2015) 255-265.
- [84] S.U. Khan, T. Ayub, Modelling of the pre and post-cracking response of the PVA fibre reinforced concrete subjected to direct tension, *Construction and Building Materials* 120 (2016) 540-557.
- [85] A.J. Babafemi, W.P. Boshoff, Pull-out response of macro synthetic fibre from concrete matrix: Effect of loading rate and embedment length, *Construction and Building Materials* 135 (2017) 590-599.
- [86] X. Lyu, Y. Song, W. Feng, W. Zhang, Direct Observation of Single-Molecule Stick–Slip Motion in Polyamide Single Crystals, *ACS Macro Letters* 7(6) (2018) 762-766.
- [87] Y. Song, Z.W. Ma, P. Yang, X.Y. Zhang, X.J. Lyu, K. Jiang, W.K. Zhang, Single-Molecule Force Spectroscopy Study on Force-Induced Melting in Polymer Single Crystals: The Chain Conformation Matters, *Macromolecules* 52(3) (2019) 1327-1333.
- [88] L. Luo, J.-h. PENG, J.-d. QU, Modification of Polypropylene Fiber by Silane Coupling Agent and Its Influence on the Anti-crack Property of Cement Mortar, *Journal of Chongqingjianzhu university* 29(4) (2007) 118.
- [89] J.P. Won, D.H. Lim, C.G. Park, Bond behaviour and flexural performance of structural synthetic fibre-reinforced concrete, *Magazine of Concrete Research* 58(6) (2006) 401-410.
- [90] R. Bornemann, S. Faber, UHPC with steel-and noncorroding high strength polymer fibres under static and cyclic loading, *Proceedings of the International Symposium on Ultra-High Performance Concrete*, Kassel, Germany, 2004, pp. 673-681.
- [91] W. Meng, K.H. Khayat, Effect of Hybrid Fibers on Fresh Properties, Mechanical Properties, and Autogenous Shrinkage of Cost-Effective UHPC, *Journal of Materials in Civil Engineering* 30(4) (2018) 04018030.

- [92] S. Yin, R. Tuladhar, T. Collister, M. Combe, N. Sivakugan, Z.C. Deng, Post-cracking performance of recycled polypropylene fibre in concrete, *Construction and Building Materials* 101 (2015) 1069-1077.
- [93] S. Yin, R. Tuladhar, J. Riella, D. Chung, T. Collister, M. Combe, N. Sivakugan, Comparative evaluation of virgin and recycled polypropylene fibre reinforced concrete, *Construction and Building Materials* 114 (2016) 134-141.
- [94] F. Shi, T.M. Pham, H. Hao, Y. Hao, Post-cracking behaviour of basalt and macro polypropylene hybrid fibre reinforced concrete with different compressive strengths, *Construction and Building Materials* 262 (2020) 120108.
- [95] F. Shi, T.M. Phama, R. Tuladhar, Z. Deng, S. Yin, H. Hao, Experimental Study on the Performance of Ground Slabs and Beams Reinforced with Macro Polypropylene Fibre, Steel Fibre and Steel Mesh, *Construction and Building Materials* Submitted (2020).
- [96] V. Bindiganavile, N. Banthia, Fiber reinforced dry-mix shotcrete with metakaolin, *Cement & Concrete Composites* 23(6) (2001) 503-514.
- [97] J. Hugenschmidt, R. Mastrangelo, GPR inspection of concrete bridges, *Cement & Concrete Composites* 28(4) (2006) 384-392.
- [98] C. Jiang, K. Fan, F. Wu, D. Chen, Experimental study on the mechanical properties and microstructure of chopped basalt fibre reinforced concrete, *Materials & Design* 58 (2014) 187-193.
- [99] J.-M. Yang, K.-H. Min, H.-O. Shin, Y.-S. Yoon, Effect of steel and synthetic fibers on flexural behavior of high-strength concrete beams reinforced with FRP bars, *Composites Part B: Engineering* 43(3) (2012) 1077-1086.
- [100] C. Qian, P. Stroeven, Fracture properties of concrete reinforced with steel–polypropylene hybrid fibres, *Cement & Concrete Composites* 22(5) (2000) 343-351.
- [101] H. Fukuyama, S. Sugano, Japanese seismic rehabilitation of concrete buildings after the Hyogoken-Nanbu Earthquake, *Cement & Concrete Composites* 22(1) (2000) 59-79.
- [102] K.M. Bi, H. Hao, Modelling and simulation of spatially varying earthquake ground motions at sites with varying conditions, *Probabilistic Engineering Mechanics* 29 (2012) 92-104.
- [103] R. Yu, P. Spiesz, H.J.H. Brouwers, Energy absorption capacity of a sustainable Ultra-High Performance Fibre Reinforced Concrete (UHPRFC) in quasi-static mode and under high velocity projectile impact, *Cement & Concrete Composites* 68 (2016) 109-122.
- [104] T.M. Pham, H. Hao, Behavior of fiber-reinforced polymer-strengthened reinforced concrete beams under static and impact loads, *International Journal of Protective Structures* 8(1) (2017) 3-24.
- [105] P. Lura, G.P. Terrasi, Reduction of fire spalling in high-performance concrete by means of superabsorbent polymers and polypropylene fibers Small scale fire tests of carbon fiber reinforced plastic-prestressed self-compacting concrete, *Cement & Concrete Composites* 49 (2014) 36-42.
- [106] Z. Li, L. Chen, Q. Fang, H. Hao, Y. Zhang, W. Chen, H. Xiang, Q. Bao, Study of autoclaved aerated concrete masonry walls under vented gas explosions, *Engineering Structures* 141 (2017) 444-460.
- [107] S. Pyo, K. Wille, S. El-Tawil, A.E. Naaman, Strain rate dependent properties of ultra high performance fiber reinforced concrete (UHP-FRC) under tension, *Cement & Concrete Composites* 56 (2015) 15-24.
- [108] I. Shkolnik, Influence of high strain rates on stress–strain relationship, strength and elastic modulus of concrete, *Cement & Concrete Composites* 30(10) (2008) 1000-1012.
- [109] Y. Al-Salloum, T. Almusallam, S.M. Ibrahim, H. Abbas, S. Alsayed, Rate dependent behavior and modeling of concrete based on SHPB experiments, *Cement & Concrete Composites* 55 (2015) 34-44.

- [110] H. Zhang, B. Wang, A.Y. Xie, Y.Z. Qi, Experimental study on dynamic mechanical properties and constitutive model of basalt fiber reinforced concrete, *Construction and Building Materials* 152 (2017) 154-167.
- [111] Q. Fu, D.T. Niu, J. Zhang, D.G. Huang, Y. Wang, M.S. Hong, L. Zhang, Dynamic compressive mechanical behaviour and modelling of basalt-polypropylene fibre-reinforced concrete, *Archives of Civil and Mechanical Engineering* 18(3) (2018) 914-927.
- [112] S. Yin, R. Tuladhar, F. Shi, M. Combe, T. Collister, N. Sivakugan, Use of macro plastic fibres in concrete: A review, *Construction and Building Materials* 93(15) (2015) 180-188.
- [113] S.F.U. Ahmed, H. Mihashi, A review on durability properties of strain hardening fibre reinforced cementitious composites (SHFRCC), *Cement & Concrete Composites* 29(5) (2007) 365-376.
- [114] Y.F. Hao, H. Hao, Mechanical properties and behaviour of concrete reinforced with spiral-shaped steel fibres under dynamic splitting tension, *Magazine of Concrete Research* 68(21) (2016) 1110-1121.
- [115] T.M. Pham, J. Liu, P. Tran, V.-L. Pang, F. Shi, W. Chen, H. Hao, T.M. Tran, Dynamic compressive properties of lightweight rubberized geopolymer concrete, *Construction and Building Materials* 265 (2020) 120753.
- [116] W.H. Feng, F. Liu, F. Yang, L.J. Li, L. Jing, Experimental study on dynamic split tensile properties of rubber concrete, *Construction and Building Materials* 165 (2018) 675-687.
- [117] ASTM, ASTM C496/C496M-04e1 Standard Test Method for Splitting Tensile Strength of Cylindrical Concrete Specimens, *Book of ASTM Standards* 4 (2008).
- [118] C. Yuan, W.S. Chen, T.M. Pham, L. Chen, J. Cui, Y.C. Shi, H. Hao, Effect of aggregate size on the dynamic interfacial bond behaviour between basalt fiber reinforced polymer sheets and concrete, *Construction and Building Materials* 227 (2019) 116584.
- [119] C. Yuan, W.S. Chen, T.M. Pham, H. Hao, Bond behavior between basalt fibres reinforced polymer sheets and steel fibres reinforced concrete, *Engineering Structures* 176 (2018) 812-824.
- [120] P. Smarzewski, Study of Bond Strength of Steel Bars in Basalt Fibre Reinforced High Performance Concrete, *Crystals* 10(6) (2020) 436.
- [121] S. Fallah, M. Nematzadeh, Mechanical properties and durability of high-strength concrete containing macro-polymeric and polypropylene fibers with nano-silica and silica fume, *Construction and Building Materials* 132 (2017) 170-187.
- [122] T.M. Pham, W.S. Chen, A.M. Khan, H. Hao, M. Elchalakani, T.M. Tran, Dynamic compressive properties of lightweight rubberized concrete, *Construction and Building Materials* 238 (2020) 117705.
- [123] M.Z.N. Khan, Y.F. Hao, H. Hao, F.U.A. Shaikh, Experimental evaluation of quasi-static and dynamic compressive properties of ambient-cured high-strength plain and fiber reinforced geopolymer composites, *Construction and Building Materials* 166 (2018) 482-499.
- [124] Y. Hao, H. Hao, Dynamic compressive behaviour of spiral steel fibre reinforced concrete in split Hopkinson pressure bar tests, *Construction and Building Materials* 48 (2013) 521-532.
- [125] F. Liu, G.X. Chen, L.J. Li, Y.C. Guo, Study of impact performance of rubber reinforced concrete, *Construction and Building Materials* 36 (2012) 604-616.
- [126] M.Z.N. Khan, Y. Hao, H. Hao, Mechanical properties and behaviour of high-strength plain and hybrid-fiber reinforced geopolymer composites under dynamic splitting tension, *Cement & Concrete Composites* 104 (2019) 103343.
- [127] N. Banthia, J.-F. Trottier, Deformed steel fiber—cementitious matrix bond under impact, *Cement concrete research* 21(1) (1991) 158-168.

- [128] N. Banthia, K. Chokri, Y. Ohama, S. Mindess, Fiber-reinforced cement based composites under tensile impact, *Advanced Cement Based Materials* 1(3) (1994) 131-141.
- [129] X.D. Chen, L.Y. Xu, S.X. Wu, Influence of Pore Structure on Mechanical Behavior of Concrete under High Strain Rates, *Journal of Materials in Civil Engineering* 28(2) (2016) 04015110.
- [130] A. Caverzan, E. Cadoni, M. di Prisco, Dynamic tensile behaviour of self compacting steel fibre reinforced concrete, *Applied Mechanics and Materials*, Trans Tech Publ, 2011, pp. 220-225.
- [131] D.Y. Yoo, S. Kim, Comparative pullout behavior of half-hooked and commercial steel fibers embedded in UHPC under static and impact loads, *Cement & Concrete Composites* 97 (2019) 89-106.
- [132] Y. Zheng, L.Z. Zhou, S.E. Taylor, H.W. Ma, Serviceability of one-way high-volume fly ash-self-compacting concrete slabs reinforced with basalt FRP bars, *Construction and Building Materials* 217 (2019) 108-127.
- [133] D. Soares, J. de Brito, J. Ferreira, J. Pacheco, Use of coarse recycled aggregates from precast concrete rejects: Mechanical and durability performance, *Construction and Building Materials* 71 (2014) 263-272.
- [134] L. Boyer, Decorative concrete has come a long way!, *Concrete international* 24(6) (2002) 62-67.
- [135] T.A. El-Sayed, Flexural behavior of RC beams containing recycled industrial wastes as steel fibers, *Construction and Building Materials* 212 (2019) 27-38.
- [136] S. Yin, R. Tuladhar, M. Combe, T. Collister, M. Jacob, R. Shanks, Mechanical properties of recycled plastic fibres for reinforcing concrete, In: *Proceedings of the 7th International Conference Fibre Concrete*, pp. 1-10. From: 7th International Conference Fibre Concrete, September 12-13 2013, Prague, Czech Republic., 2013.
- [137] S. Yin, R. Tuladhar, T. Collister, M. Combe, N. Sivakugan, Z.C. Deng, Post-cracking performance of recycled polypropylene fibre in concrete, *Construction and Building Materials* 101(13) (2015) 1069-1077.
- [138] S. Yin, R. Tuladhar, T. Collister, M. Combe, N. Sivakugan, Mechanical Properties and Post-crack Behaviours of Recycled PP Fibre Reinforced Concrete, In: *Proceedings of the 27th Biennial National Conference of the Concrete Institute of Australia, Construction Innovations, Research into Practice*, pp. 414-421. From: 27th International Conference Concrete 2015, 30 August-2 September, 2015, Melbourne, Australia. (2015).
- [139] S. Yin, R. Tuladhar, R.A. Shanks, T. Collister, M. Combe, M. Jacob, M. Tian, N. Sivakugan, Fiber preparation and mechanical properties of recycled polypropylene for reinforcing concrete, *Journal of Applied Polymer Science* 132(16) (2015).
- [140] J. Øverli, Experimental and numerical investigation of slabs on ground subjected to concentrated loads, *Central European Journal of Engineering* 4(3) (2014) 210-225.
- [141] A. Alani, D. Beckett, F. Khosrowshahi, Mechanical behaviour of a steel fibre reinforced concrete ground slab, *Magazine of Concrete Research* 64(7) (2012) 593-604.
- [142] J.R. Roesler, S.A. Altoubat, D.A. Lange, K.A. Rieder, G.R. Ulrich, Effect of synthetic fibers on structural behavior of concrete slabs-on-ground, *Aci Materials Journal* 103(1) (2006) 3-10.
- [143] J.R. Roesler, D.A. Lange, S.A. Altoubat, K.A. Rieder, G.R. Ulrich, Fracture of plain and fiber-reinforced concrete slabs under monotonic loading, *Journal of Materials in Civil Engineering* 16(5) (2004) 452-460.
- [144] AS, AS 1012.3.1:2014 Methods of testing concrete Determination of properties related to the consistency of concrete - Slump test, *Standards Australia* (2014).
- [145] AS, AS 1012.8.1:2014 Methods of testing concrete - Method for making and curing concrete - Compression and indirect tensile test specimens, *Standards Australia* (2014).

- [146] C.s. committee, Standard for test method of mechanical properties on ordinary concrete (2003) (in Chinese), National standard of the People's Republic of China (2002).
- [147] B. EN, BS EN 14651:2005+A1:2007 Test method for metallic fibre concrete. Measuring the flexural tensile strength (limit of proportionality (LOP), residual), (2005).
- [148] M. Sharma, S. Bishnoi, Influence of properties of interfacial transition zone on elastic modulus of concrete: Evidence from micromechanical modelling, *Construction and Building Materials* 246 (2020) 118381.
- [149] E.T. Dawood, M. Ramli, High strength characteristics of cement mortar reinforced with hybrid fibres, *Construction and Building Materials* 25(5) (2011) 2240-2247.
- [150] D. Jamet, R. Gettu, V.S. Gopalaratnam, A. Aguado, Toughness of fiber-reinforced high-strength concrete from notched beam tests, *Testing of Fiber Reinforced Concrete* 155 (1995) 23-39.
- [151] M.N. Soutsos, T.T. Le, A.P. Lampropoulos, Flexural performance of fibre reinforced concrete made with steel and synthetic fibres, *Construction and Building Materials* 36 (2012) 704-710.
- [152] C. Society, *Concrete industrial ground floors: a guide to design and construction*, Concrete Society 2003.

Appendix I

STATEMENTS OF CONTRIBUTION OF CO-AUTHORS

To whom it may concern

I, Feng Shi, conducted experimental, analytical, data processing & analysis and prepared manuscripts of the papers titled below, which were revised and edited by the co-authors. They also provided insights on experimental preparation, data processing and data analysis.

1. Post-cracking Behaviour of Basalt and Macro Polypropylene Hybrid Fibre Reinforced Concrete with Different Compressive Strengths

2. Pullout and Flexural Performance of Silane Groups and Hydrophilic Groups Grafted Polypropylene Fibre-reinforced UHPC

3. Mechanical Properties of Hybrid Fibre-Reinforced Concrete under Dynamic Compression and Split Tension

4. Experimental Study on the Performance of Ground Slabs and Beams Reinforced with Macro Polypropylene Fibre, Steel Fibre and Steel Mesh



I, as a co-author, endorse that this level of contribution by the candidate indicated above is appropriate.

(Prof. Hong Hao)

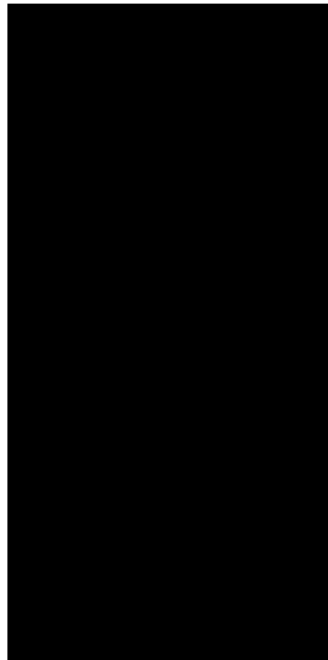
(Dr. Thong M. Pham)

(Prof. Yifei Hao)

(Dr. Shi Yin)

(A/Prof. Rabin Tuladhar)

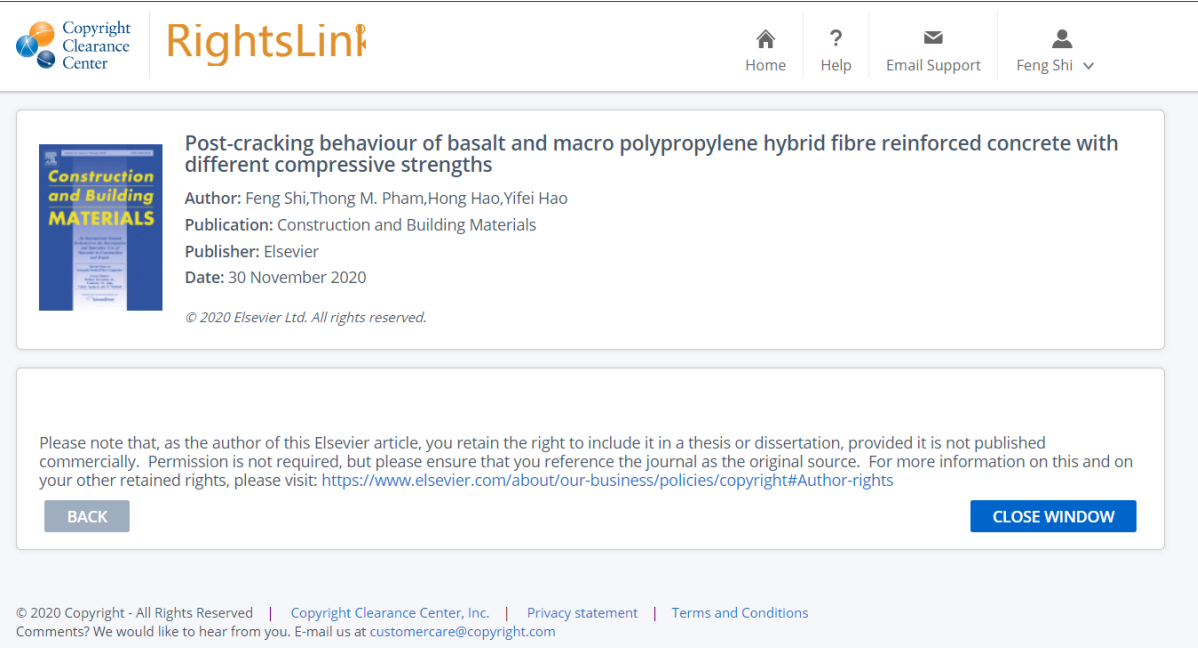
(Prof. Zongcai Deng)



Appendix II

Copyright Clearance

The proof of the rights, granted by the publisher for the publications that form the chapters of this thesis are attached below.



The screenshot shows the RightsLink interface. At the top left is the Copyright Clearance Center logo. To its right is the RightsLink logo. On the top right, there are navigation links: Home, Help, Email Support, and a user profile for Feng Shi. The main content area displays a book cover for 'Construction and Building MATERIALS' on the left. To the right of the cover, the following text is shown: 'Post-cracking behaviour of basalt and macro polypropylene hybrid fibre reinforced concrete with different compressive strengths', 'Author: Feng Shi, Thong M. Pham, Hong Hao, Yifei Hao', 'Publication: Construction and Building Materials', 'Publisher: Elsevier', and 'Date: 30 November 2020'. Below this is the copyright notice: '© 2020 Elsevier Ltd. All rights reserved.'. A disclaimer follows: 'Please note that, as the author of this Elsevier article, you retain the right to include it in a thesis or dissertation, provided it is not published commercially. Permission is not required, but please ensure that you reference the journal as the original source. For more information on this and on your other retained rights, please visit: <https://www.elsevier.com/about/our-business/policies/copyright#Author-rights>'. At the bottom of the disclaimer are two buttons: 'BACK' and 'CLOSE WINDOW'. At the very bottom of the page, there is a footer with copyright information: '© 2020 Copyright - All Rights Reserved | Copyright Clearance Center, Inc. | Privacy statement | Terms and Conditions' and a contact note: 'Comments? We would like to hear from you. E-mail us at customer-care@copyright.com'.

Feng Shi, Thong M. Pham, Hong Hao, Yifei Hao. Post-cracking behaviour of basalt and macro polypropylene hybrid fibre reinforced concrete with different compressive strengths. *Construction and Building Materials*, 2020, 262: 120108.

DOI: 10.1016/j.conbuildmat.2020.120108



Pullout and flexural performance of silane groups and hydrophilic groups grafted polypropylene fibre reinforced UHPC

Author: Feng Shi, Shi Yin, Thong M. Pham, Rabin Tuladhar, Hong Hao

Publication: Construction and Building Materials

Publisher: Elsevier

Date: 29 March 2021

© 2021 Elsevier Ltd. All rights reserved.

Journal Author Rights

Please note that, as the author of this Elsevier article, you retain the right to include it in a thesis or dissertation, provided it is not published commercially. Permission is not required, but please ensure that you reference the journal as the original source. For more information on this and on your other retained rights, please visit: <https://www.elsevier.com/about/our-business/policies/copyright#Author-rights>

BACK

CLOSE WINDOW

Feng Shi, Shi Yin, Thong M. Pham, Rabin Tuladhar, Hong Hao. Pullout and flexural performance of silane groups and hydrophilic groups grafted polypropylene fibre reinforced UHPC. Construction and Building Materials, 2021, 277: 122335.

DOI: 10.1016/j.conbuildmat.2021.122335.

Bibliography disclaimer

Every reasonable effort has been made to acknowledge the owners of copyright material. I would be pleased to hear from any copyright owner who has been omitted or incorrectly acknowledged.